Fall 11-19-2019

Predicting Agricultural Implement Hydraulic Power Demand Using Synchronized Controller Area Network and Ancillary Sensor Data

Gabriel P. Stoll
University of Nebraska-Lincoln, gpstoll.95@gmail.com

PREDICTING AGRICULTURAL IMPLEMENT HYDRAULIC POWER DEMAND USING SYNCHRONIZED CONTROLLER AREA NETWORK AND ANCILLARY SENSOR DATA

by

Gabriel P. Stoll

A THESIS

Presented to the Faculty of

The Graduate College at the University of Nebraska

In Partial Fulfillment of Requirements

For the Degree of Master of Science

Major: Agricultural and Biological Systems Engineering

Under the Supervision of Professors Joe D. Luck & Santosh K. Pitla

Lincoln, Nebraska

December, 2019

PREDICTING AGRICULTURAL IMPLEMENT HYDRAULIC POWER DEMAND USING SYNCHRONIZED CONTROLLER AREA NETWORK AND ANCILLARY SENSOR DATA

Gabriel Paul Stoll, M.S.

University of Nebraska, 2019

Advisors: Joe D. Luck & Santosh K. Pitla

As agricultural implement designs have progressed in recent years, there has been an increase in hydraulic power demand from the tractor. Current power estimation standards do not accurately estimate hydraulic power demand for implements designed with higher hydraulic power requirements. Several stakeholders, including agricultural producers, tractor and implement manufacturers, and government agencies would benefit from accurate published data on these power requirements.

While an increasing amount of operational data available on the Controller Area Network (CAN) of tractors has assisted researchers in more easily obtaining machinery performance data, hydraulic control valve flow rate and pressure measurements are not currently publically available on modern tractor CAN systems. Thus, this study attempted to determine the minimal amount of additional instrumentation needed to measure these parameters.

Results validated that CAN-reported valve spool position could successfully predict flow rate when the tractor's pump was capable of producing a sufficient flow rate to satisfy the overall tractor and implement flow demand. However, this message failed to predict flow rate in all valves whenever the pump became flow-limited due to

circumstances including multiple valves actuated simultaneously, low engine speeds, or high circuit pressure requirements. A customized orifice flowmeter was found to be a compact, cost-effective solution to estimate flow rate under such flow-limited pump conditions. A flow rate prediction method was tested incorporating temperature compensation using CAN-reported valve spool position in flow-sufficient conditions and the orifice flowmeter in flow-limited conditions. Mean absolute errors below 3 Lpm (5.5% MAPE) were observed between the predicted flow rate and measurements from a laboratory-based turbine flowmeter for various simulated tests.

Once determining the flow rate prediction methodology was acceptable, hydraulic power requirements were analyzed between two no-till air drills utilized for small grain planting operations in Eastern Nebraska. To allow a CAN data logger to serve as the sole data acquisition system, a customized instrumentation integration device, the Sensor CAN Gateway (SCANGate), was developed and used to publish all added pressure sensor data onto the CAN bus. In addition to quantifying both planters' hydraulic power requirements, comparisons were made between the time and fuel requirements per area for both operations.

Acknowledgements

As I reflect on how I wound up here submitting this thesis, I am grateful to the numerous people who got me here.

First and foremost, I need to thank God for the countless blessings he's given me. Without Him, I am nothing!

Next, I need to thank my fiancé turned wife, Hannah. Without her, I likely would not have wound up in Lincoln. Not everybody gets the chance to do grad school the same time as their "life-partner," and I learned through this process how wonderful it was to have her along the way. I appreciated being able to vent with her on a nightly basis as both of us went through the toils of the graduate student life.

Third, I need to thank both sets of grandparents. Without my maternal grandparents (Drs. Joe and Charlotte Talkington) supporting me along the way with my schooling, I likely would not have pursued graduate school following completion of my undergraduate degree. Because of them, I would say that I have a greater appreciation for the value of a good education and the importance of being a life-long learner too! As for my paternal grandparents (Hubert and Jean Stoll), I credit them for being my first inspiration for wanting to pursue a career in agriculture. I believe the work ethic I have today is in large part because of the example they set before me as the dairy-farmers that they were.

Finally, I need to thank all who I have worked with in Lincoln. I have been truly blessed to have gotten the chance to work with all of the characters that made up the AMS Lab Group as well as the supporting cast that was always there for us along the way. Showing up to the lab everyday was enjoyable thanks to the friendship and

camaraderie I shared with these individuals and the tremendous amount of respect I have for them. Joe and Santosh, thanks for your work in assembling the group that we were!

It is my hope that, when it's said and done with my career, I will be pointing towards this research work discussed in this thesis as the catalyst that sparked my career. I have learned a great deal through my time at the University of Nebraska. While I felt prepared to take on an engineering career after finishing my bachelor's at the University of Illinois, I believe I am a better critical thinker and more refined individual thanks to the work I conducted here. Thanks to everyone, especially Joe and Santosh, for helping me progress as an engineer in my time here.

I guess that's enough yapping; there's still a lot of pages to digest!

Table of Contents

List of Figures

List of Tables

Chapter 1: Thesis Introduction and Goals

How much power does an agricultural implement require? This question generally cannot be easily answered without the consideration of numerous parameters. The complexity of the possible levels within these parameters further complicates the ability to answer this question. While some parameters can be controlled independently by the operator, others are dependent on factors difficult to quantify such as field conditions and weather. While academic research has been conducted over decades attempting to quantify power requirements for various operations, continued research is needed to improve estimated predictions and account for the latest machinery technology.

As part of a larger effort towards determining modern implement power requirements across different crops, sizes, manufacturers, and field conditions, work conducted for this thesis focused on determining methods to measure hydraulic power demand. The overall purpose of this thesis was to determine the simplest auxiliary sensor instrumentation method capable of effectively inferring agricultural implement hydraulic power requirements. In total, four chapters included in this thesis dissect the challenges encountered towards achieving this goal, detail solutions developed to overcome these challenges, and provide results on the success in these solutions.

Using machine CAN messages available on modern tractors eliminates the need for additional sensors for variables that are reported in a standard format. However, if additional sensors are needed to log all necessary variables for a machinery performance study, a data acquisition system that effectively merges machine CAN messages with auxiliary sensor data is needed. Chapter 2 focuses on the development of an effective

method to allow a CAN data logger to serve as the sole data acquisition system for studies requiring auxiliary sensor installation.

Of the standardized CAN messages commonly available on modern tractors, the estimated flow rate message based on hydraulic control valve spool position is analyzed in great detail in Chapter 3 to determine the ability it possesses in representing actual flow rate. Specific objectives included assessing the accuracy with which the message predicted rate, developing a prediction matrix defining when the message represented flow rate, and determining the amount of additional instrumentation needed to infer hydraulic power demand.

Building upon the results of Chapter 3, Chapter 4 assesses the accuracy of using a combination of CAN-indicated valve spool position and the pressure drop across a customized orifice flowmeter to predict flow rate. Consideration towards incorporating temperature effects on both flow rate prediction methods is given and discussed. Successful implementation of a prediction method using these inputs eliminates the potential difficulties of installing a turbine flowmeter between the tractor and implement.

Chapter 5 discusses a field machinery performance study for two no-till air drills planting small grains. In addition to quantifying hydraulic power demanded by the implement, the overall power, time, and fuel requirements for the operation were analyzed amongst different field terrains and varying vehicle speeds. Assessing hydraulic power involved the deployment of the simplified auxiliary sensor instrumentation method developed in a lab setting and discussed in Chapters 3 and 4.

Chapter 2: Integration of Auxiliary Sensor Data to Tractor ISOBUS for Field Data Collection

2.1. Introduction

For years, researchers have relied on additional sensors connected to data acquisition systems to measure variables needed to better understand agricultural machinery performance. This pursuit, in some instances, resulted in modifications to tractor components to fit the necessary sensors and data acquisition systems on the machinery (McLaughlin et al., 1993).

As technology has evolved, sensors have been incorporated into tractor and implement designs to improve functionality, efficiency, and reduce emissions (Stone et al., 2008). The need for multiple sensors and controllers to communicate with one another in the simplest possible infrastructure led to the development of the Controller Area Network (CAN). To allow components from different manufacturers to communicate with one another on CAN bus systems, standards including SAE J1939 and ISO 11783 were developed to establish benchmarks including common connectors, bus physical structures, and message protocols on heavy duty machinery (Stone et al., 1999). As a result, messages published in a standard format could be decoded into engineering units. Thus, logging CAN Bus data can be valuable in measuring machinery performance characteristics without the installation of additional sensors (Darr, 2012).

As a result, agricultural machinery systems researchers have focused on using the CAN bus as a data acquisition device for tractor and implement studies in recent years. Examples of engineering variables available in a standard CAN message format on

modern tractors include fuel rate, engine speed, engine load percentage, GPS position, wheel slippage, and vehicle ground speed (Al-Aani et al., 2016; Molari et al., 2013; Pitla et al., 2016; Pitla et al., 2014). From measuring these quantities with CAN data, researchers have determined field capacity and efficiencies, conducted time studies, and measured fuel usage and engine power requirements for various field operations involving a tractor and implement (Al-Aani et al., 2016; Kortenbruck et al., 2017; Pitla et al., 2016; Pitla et al., 2014).

In many instances, the sensors and methods used to determine the engineering variables reported on the CAN bus are not traceable. Thus, studies have been conducted attempting to validate the accuracy of certain CAN messages on the tractor (Marx et al., 2015; Rohrer, 2017). Results from these studies have varied. Some variables, such as engine speed and fuel rate, closely matched sensor data measured in a lab setting (Marx et al., 2015; Rohrer, 2017). However, CAN reported engine torque percentage was found to be significantly different than measured torque on a dynamometer connected to an engine (Rohrer, 2017). Thus, the acceptance of error associated with the CAN measurement method must be acknowledged when using CAN variables rather than traceable auxiliary sensors as a measurement device.

Despite many variables being available on the CAN Bus, other variables that could be beneficial in machinery performance studies are either published in a proprietary format on the CAN Bus (at the decision of the manufacturer) or not measured at all. Thus, to measure these variables, additional auxiliary sensors must still be incorporated. For studies where both CAN and added sensor data need collected, the ability to merge and synchronize the two forms of data is required.

Methods for merging CAN and added sensor datasets have varied in past studies. Some studies collected CAN data and added sensor data using two separate data acquisition systems (Burgun et al., 2013; Lacour et al., 2014; Marx et al., 2015). In post-processing, the two datasets were synchronized using the superposition of at least two variables, one from each data acquisition system, that were directly related to one another. Other studies utilized a data acquisition system featuring software to simultaneously merge both CAN and analog data connected to inserted modules of the data acquisition system (Hanigan, 2018; Rohrer, 2017). While the latter data acquisition method eliminates potential difficulty in merging datasets, the combination of purchase price associated with these systems and preference to use existing resources may hinder the ability for the method to be commonly used depending on the scope and background of a study.

2.2. Objectives

The goal of this study was to enable a CAN data logger to serve as the data acquisition system for agricultural machinery studies involving the addition of sensors to measure necessary operational parameters. To accomplish this goal, specific objectives included 1) developing a hardware and software system that could seamlessly merge field performance sensor data into CAN Messages, 2) interfacing the device with modern agricultural machinery, and 3) investigating the effects of added sensor data (sampling frequency and total message number) on bus load.

2.3. Materials and Methods

2.3.1. ECU Selection

An electronic controller unit (ECU) was needed in this study to publish sensor data over the CAN bus to enable data collection with a CAN data logger. Certain features were prioritized in selecting an ECU, including the number of input ports available, the ease in programming the unit to convert sensor data into CAN messages, and the ability to handle rugged field conditions. The ECU (PLUS+1 MC024-110, Danfoss North America, Ames, Iowa) selected excelled in each criteria.

While an adequate number of analog and digital input ports were available on the ECU directly, if more inputs were needed than available on the ECU, an expansion module (IX024-010, Danfoss North America, Ames, Iowa) could be added to create more inputs. For both the ECU and expansion module, the input pins were configurable to allow for flexibility in usage with different combinations of sensor types. The input capabilities for both devices are listed in table 2.1.

Table 2.1: Danfoss PLUS+1 ECU and expansion module input configuration

Maximum Number of Input Types Available for Device	MC024-110 ECU	IX024-010 Expansion Module
Total	14	18
Digital	11	13
Analog	8	12
Frequency	5	7
Temperature / Rheostat	2	4

The selected ECU was programmable via a graphical programming proprietary software (PLUS+1 GUIDE, Danfoss North America). Within the ECU application programming software, numerous settings for the ECU were adjustable to properly

configure it to a given CAN application, including the CAN Bus baud rate and input and output pin configuration. CAN messages were produced by the ECU through using a special CAN transmit block within a given application. Other configurable components and functions allowed the transmitted CAN messages to contain analog voltage readings from various ECU input pins. Figure 2.1 illustrates a sample sub-application from the created program.

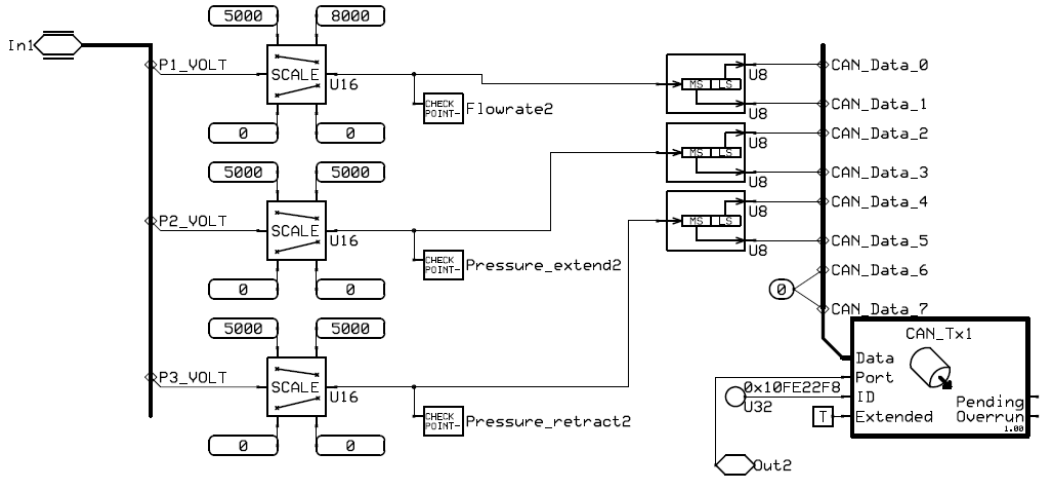

Figure 2.1: *Plus+1 GUIDE sub-application programmed for CAN message transmission using input pin readings.*

For each CAN message created by the added ECU, consideration to the SAE J1939 and ISO 11783 standards was given in forming the identifier and data byte arrangement. As most connected sensors would supplement a CAN message not published in a standard format, the identifier for the created message typically was set to the standard identifier associated with that data. For measured variables not defined by either standard, rather than creating additional messages, sensor data were instead placed in data bytes not used by other created messages following a standard format to reduce the number of messages required to be published over the bus. Additionally, the frequency at

which the messages were published could be adjusted within the CAN transmit function block. As shown in figure 2.2, the function utilized an oscillator and positive trend component to allow adjustment to the message frequency.

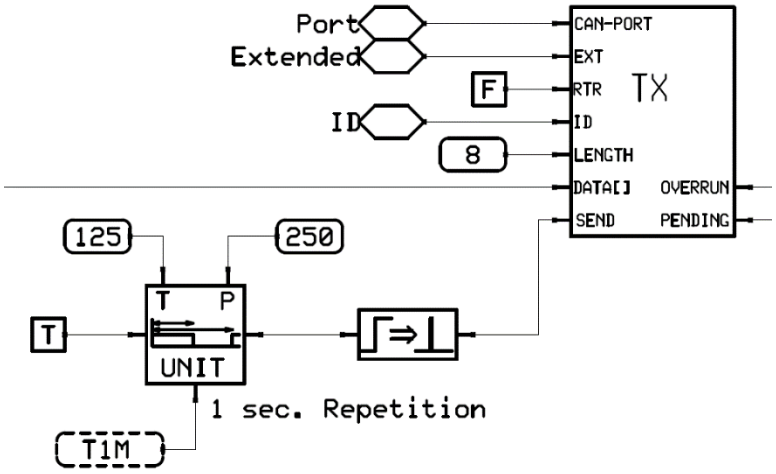

Figure 2.2: *Within the CAN TX function block, adjustment to the message frequency was made by altering the oscillator period that was tied to the Transmit CAN component "send" setting.*

2.3.2. CAN Connection Location

Typically, there are two main CAN bus channels on a tractor. One, intended for tractor related messages, is commonly referred to as the tractor bus, while the other, intended for implement related messages, is known as the ISOBUS. ISOBUS channels on tractors today have a baud rate, which defines the rate of data that can be transmitted over the bus, of 250 kbit/s, while the tractor bus is either 250 kbit/s or 500 kbit/s. A standard J1939 message containing 8 data bytes is 128 bits in length excluding stuffing bits (Kvaser, 2019; Voss, 2018). These baud rates have been selected to accommodate the expected number of messages published over the bus.

While the baud rate defines the maximum rate that data can be transmitted, in reality, the bus load, or percentage of the baud rate used, should be kept lower. Deere (2018)

suggests that bus loads 45% and greater increase potential for communication errors to occur, while according to Kvaser (2019), most systems are designed with a corresponding bus load maintained below 50%. Additionally, certain implements with ISOBUS compatibility do not work with bus loads higher than 25% (Deere, 2018). Unlike the tractor bus, the bus load on the ISOBUS varies with different implements connected to the tractor. For implements that do not feature ISOBUS technology, sufficient room for the addition of auxiliary sensor data exists. However, there are advantages in placing auxiliary sensor data on the tractor bus if there is available room due to no change in required bus load based on the implement used.

Two standard tractor CAN connection ports that were considered for connection of the added ECU were the CAN diagnostic port and the ISOBUS breakaway connector (IBBC). The addition of sensor data to the machine CAN was simplest through connection into one of these two ports. The diagnostic port, which allows for connection of a CAN data logger or diagnostic tool into either channel, is typically located in the tractor cab. The IBBC, generally located behind the tractor cab, allows an implement to communicate with the tractor CAN system via the ISOBUS channel. For either port, an additional port connection was needed to allow the CAN data logger or implement CAN system to simultaneously function. Benefits of using the diagnostic port included the ability to connect into either bus, a more suitable environment for the ECU, and better access to the ECU to troubleshoot issues if they would occur. Benefits of using the IBBC included a closer location to sensor installation for implement data collection studies and the elimination of running additional wiring to the cab of the tractor. In an attempt to

minimize data acquisition components in the tractor cab, connection to the IBBC on the back of the tractor was selected for this study.

2.3.3. Electronics Enclosure Development

A customized electronics device, henceforth referred to as the Sensor CAN Gateway (SCANGate), was developed to integrate sensor data to the ISOBUS through the ECU. The SCANGate fulfilled several goals, including providing power to all sensors, connecting sensor outputs to the necessary ECU input pins, and connecting the ECU to the CAN system.

To connect to the tractor IBBC, an ISOBUS implement connector was used. As shown in figure 2.3 and elaborated in table 2.2, the connector pair featured 9 pins total. To allow implements access to the ISOBUS, the SCANGate featured an additional IBBC. A wiring harness to power all pins in the added IBBC was routed from the ISOBUS implement connector to the added IBBC. No terminating bias circuit (TBC) was needed at the end of the SCANGate bus segment due to the added IBBC featuring a TBC internally. Thus, only 8 wires made up the harness (no TBC disconnect).

Table 2.2: ISOBUS breakaway connector pin description

Pin Number	Description
1	Pass through ground
2	ECU Ground
3	Pass through power
4	ECU Power
5	TBC Disconnect
6	TBC Power
7	TBC Return
8	CAN high
9	CAN low

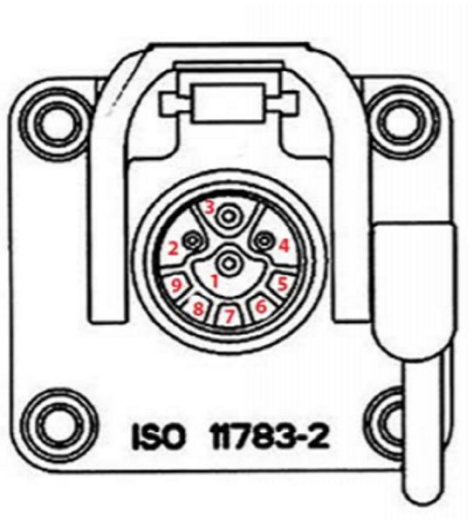

Figure 2.3: *ISOBUS breakaway connector. Numbered pins represent pin number in Table 2.2. Figure from Powell Agriculture.*

To power both the ECU and all added sensors, power and ground were provided from the ECU power and ground pins. While it was anticipated that all future sensors would have input voltage ranges compatible with the tractor battery voltage (12-24V DC), 5 V (DC) could also be provided to sensors from the ECU. To connect the ECU to the CAN bus, a pigtail from the CAN high and low wires was routed to the ECU CAN pins. Terminal blocks were fastened to the side of the enclosure box to allow easy connection of the sensor wires to power, ground, and the necessary ECU input pins. Figure 2.4 shows a picture of the resulting SCANGate electronics enclosure and wiring harness.

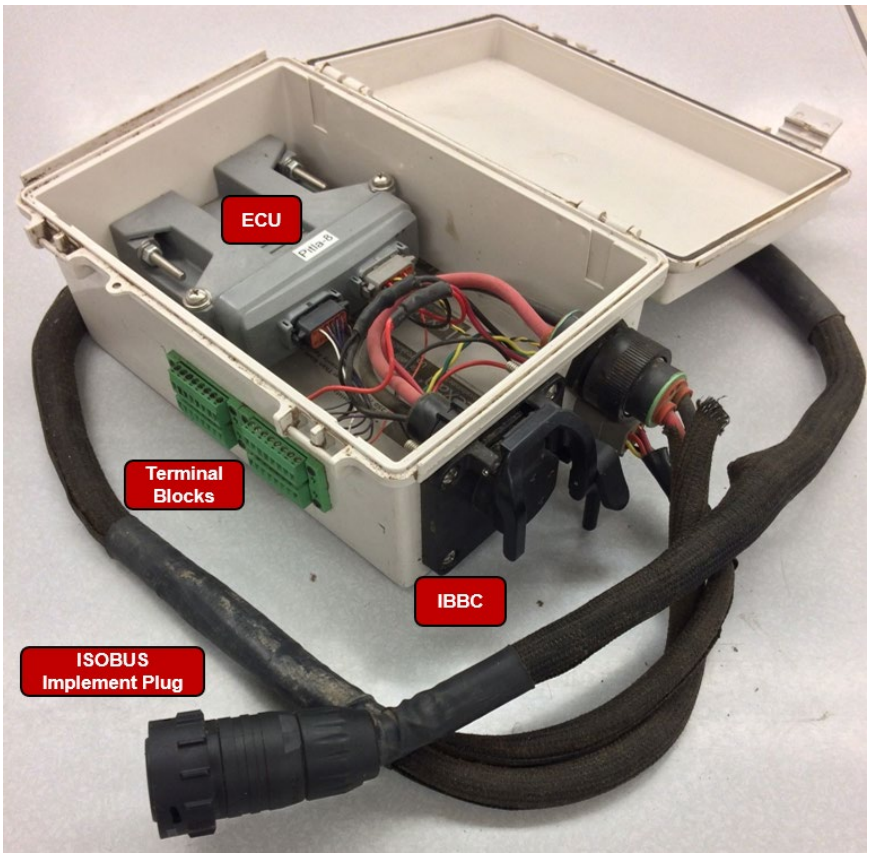

Figure 2.4: *The SCANGate electronics enclosure and wiring harness with hardware components labelled.*

2.3.4. SCANGate Data Collection Method

For studies that were to incorporate the SCANGate, all data were to be collected using a CAN data-logger connected to a tractor's CAN diagnostic port. The logger selected for use (Pro 2xHS v2, Kvaser AB, Mölndal, Sweden) featured the ability to incorporate filters to log selected desired CAN messages to an SD card. Due to the raw format of the resulting log files output by the CAN data-logger, a Matlab program was developed to convert raw CAN data into engineering units to facilitate data analysis from various tests. Figure 2.5 provides a flow diagram detailing the data collection method utilized.

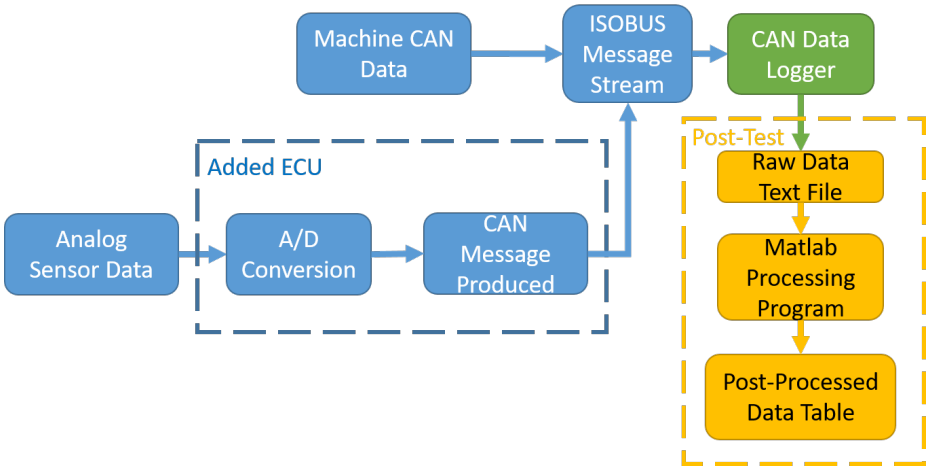

Figure 2.5: *Block diagram detailing the addition of sensor data to the ISOBUS that can be logged and post-processed into engineering units.*

2.3.5. Bus Load Test Equipment and Procedures

A modern tractor (6145R, Deere & Company, Moline, Ill.) was selected to test the developed SCANGate. Due to the tractor's physical design and the desire to use the SCANGate for mobile tests in the future, a customized mounting bracket was built to secure the device (figure 2.6b). The bracket located the SCANGate behind the tractor cab between the three point hitch, hydraulic valve assemblies, and just below the rear window opening path.

Figure 2.6: *(a) JD 6145R tractor used for this study with (b) SCANGate and bracket mounted on rear.*

The selected tractor's virtual terminal featured a Diagnostics Center tool (figure 2.7) that displayed various machine CAN performance statistics, including bus load (listed as bus utilization). The tool also provided an effective message count over a given time period among other information for each machine ECU. While the Diagnostics Center could not validate the transmission of individual messages and log data contained in these messages like the CAN data logger, the tool was sufficient for providing CAN system performance information.

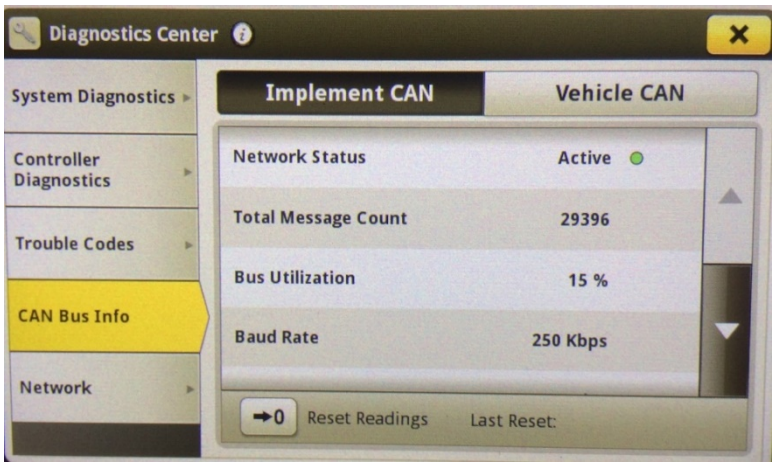

Figure 2.7: *Diagnostics Center page on tractor's virtual terminal displaying effective ISOBUS bus load.*

After plugging the SCANGate into the tractor's IBBC, a CAN bus-to-USB interface (Danfoss CG-150, Danfoss North America, Ames, Iowa) was used to connect a computer to the tractor CAN diagnostic port. This connection allowed the computer to download programmed applications to the ECU using a service tool software (Plus+1 Service Tool, Danfoss North America, Ames, Iowa). Upon successful download, the ECU began publishing CAN messages on the ISOBUS.

Different applications were developed and downloaded to the added ECU to determine the effect of the number of messages published and their set frequencies on the

ISOBUS bus load. In total, 5 different number of messages (1,2,4,6,8) were each tested at 5 different message frequencies (1,2,5,10,20 Hz). All data bytes in every SCANGate CAN message transmitted were set to broadcast at a constant value (255). Additionally, all SCANGate messages were broadcast with lowest priority to ensure existing CAN messages would broadcast first.

An additional variable altered amongst different applications downloaded to the ECU was the source address contained within the CAN message identifier. Different numbers were tested to determine the interaction the added messages would have with the CAN system, including the Diagnostics Center pages on the virtual terminal.

2.4. Results and Discussion

Table 2.3 details other ISOBUS ECU names listed in the Diagnostics Center of the tractor's virtual terminal and their respective source address. For all of the messages output over the ISOBUS, the Diagnostics Center tool on the virtual terminal reported a bus load percentage that fluctuated closely around 15%. In comparison, the reported tractor bus load percentage with a 500 kbit/sec baud rate fluctuated around 45%, which indicated there was limited room for additional messages.

Table 2.3: ISOBUS ECUs Listed on Tractor Virtual Terminal

Source Address (Hex)	Device Name Shown
1C	StarFire – Vehicle Navigation
26	Vehicle Terminal Implement
2A	Vehicle Guidance
2B	Implement Message Service
D2	Documentation for Operational Information
ED	Precision Farming Reprogramming
EE	Sequence Controller Implement
F0	Tractor ECU
F7	Task Controller
FB	JDLink (Machine Monitoring System)
FC	Mobile Processor (GreenStar)

Based on the existing ISOBUS ECU source addresses listed in the Diagnostics Center, three added ECU source addresses were tested. Values included a standard J1939 source address (248), an existing ISOBUS ECU source address (247), and a number reserved for future assignment in the J1939 standard (246). CAN messages with a source address of 248 were listed under new ECU on the Diagnostics Center labeled "File Server / Printer," which matched the description defined by the J1939 standard for that source address. CAN messages with a source address of 247 did not show up under a different ECU, but were instead included within the Task Controller ECU message count along with the existing messages transmitted by that ECU. CAN messages with a source address of 246 were not displayed on the Diagnostics Center page but were recorded by a data logger. From this test, it was determined that the preferred node number was a standard J1939 source address value that was not used among existing ISOBUS ECUs, such as 248.

Table 2.4 details the overall ISOBUS bus load displayed by the Diagnostics Center for different applications containing varying combinations of added message and

message rate levels. All messages were successfully broadcasted at their assigned rates for the lowest priority assignment. As graphically shown in figure 2.8, a linear relationship was observed between the total number of added messages per second and increase in bus load. Due to the whole percentage precision level in the reported bus load, there appeared to be little change in bus load at a lower range of total messages. However, the linear trend was far more prominent at higher ranges of total messages. From a best-fit line equation, it was estimated that each added message per second would increase bus load by approximately .053% for a 250 kbit/s baud rate, which was similar to the expected increase assuming 128 bits per message.

Table 2.4: Total ISOBUS Bus Load for Various Added Message Numbers and Frequencies

Bus Load (%)		Sampling Rate (Hz)				
		1	**2**	**5**	**10**	**20**
Number of Added Messages	1	15.5	16	16	16	17
	2	16	16	16	17	18
	4	16	16	17	18	20
	6	16	16	18	19	22
	8	16	16.5	18	20	24

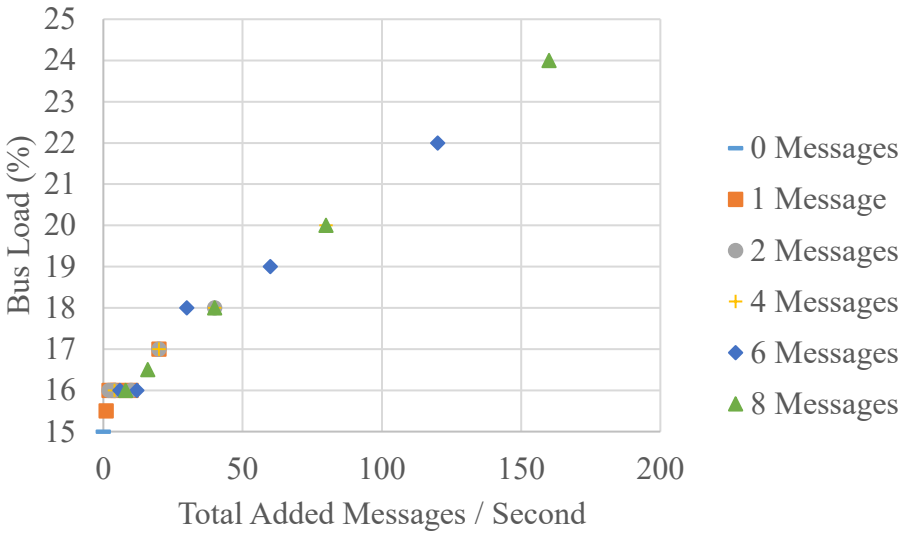

Figure 2.8: *Graphical representation of corresponding bus load for different total added messages per second to the ISOBUS.*

$$y = 0.0533x + 15.71 \quad \text{(Eq. 1)}$$

where
y = bus load (%)
x = total added messages per second

2.5. Conclusions

Being able to utilize CAN messages for data logging is beneficial in that it eliminates the need to install additional sensors to the tractor for measurements that can be obtained from the bus. However, due to a limited number of messages encoded in a standard format on current agricultural machinery, there are instances when additional sensors are still required to effectively conduct certain machinery performance studies.

While multiple companies have developed data acquisition systems capable of merging CAN messages with added sensor data into a common output file, the SCANGate developed in this study allows for a CAN data logger to serve as the sole data acquisition system for studies requiring additional sensors. The primary limitation to the SCANGate

solution is the amount of room available on the CAN bus. Results from this study found that the increase in bus load by the SCANGate can accurately be determined due to a linear relationship with the total number of additional messages the SCANGate will transmit per time interval. The ability to sample sensor data at lower frequencies and fit all sensor data into a minimal number of messages increases the likelihood that the SCANGate will work. Results found that bus load increased by only 1% if less than 15 additional messages were broadcast per second by the SCANGate. With knowledge of the existing bus load requirements of a tractor and implement, it can be determined whether the SCANGate will allow a CAN data logger to serve as the data acquisition system for a given field study based on the amount of added sensor data to be collected.

Chapter 3: Assessment of Control Valve Spool Position and Flow Rate Relationship in Load Sensing Fluid Power Systems

3.1. Introduction

For decades, agricultural producers have relied on tractors to supply implement power necessary to carry out a variety of different in-field tasks. Power is transmitted from the tractor's engine to the implement through at least one of three forms. These forms are the drawbar or three-point hitch to provide draft power to an implement, the power take-off (PTO) to provide rotational power, and the hydraulic system to provide either linear or rotational power (Stoss et al., 2013).

The incorporation of hydraulics to power implements is an increasing trend in modern agricultural machinery. Love (2012) estimated that 14 percent of all power generated by agricultural tractors was devoted to fluid power components. Manufacturers now offer hydraulic systems capable of producing flow rates exceeding 435 Lpm (115 gpm) on larger models (Nebraska Tractor Test Laboratory, 2016b). Additionally, some manufacturers now offer the PTO as an added option instead of a standard feature on their highest power tractor models ("Build and Price," 2019; "Options for 9370R Cab Tractor," 2019). In anticipation of usage with tractors lacking a PTO drive, some implement manufacturers now offer equipment with functions previously controlled by the PTO instead powered by hydraulics. For example, grain cart manufacturers have begun offering models with discharge augers powered by hydraulic motors ("DEMCO Harvest Equipment," 2018).

On agricultural machinery, hydraulic power is generated by at least one pump powered by the tractor's engine that displaces oil through tractor and implement circuits that convert hydraulic power to mechanical power. There is a corresponding pressure requirement the fluid must achieve to overcome parasitic losses and perform mechanical work. As shown in equation 2, the power requirement of the pump is a function of the oil's flow rate and pressure requirement.

$$P_{pump}(kW) = \frac{Fluid\ Pressure\ (MPa) * \ Flow\ Rate(Lpm)}{60\ \left(\frac{MPa * L}{min * kW}\right)} \quad \text{(Eq. Error! Bookmark not defined.2)}$$

Despite the increasing usage of hydraulics, fluid power systems on mobile equipment applications possess an estimated efficiency of just 21.1 percent (Love, 2012). Inefficiencies stem from several components within the hydraulic system. However, Love (2012) estimates that 43 percent of losses occur in control valves and 25 percent occur from power requirements for the fan and charge pump. To gain an understanding of how these losses occur, knowledge of the hydraulic system is needed.

3.1.1. Tractor Hydraulic System Background

Hydraulic pumps on modern tractors are responsible for supplying hydraulic power both to functions on a connected implement as well as internal tractor functions, commonly referred to as primary functions. Examples of primary functions include steering, braking, and control of the three-point hitch. The pump typically supplies energy to an accumulator that provides control to these primary functions; the

accumulator can provide temporary pressurized fluid for primary functions should power loss occur (Cundiff, 2001). Connections to implement circuits occur at auxiliary control valve or power beyond ports.

To improve hydraulic power production and transmission efficiency, most modern tractors utilize a load-sensing, pressure-compensated (LSPC) auxiliary piston pump design. Pump displacement is controlled by a swash plate angle; thus, the flow rate produced by the pump is a function of engine speed and swash plate angle. Two compensators within the pump are used to control a piston that adjusts the swash plate angle. One, commonly referred to as the pressure compensator, is engaged when the maximum tolerable working pressure is reached at the pump outlet. When engaged, the pressure compensator moves the swash plate towards zero pump displacement. The other, commonly known as the flow compensator, is used to control the pump displacement in the operating pressure range below the pressure compensator setting.

For hydraulic circuits connected to a load-sensing system, a system of shuttle valves is used to determine the highest pressure requirement of all functions in the hydraulic system, commonly referred to as the load sense pressure. The flow compensator balances the force generated by fluid pressure at the pump with the combination of forces generated by the load sense pressure and a compressed spring within the compensator (Dell, 2017). The compensator works with the LSPC pump to attempt to maintain a constant pressure difference, commonly referred to as margin pressure, between the pump and load sense fluid pressures. When the difference between the pump and load sense pressure is less than the margin pressure setting in the flow compensator, the swash plate angle increases, if possible, to achieve a higher flow rate. If the difference between

pump and load sense pressure is greater than the margin pressure setting, the control piston decreases the swash plate angle to reduce the pump flow rate.

Auxiliary control valves used with LSPC pumps feature an adjustable main spool that creates a variable-sized fluid passageway controlled by the spool's position. Depending on the passageway size and fluid flow rate passing through the valve, a certain pressure drop occurs across the spool. The auxiliary control valve features an additional pressure compensator to attempt to maintain a constant pressure difference across the spool. Thus, flow rate through a control valve can solely be dictated by valve spool position. Each valve's load sense pressure is recorded just beyond the main spool on the load side. Therefore, the pressure difference between pump and load sense closely represents the pressure drop that occurs across the control valve with the highest load sense pressure. A higher pressure drop occurs across the pressure compensators in control valves with lower load sense pressures to maintain the constant pressure drop across the main spool to allow flow rate to be maintained for a given valve spool position.

Although using valve pressure compensators effectively allows multiple control valves to each receive their requested flow rate from a single LSPC pump, the pump output power efficiency is reduced. As illustrated in figure 3.1 and detailed in table 3.1, the resulting power produced by the pump is a product of the flow rate needed for all functions and the highest load sense pressure of the system. However, the implement power requirement is the sum of each individual circuit's product of flow rate and pressure requirement. Thus, the product of flow rate and difference in magnitude between the highest load sense and pressure requirement of each lower load sense valve

is wasted power. Additional wasted power occurs by a magnitude of the product of the total system flow rate and margin pressure setting. All wasted power is converted into heat, which increases fluid temperature. To prevent the fluid from reaching low viscosities, which can cause excessive hydraulic component wear and eventual failure, the system must cool the hydraulic fluid, adding an additional system energy loss.

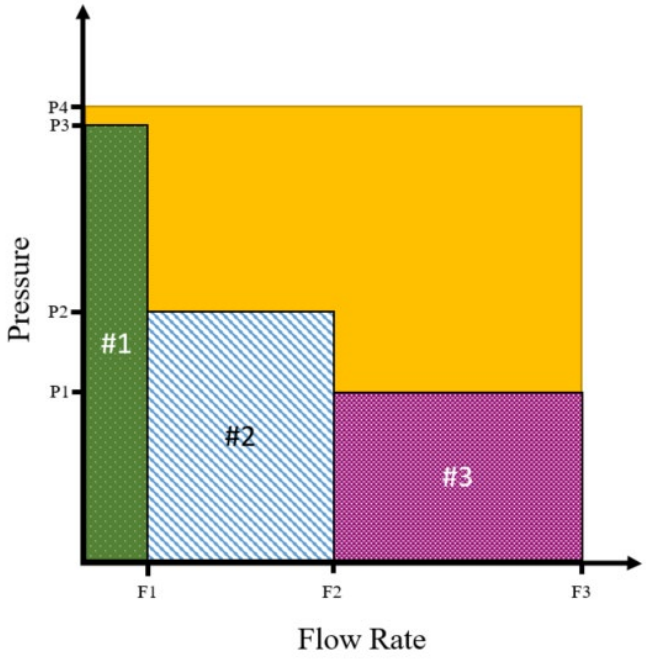

Figure 3.1: *Hydraulic power delivery breakdown for single pump. Through this figure, it is seen that individual valve flow rate and pressure measurements are needed to determine implement power.*

Table 3.1: Power Values Derived from Figure 3.1

Value Represented	Equation of Value
Margin Pressure Setting	$p_{margin} = p4 - p3$
Valve #1 Power Requirement	$P_1 = p3 * f1$
Valve #2 Power Requirement	$P_2 = p2 * (f2 - f1)$
Valve #3 Power Requirement	$P_3 = p1 * (f3 - f2)$
Implement Power Requirement	$P_{imp} = P_1 + P_2 + P_3$

Pump Power Produced	$P_{pump} = p4 * f3$
Wasted Power	$P_{loss} = P_{pump} - P_{imp}$
Pump Power Efficiency	$\varepsilon = \frac{P_{imp}}{P_{pump}}$

Stoss et al. (2013) discussed how manufacturers have begun incorporating multiple pumps on tractors to more efficiently provide power for implements. Division of high and low pressure functions to different pumps reduces the power wasted at the control valves. Additionally, the evolution of digital hydraulics has a strong potential to drastically reduce inefficiencies throughout the hydraulic system (Breidi et al., 2017). Digital hydraulics presents the opportunity to more precisely deliver the desired flow rate to each control valve.

3.1.2. Means to Measure Implement Hydraulic Power Components

Because implement power is the product of each individual circuit's fluid pressure requirement and flow rate, both variables of each control valve must be measured to accurately determine this quantity.

For implements where only one control valve is used at a time, measuring total flow rate sent to the tractor's control valve stack, as done by Lacour et al. (2014), is suitable. However, complications in flow rate measurements inferred at the pump with swash plate angle and engine speed exist due to the pump also potentially supplying flow to primary tractor functions and internal leakages which are dependent on the fluid pressure, the viscosity of the fluid, and the area of the leakage path (Srivastava et al., 2012). Similarly, measurement of the load sense and return fluid pressures are effective pressure measurements in instances when only one valve is used at a time. Pressure measurement

at the pump is not suitable as it would not account for losses in the tractor hydraulic system design between the pump and implement circuit.

Unfortunately, methods capable of measuring flow rate and pressure for single-valve usage would not be effective for many implements that require multiple control valves actuated simultaneously. When this is the case, the flow rate and pressure of each valve must be measured individually. Potential methods to measure these quantities are discussed below.

3.1.2.1. CAN Bus Messages

As technology has progressed in agricultural machinery designs, rather than adding sensors and a data acquisition system for machinery data collection studies, researchers have utilized CAN messages derived from existing sensor hardware on machines to obtain available data of interest. Certain CAN messages produced by the machinery are encoded in a format defined by either the SAE J1939 or ISO 11783 standards. Anyone with access to the standard can interpret these messages into engineering units. However, many engineering variables are either not currently reported on the CAN Bus of modern agricultural machinery or are instead published in a propriety format at the discretion of the manufacturer. If valve flow rates and pressures on the inlet and outlet of the valve are logged on the CAN Bus in a standard format, implement hydraulic power magnitude can be inferred through CAN data.

3.1.2.2. Flowmeters / Pressure Sensors

If the CAN bus does not directly offer the needed flow rate and pressure variables in a standard format, other methods must be explored. Ideally, a direct measurement of fluid flow rate and pressure is preferred to an indirect method; thus, the addition of flowmeters

and pressure sensors are needed. Pressure sensors are needed on both the extend and retract sides of each control valve due to the potential for pump flow being sent through either valve side and to account for fluid flow restrictions to tank that could vary by tractor design. Unlike pressure sensors, a single flowmeter can be installed on either valve side. Circuits featuring single-rod cylinders with differing flow rates entering and exiting the cylinder require knowledge of cylinder bore and rod dimensions to prevent the need for multiple flowmeters on each circuit.

The feasibility of adding sensors to machinery that accurately measure such variables is an important criteria to consider. The selected flowmeter for use must be capable of fitting between the valve stack behind the tractor cab and the attached implement hydraulic circuit. Due to potential for flow moving in either direction, the flowmeter must be capable of measuring bidirectional flow rate. Compatible turbine flowmeters available require uninterrupted flow lengths equivalent to 10 times the port diameter size upstream and 5 times the port diameter downstream of the sensor (Badger Meter, 2018). Roeber et al. (2016) tested hose bend angles both upstream and downstream of a turbine flowmeter and concluded measurement accuracy was sufficient for any hydraulic hose bend angle. However, alternative means to measure flow rate are preferred due to minimal room between the tractor and implement conflicted with the long upstream and downstream hose-length requirements for turbine flowmeter accuracy.

Indirect methods of determining flow rate, using quantities that were simple to measure and required minimal space, were considered. Unlike turbine flowmeters, orifice flowmeters offer a compact solution. These flowmeters rely on the standard orifice equation (equation 3), derived from Bernoulli's equation, to infer flow rate as a

function of the pressure drop measured across an orifice. The same relationship between pressure drop and flow rate occurs in fluid flow path geometry changes, commonly referred to as minor losses. Given that minor losses commonly exist in a hydraulic system, the estimation of flow rate from a minor loss versus an orifice flowmeter would eliminate the creation of an additional system loss.

$$Q = C_d A \sqrt{\frac{2\Delta p}{\rho}} \quad \text{(Eq. 3)}$$

where
Q = flow rate
C_d = discharge coefficient
A = orifice area
Δp = pressure drop across orifice
ρ = fluid density

Manring (2005) proposed a model based on the standard orifice equation to predict flow rate produced from a control valve. Shown in equation 4, the model determines flow rate as a function of the valve's pressure drop and spool linear position. If a constant pressure drop can be maintained across the valve spool, as is intended in load sensing hydraulic system designs, then flow rate that passes through the valve can theoretically be modeled by the valve spool position alone. However, pressure drop must also be monitored for any instance when the constant pressure drop across the valve spool cannot be maintained.

$$Q = \frac{1}{2} Q_o + K_q x + K_c \Delta p \quad \text{(Eq. 4)}$$

where
Q = flow rate
x = control valve spool position
Q_o = nominal flow rate when x = 0.
$K_c \equiv \frac{\delta Q}{\delta A}\frac{\delta A}{\delta x} = C_d \sqrt{\frac{2\Delta p}{\rho}}\frac{\delta A}{\delta x}\Big|_o$ = flow gain coefficient

$$K_c \equiv \frac{\delta Q}{\delta \Delta p} = \frac{AC_d}{\sqrt{2\rho\Delta p}}\Bigg|_o$$ = pressure flow coefficient

3.2. Objectives

The main goal of this study was to determine the feasibility of quantifying agricultural implement hydraulic power requirements using existing machinery CAN messages. Specific objectives to accomplish this goal included 1) confirming whether hydraulic pressure and flow rate measurements were available on a modern tractor's CAN system, 2) assessing the accuracy of the CAN messages at reporting the actual pressures and flow rates, and 3) determining the minimal additional instrumentation needed if CAN messages alone cannot provide information to determine implement hydraulic power consumption.

3.3. Materials and Methods

3.3.1. Equipment / Materials Used

Two modern tractors of the same model number (6145R, Deere & Company, Moline, Ill.) were selected for use in this study. Test results from the Nebraska Tractor Test Laboratory for this model indicated that the maximum system fluid pressure achieved was 20.5 MPa, while the maximum flow rate achieved at rated engine speed was 115.8 Lpm through a single outlet and 116.8 Lpm through three outlets (Nebraska Tractor Test Laboratory, 2016a). Both selected tractors featured auxiliary control valves with electronically adjustable spools. Control valve settings that could be adjusted from the tractor's virtual terminal included a maximum spool position setting (on a range of 0 to 10 in 0.04 increments) and detent time length. A lever for each valve was provided in the

cab to control the valve actuation direction, percentage of maximum spool position setting, and the initiation of detent or float mode.

An investigation was conducted on available standard hydraulic-related CAN messages published on the selected tractors. Table 3.2 details relevant hydraulic messages outlined in either the ISO 11783 or SAE J1939 standard. The standard message for extend and retract port flow rates and pressures was not available on either tractor. The only hydraulic-related variables published on the CAN bus in a standard format were engine speed, hydraulic fluid temperature, and estimated flow rates. It was determined that estimated flow rate, published as a percentage, was directly related to each valve's spool position. While the CAN reported estimated flow percentage did not directly match the input setting from the virtual terminal, it maintained a constant percentage for each actuated position. With ability to collect valve spool position data for each control valve on the CAN bus, the focus of this study was directed towards understanding the scenarios during operation when the estimated flow message accurately predicted flow rate.

Table 3.2: SAE J1939 / ISO 11783 assigned PGNs related to hydraulics

PGN Identifier		Description	Availability on Tractor
Hexadecimal	Decimal		
F004	61444	Engine Speed	Available
F008	61448	Hydraulic fluid pressure at pump	Unavailable
FE10	65040	Extend port and retract port estimated flow for auxiliary valves numbered 0,1,2,3, and 4, respectively	Available
FE11	65041		
FE12	65042		
FE13	65043		
FE14	65044		
FE20	65056	Extend port and retract port pressure and measured flow for auxiliary valves numbered 0,1,2,3, and 4, respectively	Unavailable
FE21	65057		
FE22	65058		
FE23	65059		
FE24	65060		
FE68	65128	Hydraulic oil temperature and level	Available

A testing apparatus was developed to simulate connected implement circuits and measure fluid flow rate. The apparatus (figure 3.2) featured two duplicate circuits containing a turbine flowmeter (Flo-tech Activa F6206-AVB-NN, Badger Meter, Milwaukee, Wisc.) that served as the baseline flow rate measurement and an adjustable flow control valve, or needle valve, to allow adjustment to the circuit pressure requirement. An analog pressure gauge was also incorporated into the circuit to provide the operator with an estimated circuit fluid pressure during testing.

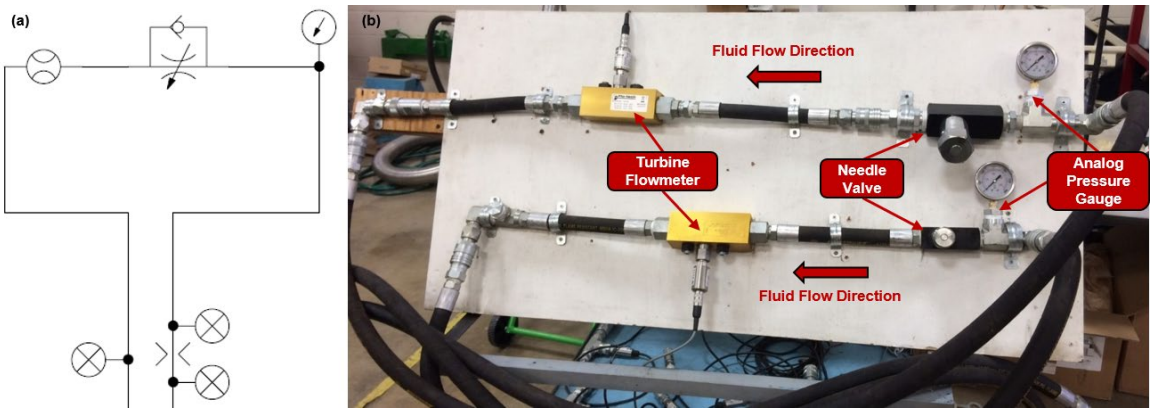

Figure 3.2: *(a) Schematic of the (b) hydraulic testing apparatus used throughout the study.*

In order to understand hydraulic system performance characteristics, including power magnitudes, pressure was measured on the extend and retract ports of each control valve and the pump and load sense diagnostic ports available on the tractor (figure 3.3). All pressure measurements were conducted using a common electronic pressure sensor (Omega PX309, Omega Engineering Inc., Norwalk, Conn.). To measure control valve pressures, sensors were added to tee fittings with ISO quick couplers to allow location between the control valve and implement.

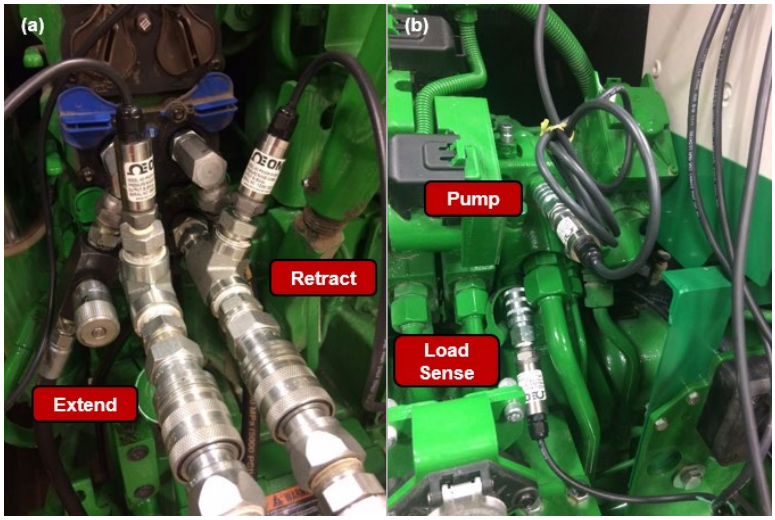

Figure 3.3: *Common pressure sensor locations included (a) on the extend and retract port immediately beyond each valve and (b) on diagnostic ports of the pump and load sense.*

3.3.2. Data Collection Method

To synchronize data collection, auxiliary sensor data were published as CAN messages to the tractor's ISOBUS. This allowed for all data to be logged with a CAN data logger. An electronic controller unit (ECU) (Danfoss MC024-110, Danfoss North America, Ames, Iowa) was programmed through a graphically programmable proprietary software (Danfoss PLUS+1 GUIDE, Danfoss North America) to convert analog sensor data into CAN messages. A customized electronics enclosure (figure 3.4), named the Sensor CAN Gateway (SCANGate), was developed to house the selected ECU and connect it to the tractor CAN system using an implement-end ISOBUS breakaway connector (IBBC). Furthermore, the SCANGate supplied power to the sensors and connected their output readings to the ECU. For this study, the SCANGate published three additional CAN messages containing all auxiliary sensor data at a frequency of 4 Hz.

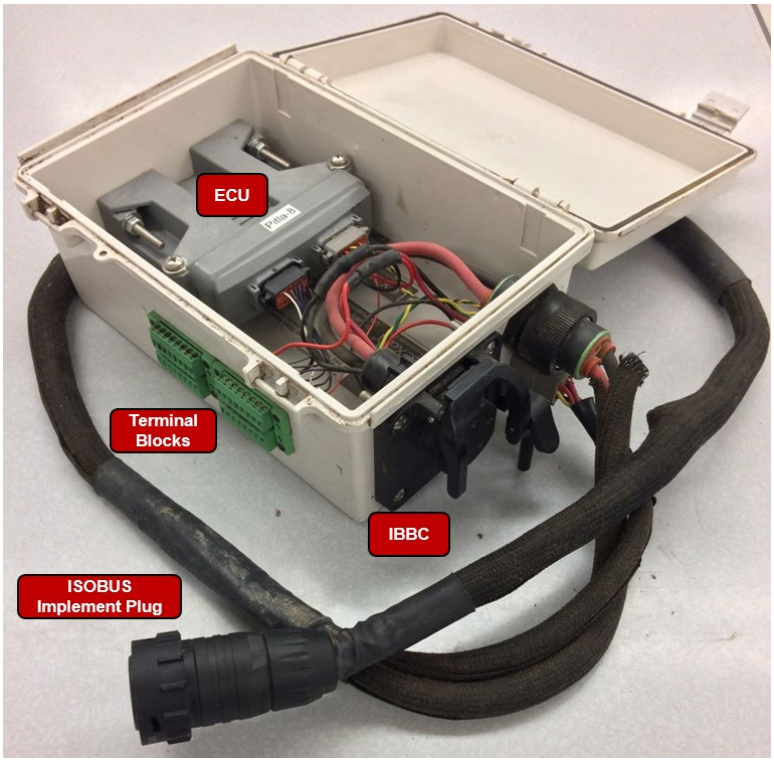

Figure 3.4: *Picture of the developed SCANGate design with hardware components labelled.*

The tractor's in-cab CAN diagnostic port was accessed to enable two different data logging systems (figure 3.5) to be utilized throughout the study. A standalone data-logger (Pro 2xHS v2, Kvaser AB, Mölndal, Sweden) saved CAN bus data to an SD card. A CAN bus-to-USB interface (Danfoss CG-150, Danfoss North America, Ames, Iowa), logged messages to a connected computer through a proprietary software (Danfoss CANKing, Danfoss North America). Various filters were incorporated for both data logging methods to only record desired messages from the bus.

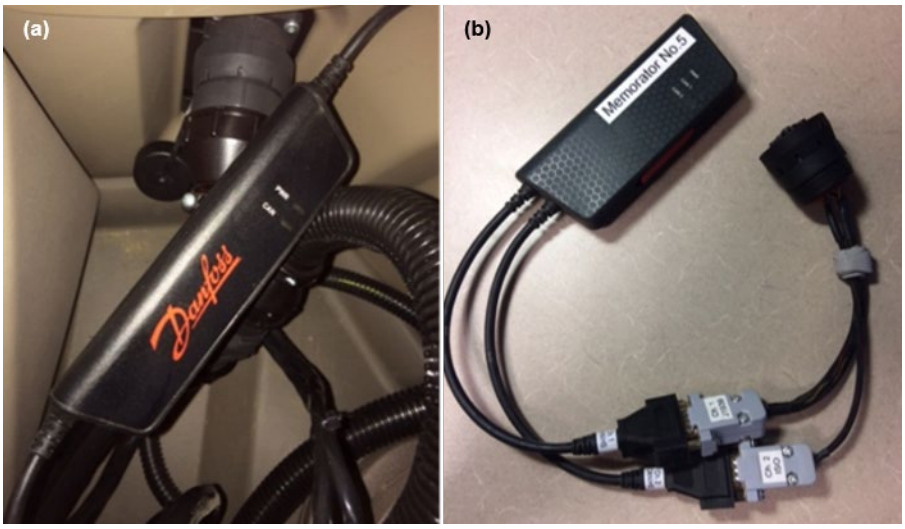

Figure 3.5: *CAN data loggers used in study included (a) Danfoss CG-150 CAN-to-USB interface and (b) Kvaser Memorator Pro 2xHS v2 standalone CAN data logger.*

Log files generated by either data logger were produced in a raw hexadecimal format. A MATLAB program was created to post-process the CAN log files. Steps in the data post-processing included sorting different messages by their parameter group number (PGN), converting raw data bytes into engineering units, and resampling calculated engineering values to common time intervals. Additionally, neutral valve position and transient data points were filtered out of the dataset to isolate data with steady-state flow characteristics. Additional MATLAB programs used the filtered dataset to further analyze each test's results. Figure 3.6 provides a flow diagram detailing the data collection method utilized.

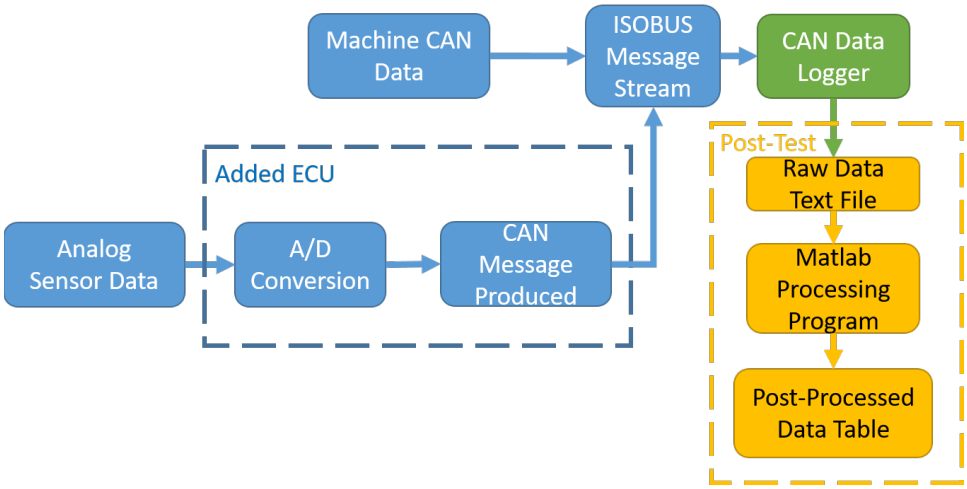

Figure 3.6: *Block diagram detailing the addition of sensor data to the ISOBUS that can be logged and post-processed into engineering units.*

3.3.3. Test Types

Tests analyzing different variables' effects on the ability to predict flow rate using the estimated flow rate CAN message were developed and executed. Variables of interest included engine speed, implement load, the usage of multiple control valves, and hydraulic fluid temperature. Three input variables were adjusted for each test setup: 1) the needle valve setting representing implement load, 2) the engine speed, and 3) the spool position of each control valve. While it was preferred to be able to control the circuit pressure requirement, the associated pressure requirement would change for a given needle valve setting as flow rate changed. With exception to the temperature test, the fluid was always preheated to a stable value prior to testing to eliminate any potential effects of fluid temperature. This was particularly important given all power produced by the needle valve circuit was converted to heat, which could increase fluid temperature quickly during a test. Discussion on specific tests and their purpose is presented in greater detail in the following sections.

3.3.3.1. Variable Engine Speed Test

The purpose of the variable engine speed test was to determine the effect of engine speed on the flow rate produced through a control valve for a given spool position setting. Two spool position settings were used in this test; one corresponded to a mid-level estimated flow percentage while the other was fully open to maximize the passageway area. In either case, valve spool position was held constant for the test duration. The circuit needle valve was set to a low pressure requirement setting held constant over the test duration to prevent the pressure compensator from engaging due to high system pressure. Different engine speeds ranging from low to high idle were tested. Typically, at each engine speed, the control valve was placed into detent between 10 to 20 seconds to gather a sufficient amount of data.

3.3.3.2. Variable Implement Pressure Requirement Test

A variable implement pressure requirement test was conducted to evaluate the effects of different simulated implement pressure requirements on flow rate for a given valve spool position. A high idle engine speed was maintained to ensure the pump was not flow-limited for reasons other than pressure magnitude. The control valve spool was preset to be actuated to a constant position correlating to a mid-level estimated flow percentage throughout the test duration. Different needle valve settings were tested to simulate different implement pressure requirements ranging from the lowest achievable pressure requirement with a fully open needle valve to a setting that resulted in maximum system pressure. Similar to the variable engine speed test, the control valve was placed into detent between 10 to 20 seconds to gather a sufficient amount of data for each tested implement pressure requirement setting.

3.3.3.3. Multiple Valve Test

Due to the likelihood of multiple control valves actuated simultaneously in field operations with implements, testing of multiple valves was conducted. The purpose of these tests was to validate expected flow rate distribution between multiple valves for different anticipated cases. According to Dell (2017), distribution of flow rate amongst multiple valves in LSPC systems was dependent on where the valve pressure compensator is located. If located before the main spool, known as pre-spool compensation, a valve with a lower fluid pressure requirement would receive all flow before a valve with a higher fluid pressure requirement received any flow (Dell, 2017). If located after the spool, known as post-spool compensation, flow would be divided based on spool position setting in each valve (Dell, 2017). Location of valve compensators in each tractor was unknown prior to testing.

Three scenarios with multiple valves actuated simultaneously were tested. Two of these involved only two valves. In one test, different needle valve settings were used in each valve, while the other test featured similar needle valve settings in both valves. The third test featured a third valve also actuated, but connected to no circuit. Load check valves within the control valve prevented a flow rate from being produced through the third valve. Therefore, the desired flow rate produced through the third valve would never be achieved. This, in theory, would send the pump pressure to its maximum system pressure setting.

For all tests, all tested valves were placed into continuous detent. Each test featured one connected valve that was held at a constant spool position correlating to a mid-level estimated flow percentage for the test duration. The other connected valve, after starting

fully closed, had its spool position increased in approximately 10% estimated flow rate increments roughly every 10 seconds, or enough time to collect a sufficient amount of steady-state data. Once the valve was fully-open, its spool position was reduced at the same increments over a similar timeline until the valve was fully closed. For the test with three valves actuated, the unconnected valve maintained a constant, low-spool position setting throughout the test. To prevent potential flow-limited circumstances, a high engine speed was maintained and needle valve settings on each circuit were always set at positions that prevented the pressure compensator engaging at high flow rates.

3.3.3.4. Fluid Temperature Test

A temperature test was conducted to determine if fluid temperature affected flow rates produced at a particular valve spool position. Unlike the other variables tested, fluid temperature was not easily adjustable by changing an input variable. As fluid temperature increased as work was performed, the hydraulic oil temperature at the beginning of each test was required to be at ambient air temperature. Engine speed and circuit pressure parameters were set such that they would not hinder the pump's ability to produce a requested flow rate. However, a needle valve setting that resulted in a higher circuit pressure requirement was preferred to create more wasted power, thus increasing fluid temperature at a faster rate. A valve was placed into continuous detent for a single valve spool position throughout the test duration. Hydraulic oil temperature was monitored on the tractor's virtual terminal to determine when a steady-state temperature was maintained.

3.4. Results & Discussion

3.4.1. Effect of Engine Speed on Hydraulic Flow Rate Delivery

A variable engine speed test was conducted at a valve spool position corresponding to an estimated flow rate percentage CAN message of 54%. Table 3.3 details results for the mean measured flow rate and pressure difference between pump and load sense for different engine speeds tested. At the two lowest tested engine speeds, the actuated valve was not able to achieve the consistent flow rate seen at higher engine speeds. Thus, the estimated flow rate CAN message did not accurately predict actual flow rate in instances where the pump was flow-limited due to engine speed.

Table 3.3: Variable Engine Speed Test Results at 54% Estimated Flow Rate

Engine Speed (rpm)	Mean Flow Rate (Lpm)	Flow Rate Variance (Lpm)	Pump - LS Mean Pressure Difference (MPa)
848.87	46.47	0.0275	1.704
1072.06	58.63	0.0367	2.176
1239.02	58.88	0.0154	2.509
1381.59	58.90	0.0184	2.505
1536.26	58.91	0.0181	2.496
1641.47	58.85	0.0206	2.499
1780.36	58.82	0.0124	2.509
1924.77	58.85	0.0178	2.509
2055.67	58.89	0.0210	2.501
2240.52	58.93	0.0249	2.486

Additionally, the pressure difference between the pump and load sense at low engine speeds failed to maintain the constant difference seen at engine speeds where flow rate was constant. From the test, it is inferred that the margin pressure setting of the pump's flow compensator was approximately 2.50 MPa. When the pump reached a flow-limited condition, the pressure difference between pump and load sense dropped below the

margin pressure magnitude. Therefore, monitoring the difference between pump and load sense is beneficial in determining when the estimated flow rate CAN message will accurately predict flow rate in a control valve.

Having determined that at lower engine speeds, the tested tractor's pump was potentially incapable of meeting control valve flow rate requests, another variable engine speed test was conducted with a fully open valve (estimated flow rate CAN message of 100%) to quantify the flow rate available to a control valve at different engine speeds. Figure 3.7 shows the resulting linear relationship observed between engine speed and the measured flow rate through the control valve. Equation 5 details the resulting line of best fit, which had a coefficient of determination (R^2) of 0.9997.

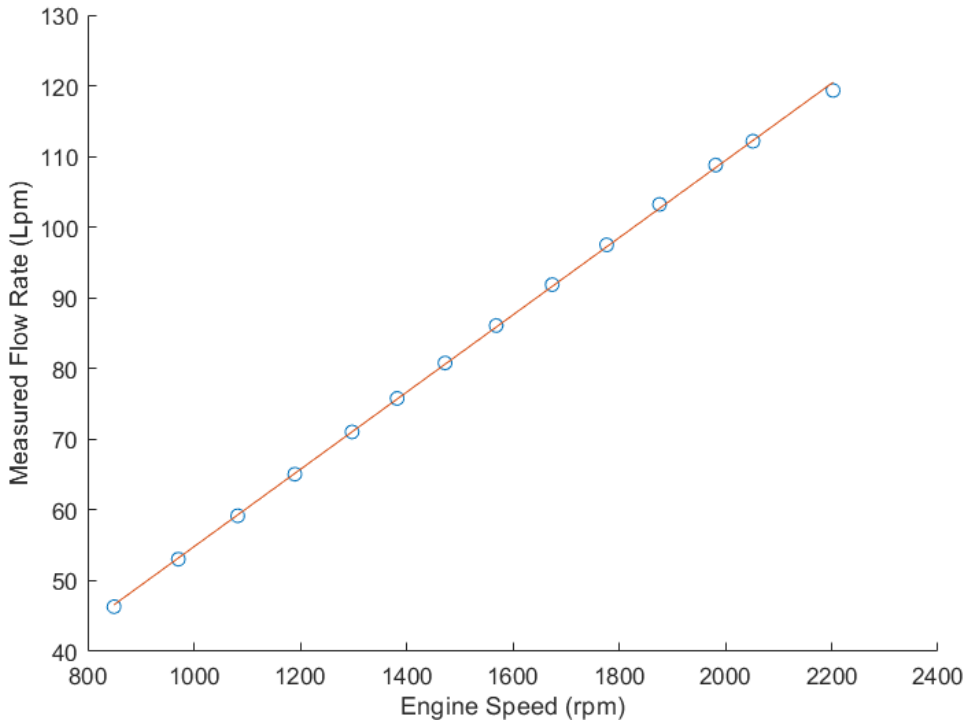

Figure 3.7: *Measured flow rate versus engine speed test for a fully open spool. Line of best fit given in equation 5.*

$$q = 0.0546n + 0.1961 \quad \text{(Eq. 5)}$$

where

q = flow rate produced from valve (L min^{-1})
n = engine speed (rpm)

Equation 5 provides an understanding of the minimum engine speed needed for an implement to achieve its hydraulic functions based on its flow rate requirement. Typically, engine speed would not be used to adjust the desired flow rate for an operation; however, if an operation required a high flow rate, the engine speed setting could limit the ability for the pump to achieve the requested flow rate. This issue could occur for tractors equipped with IVT or CVT transmissions where lower engine speeds must be set to ensure proper implement functions.

3.4.2. Effect of Pressure Requirement on Control Valve Flow Rate

A variable implement pressure requirement test was conducted at a valve spool position generating a 69% estimated flow rate CAN message. Figure 3.8 details flow rate, circuit pressure requirement, and the difference between pump and load sense pressure measurements for different tested needle valve settings. The data shown illustrate the system's ability to maintain a consistent flow rate for a given control valve setting over varying implement loads resulting in different fluid pressure requirements. However, at the highest two pressure requirements tested, the resulting flow rate delivered from the control valve was below the measured flow rate seen at lower fluid pressures. Thus, the pump could not maintain a consistent flow rate at high pressures for this valve position. Therefore, estimated flow rate CAN message cannot be used to predict flow rate for circuits with fluid pressures at maximum system pressure.

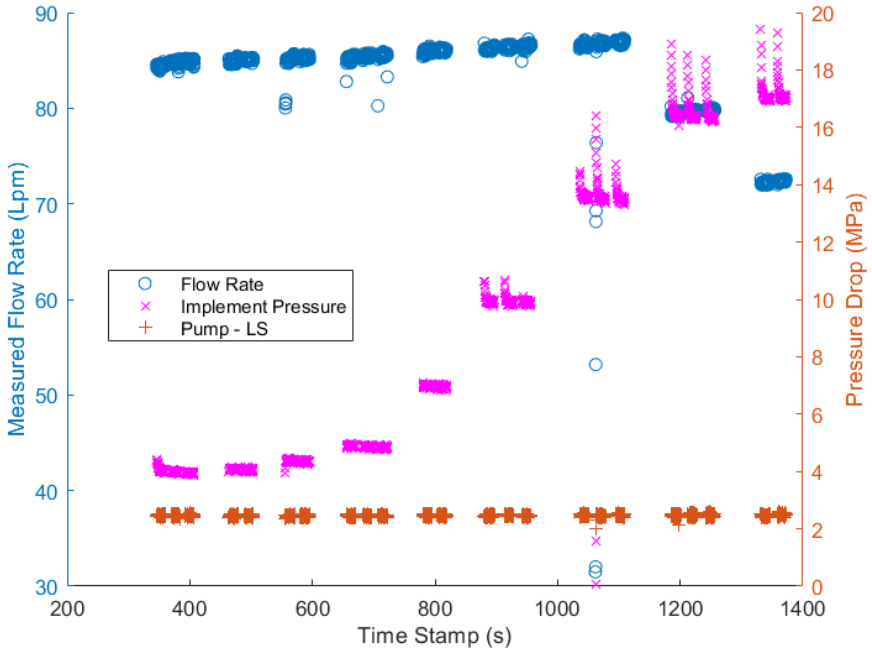

Figure 3.8: *Flow rate, implement pressure, and pressure difference between pump and load sense versus time for a variable implement load test.*

Unlike the engine speed test results, where the pressure difference between the pump and load sense indicated flow-limited conditions, the pressure difference between the pump and load sense pressures maintained the nominal margin pressure value throughout the test despite the reduction in flow rate at high implement pressures. Upon investigation of each individual pressure measurement (figure 3.9), the pump fluid pressure reached a maximum magnitude (~20.25 MPa) over the last two trials, where flow rate was reduced. Additionally, the load sense magnitude did not change between the last two tested implement loads despite the implement pressure requirement increasing in the last test. Thus, the load sense did not accurately represent the highest circuit pressure requirement when the pump was at its maximum pressure magnitude.

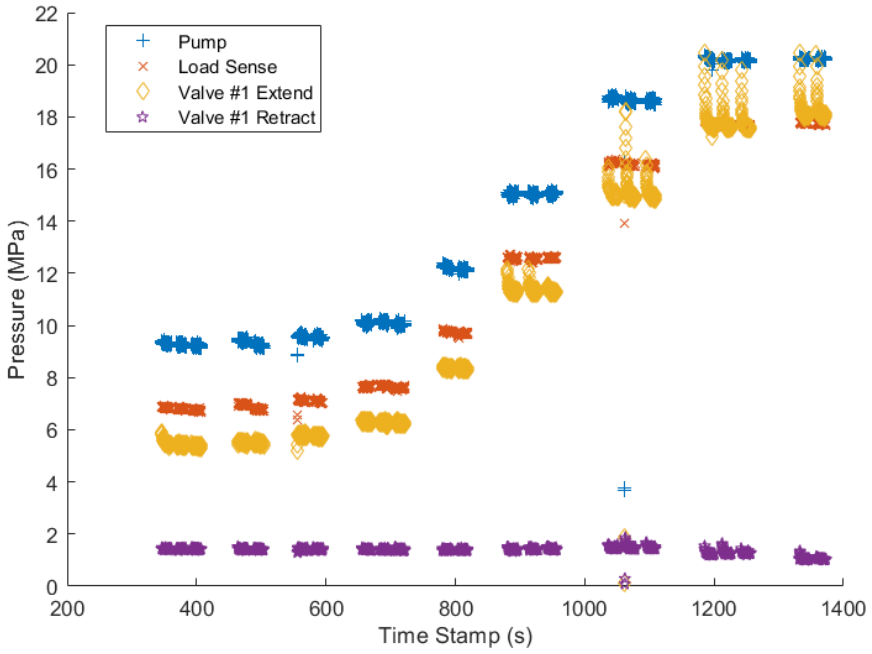

Figure 3.9: *Pressure measurements for conducted implement load test*

Characteristics of the pressures measured in this test indicated that the load sense system of the selected tractor contained a signal relief valve. According to Dell (2017), load sense signal relief valves are commonly used in systems with post-spool compensated valves. At implement circuit pressure requirements higher than the signal relief valve setting, the effective system load sense pressure sent to the pump was the relief valve setting (~17.75 MPa). While it is possible the pump was destroked by the pressure compensator upon reaching the maximum pressure setting (20.5 MPa), the addition of the signal relief valve to the load sense system allows the flow compensator to also destroke the pump. As previously discussed, the flow compensator reduces pump displacement when pump pressure exceeds the sum of the load sense signal and margin pressure. Given the load sense signal becomes the constant relief valve pressure setting when the implement circuit pressure exceeds this value, the pump would destroke to maintain a constant pump pressure equal to the sum of margin pressure and the relief

valve setting. This aligns with results obtained in this test where the difference between pump and load sense did not change even in flow-limited conditions. Thus, with this design, the pump pressure compensator could simply serve as a failsafe in the event issues arose with the flow compensator.

From this test, it was determined that when the pump was at its maximum system pressure setting, potential existed for at least one valve to be flow-limited. Rather than detecting flow-limited circumstances using the pressure difference between pump and load sense, instead detection must be made by monitoring the pump pressure magnitude.

3.4.3. Effect of Multiple Actuated Control Valves on Flow Rate Delivery

3.4.3.1. Flow Rate Distribution: Different Valve Load Sense Requirements

Table 3.4 breaks down mean flow rate and pressure measurements of different spool position combinations for a multiple valve test conducted with different load settings between two control valves. As shown in the table, valve 1, the valve with the lower load setting, was held at a constant spool position while adjustments in spool position were made to valve 2, the valve with the higher load setting. A relatively constant flow rate in valve 1 was maintained independent of valve 2's spool position, while the flow rate in valve 2 was relatively constant at spool positions 60% and greater. When flow rate was constant in valve 2, the difference in pressure measurement between pump and load sense dropped below the margin pressure setting. Thus, flow rate was limited in the circuit with a higher pressure requirement, while the circuit with a lower pressure requirement still was flow-sufficient. This flow distribution characterized valves featuring pre-spool compensation. Therefore, valve spool position still closely related to flow rate for valves

with lower pressure requirements than the system load sense even when the pump became flow-limited.

Table 3.4: Multiple Valve Test: Different Valve Load Requirements Mean Results

Estimated Flow Rate #1 (%)	Estimated Flow Rate #2 (%)	Flow Rate #1 (Lpm)	Flow Rate #2 (Lpm)	Valve #1 Pressure (MPa)	Valve #2 Pressure (MPa)	Pump - Load Sense (MPa)
60	10	67.08	0.77	3.775	0.246	2.596
60	20	67.11	17.56	3.800	0.646	2.576
60	30	67.05	29.25	3.842	1.260	2.552
60	40	66.77	43.05	3.862	2.828	2.512
60	50	67.66	55.94	4.036	4.897	2.446
60	60	67.08	57.84	3.977	5.236	1.602
60	70	66.89	58.08	3.949	5.283	1.416
60	80	66.75	58.22	3.926	5.306	1.316
60	90	66.61	58.34	3.918	5.330	1.248
60	100	66.52	58.48	3.913	5.352	1.206

3.4.3.2. Flow Rate Distribution: Similar Valve Circuit Pressure Requirements

Table 3.5 details mean flow rates, pressure requirements, and resulting differences between pump and load sense pressures for a multiple valve test with similar implement load settings in both valves. Results indicated the pump became flow-limited as valve 2 reached a spool position corresponding to an estimated flow rate message of 60%. Both valves had similar circuit pressure requirements with spool positions corresponding to 60% estimated flow. When the pump became flow-limited, both valve 1 and valve 2 achieved a lower flow rate than requested. Thus, the estimated flow rate message did not properly represent flow rate in either valve under flow-limited conditions.

Table 3.5: Multiple Valve Test: Similar Valve Load Requirements Mean Results

Estimated Flow Rate #1 (%)	Estimated Flow Rate #2 (%)	Flow Rate #1 (Lpm)	Flow Rate #2 (Lpm)	Valve #1 Pressure (MPa)	Valve #2 Pressure (MPa)	Pump Pressure (MPa)	Pump - Load Sense (MPa)
60	10	66.741	0.970	4.122	0.284	7.483	2.605
60	20	66.846	17.255	4.138	0.533	7.468	2.576
60	30	66.955	28.725	4.144	1.014	7.454	2.550
60	40	66.730	42.303	4.151	1.864	7.407	2.512
60	50	66.310	55.878	4.164	3.038	7.369	2.470
60	60	61.853	62.652	3.683	3.712	6.193	1.692
60	70	60.909	63.352	3.572	3.766	6.022	1.593
60	80	60.434	63.729	3.509	3.800	5.936	1.406
60	90	60.140	63.994	3.472	3.829	5.879	1.316
60	100	59.881	64.247	3.450	3.855	5.840	1.251

Minor changes in flow rate continued to occur in both valves as spool position changed in valve 2 under flow-limited circumstances (contrary to the multiple valves test with different load settings). When multiple valves are simultaneously actuated, the total pressure requirement of each circuit must be the same in order for both valves to receive flow. When different implement circuit pressure requirements exist, in flow-sufficient conditions, the pre-spool compensator in the lower load sense valve introduces additional resistance to its circuit to prevent excessive flow rates from occurring. However, the pre-spool compensator would not intervene when a valve did not receive its full requested flow. Therefore, changes in resistance to one circuit must result in resistance changes to the other to maintain equilibrium allowing both valves to receive flow.

When increasing the spool position in valve 2, the resistance to pass fluid through the valve decreased. With reduced resistance, the flow rate in valve 2 increased. However, to achieve the higher flow rate, the pressure requirement increased through the valve 2

circuit. With limited total flow rate available, flow rate decreased in valve 1. Decreased flow rate decreased the pressure required to achieve the new flow rate through the valve 1 circuit. Thus, the change in flow rate worked to continuously balance the pressure requirements in both valves. This explains why flow rate continued to change in both valves when changing spool position in valve 2 after the pump became flow-limited.

When both valves were flow-limited, a potential incorrect assumption that could be drawn is that the load sense in both valves were the same. However, with flow rate continuing to change in both valves and flow rate directly impacting the pressure requirement of both circuits, the load sense of each valve changed as spool position in valve 2 continued to increase. Thus, the load sense pressure measurement only represented the higher load sense valve, although both valves had similar load sense requirements. If load sense pressure were used as a method to predict flow rate in flow-limited valves, this could negatively affect estimates. However, differences in load sense between flow-limited valves did not affect pump displacement as the pump was already at maximum displacement.

Unlike the simulated implement circuit tested, most implement circuits likely have relatively constant pressure requirements independent of flow rate to move a cylinder or motor. However, pressure requirements of a circuit will change slightly by flow rate due to any minor losses that exist in an implement circuit. Implement manufacturers may attempt to reduce power inefficiencies for multiple valves actuated simultaneously by sizing their cylinders and motors to have similar fluid pressure requirements. Thus, the possibility of implements having similar load requirements is quite realistic. Therefore, the possibility of having multiple valves simultaneously flow-limited exists. Similarities

between the system load sense pressure and the pressure measured in each circuit can be used to identify both valves as flow-limited.

3.4.3.3. Flow Rate Distribution: High Flow Rate Request versus Flow Capability

For the multiple valve test involving actuation of three valves, the two valves that connected to the test stand had the same similar load settings as the multiple valve test discussed in section 3.4.3.2. The only difference between these tests was the continuous actuation of the third valve not connected to any circuit. Thus, comparisons between the two tests could be made.

Mean recorded flow rate and pressure measurements for the connected valves during the test are shown in table 3.5. Comparing test results provided in tables 3.4 and 3.5, both connected valves received their requested flow rate until valve 2 reached a spool position corresponding to an estimated flow message of 60%. The greatest difference in mean flow rate for valve 1 between tests was 2.91 Lpm, when valve 2 had an estimated flow rate of 20%. In comparison, the greatest difference in flow rate for valve 2 between tests was 1.06 Lpm, which occurred when valve 2 had an estimated flow rate of 50%.

Table 3.6: Multiple Valve Test: Three Valves (Two Connected) Results

Estimated Flow Rate #1 (%)	Estimated Flow Rate #2 (%)	Flow Rate #1 (Lpm)	Flow Rate #2 (Lpm)	Valve #1 Pressure (MPa)	Valve #2 Pressure (MPa)	Pump Pressure (MPa)	Pump - Load Sense (MPa)
60	10	63.83	0.84	3.510	0.238	17.323	2.579
60	20	63.91	17.73	3.503	0.496	20.332	2.516
60	30	64.59	29.28	3.593	0.956	20.330	2.507
60	40	64.65	41.55	3.694	1.689	20.256	2.492
60	50	65.09	54.82	3.862	2.773	17.727	2.128
60	60	62.00	63.08	3.630	3.639	6.152	0.770
60	70	60.91	63.92	3.524	3.708	5.934	0.756
60	80	60.42	64.34	3.478	3.756	5.868	0.756
60	90	60.11	64.60	3.442	3.782	5.808	0.748
60	100	59.88	64.83	3.424	3.809	5.782	0.752

As seen in table 3.5, pump pressure was near maximum system pressure when the desired flow rate in both connected valves was attained. However, when the connected valves became flow-limited, pump pressure dropped to similar magnitudes seen in the test with only the two connected valves actuated. Because of the pre-spool compensation flow distribution used in this system, where a valve with a lower circuit pressure requirement receives requested flow before a valve with a higher requirement, the unconnected valve did not receive any flow from the pump unless the two connected valves were satisfied. When no flow was available for the unconnected valve, the pump pressure dropped.

As for the difference between pump and load sense pressures, the margin pressure difference between the two variables was maintained when the two connected valves received their requested flow rate. As proven in the variable pressure requirement test discussed in 3.4.2, due to a signal relief valve incorporated into the load sense signal, the

margin pressure difference between pump and load sense exists when the pump is at the maximum system pressure despite the unconnected valve not achieving its desired flow rate. However, observing the high pump pressure indicated the estimated flow rate message in the unconnected valve would inaccurately predict flow rate. Simultaneously, comparisons of circuit pressure requirements in the connected valves to the pump pressure indicated that flow rate still correlated to valve spool position in the connected valves. Once the connected valves were flow-limited, the lack of correlation between valve spool position and flow rate could be identified by the pressure difference between pump and load sense being less than margin pressure and circuit pressure requirements that closely resembled the load sense.

3.4.4. Effect of Fluid Temperature on Flow Rate

A fluid temperature test was conducted at a valve spool position correlating to an estimated flow rate message of 84%. Results for the mean flow rate and pressure difference between pump and load sense measurements for different oil temperatures are shown in table 3.7. Additionally, a graphical representation of the relationship observed between fluid temperature and flow rate is provided (figure 3.10). A temperature increase of 40°C was seen throughout testing. At the coldest oil temperature tested (27°C), the mean flow rate was 3.97 Lpm, or 3.98%, lower in magnitude than the flow rate measured at the observed steady-state oil temperature (67°C). Despite changes in flow rate for a given valve position, the pressure difference between pump and load sense was essentially unchanged at different temperatures.

Table 3.7: Relevant Variable Fluid Temperature Test Data

Valve Spool Position (%)	Oil Temperature (°C)	Mean Flow Rate (Lpm)	Difference vs. Flow Rate at 67°C (%)	Pump - LS Pressure (MPa)
84	27	95.72	-3.98	2.515
84	30	96.41	-3.29	2.510
84	35	97.07	-2.64	2.534
84	40	97.40	-2.30	2.546
84	45	97.91	-1.79	2.542
84	50	98.29	-1.41	2.525
84	55	98.76	-0.94	2.537
84	60	99.39	-0.30	2.527
84	65	99.61	-0.09	2.538
84	67	99.69	0.00	2.540

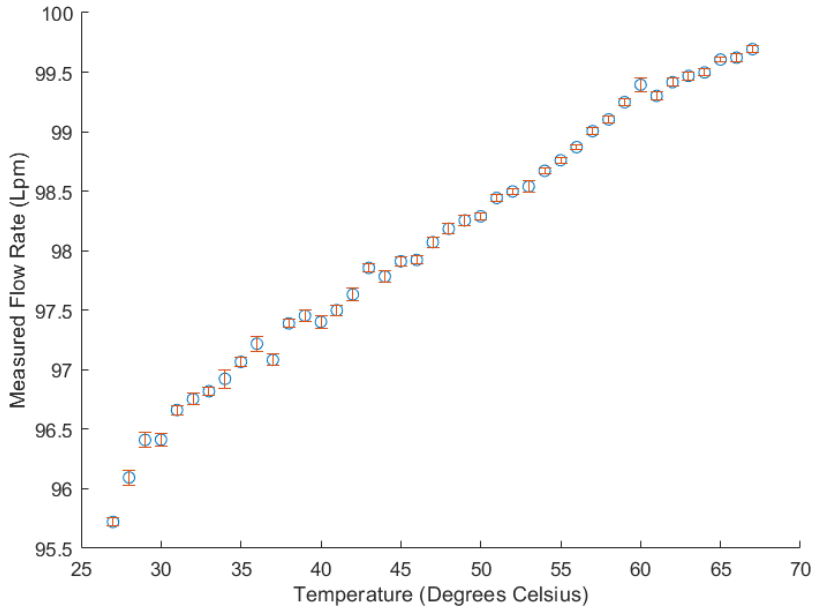

Figure 3.10: *Flow rate versus oil temperature for an 84% estimated flow rate spool position.*

Despite all of the fluid power produced being converted to heat and a high flow rate maintained, it took just under 15 minutes to achieve a stable fluid temperature in this test. While the expectation is that most agricultural machinery field data would occur at a stable fluid temperature, flow rates will differ within a given flow-sufficient spool position across different fluid temperatures.

3.5. Conclusions

Because hydraulic control valve flow rate is not interpretable on existing agricultural machinery CAN systems, the accuracy of predicting flow rate using valve spool position, which was available in a standard encoded CAN message, was investigated. It was determined from this study that while valve spool position closely related to flow rate in flow-sufficient conditions, the two quantities were unrelated in at least one valve when the fluid power system became flow-limited. Any combination of low engine speeds, multiple valves actuated simultaneously, or high implement pressure requirements presented opportunities where flow-limited conditions occurred.

Additionally, no hydraulic fluid pressure measurements were published in a standard format on the CAN bus of the selected tractors. Thus, hydraulic power requirements cannot be determined using existing machine CAN data alone. With the addition of pressure sensors needed to determine implement hydraulic power consumption, data from these sensors could additionally be used to determine when valve spool position would accurately predict flow rate. Using the test results from this study, figure 3.11 summarizes how to use pressure measurements to determine if valve spool position can predict flow rate.

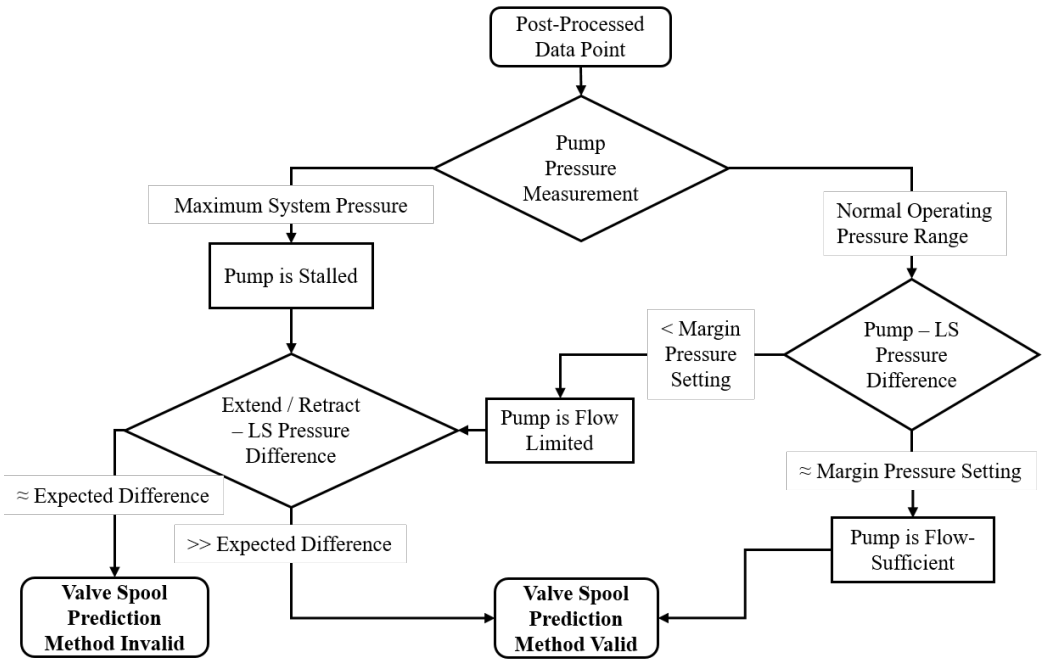

Figure 3.11: *Flowchart detailing how to determine if valve spool position could be used to predict flow rate for a given data point using pump, load sense, and implement pressure.*

For implement operations where the pump was neither in a flow-limited condition nor at its maximum pressure during usage, flow rate for a valve position was relatively constant. However, minor changes in flow rate were observed based on changes in hydraulic oil temperature. Thus, for a more accurate flow rate prediction using valve spool position, compensation for fluid temperature should be considered.

An additional method must be utilized to predict hydraulic flow rate for instances when valve spool position will not accurately represent flow rate. Due to the difficulty in installing turbine flowmeters between the tractor and implement, given the relationship between flow rate and pressure drop across a minor loss, potential for using a measured pressure drop across a minor loss to predict flow rate is worthy of examination. Further work related to flow rate prediction using this method is discussed in Chapter 4.

Chapter 4: Investigation of Utilizing CAN Messages and Minimal Added Sensors to Predict Agricultural Implement Hydraulic Power Requirements

4.1. Introduction

A growing power source demand required by agricultural implements is hydraulics. Fluid power, initially added to agricultural machinery to raise implements at the end of a field pass, now is utilized for numerous functions (eg. fans, augers, implement folding, planter unit downforce, tractor primary functions) through cylinders and motors (Stoss et al., 2013).

Modern tractors commonly feature a load sensing pressure compensated (LSPC) pump to allow hydraulic control valves to command pump flow rate and reduce power losses when an implement is not requesting hydraulic power. However, despite improved efficiency in utilizing these pumps over other designs, Love (2012) estimated that fluid power system usage on mobile equipment applications in the US possessed a power efficiency of just 21.1%. While power losses stemmed from several hydraulic system components, 43% of losses were attributed to valves and 25% to power usage in charge pumps and cooling systems (Love, 2012). With room for improvement in mobile equipment fluid power systems, there is value in understanding agricultural implement hydraulic power requirements and the efficiency in providing this power to them by various tractor designs.

Because implement power requirements are a function of each individual circuit's fluid pressure requirement and flow rate, both variables of each circuit must be measured

to accurately determine this quantity. Despite usage of CAN data becoming a more effective way to measure agricultural machinery performance characteristics, direct flow rate and pressure measurements are not typically published in a standard format on modern tractors. While the addition of sensors would allow for these quantities to be directly measured, turbine flowmeters present potential issues due to high costs and long upstream and downstream uninterrupted flow length requirements (Badger Meter, 2018). Despite Roeber et al. (2016) concluding turbine flowmeter measurement accuracy to be acceptable for any hose bend angle, the ability to avoid using these flowmeters is desired given limited space between the tractor and implement.

As an alternative to turbine flowmeters, numerous industries utilize differential pressure flowmeters to estimate fluid flow rate. These differential pressure devices include venturis, standard orifice plates, v-cones, and wedge flowmeters (Hollingshead, 2011). Each differential pressure flowmeter relies on measured changes in pressure energy to predict flow rate. For example, the standard orifice equation (eq. 6) can be used with an orifice to quantify flow rate as a function of the pressure drop, fluid density, passageway area, and discharge coefficient.

$$Q = C_d A \sqrt{\frac{2\Delta p}{\rho}} \qquad \text{(Eq. 6)}$$

where
Q = flow rate
C_d = discharge coefficient
A = orifice area
Δp = pressure drop across orifice
ρ = fluid density

Manring (2005) derived a model from the standard orifice equation to predict control valve flow rate as a function of the valve's spool position and pressure drop across the spool. Load sensing circuits attempt to maintain a constant pressure drop across the control valve main spool to enable spool position to dictate flow rate. Thus, a standard CAN message found on modern tractors related to valve spool position, referred to as the estimated flow message in the ISO 11783 standard, can be beneficial in predicting flow rate.

Numerous past studies have worked to quantify the relationship between the discharge coefficient magnitude used in the standard orifice equation and the fluid's Reynold's number for a given orifice. As fluid viscosity is inversely related to Reynold's number, and a fluid's temperature is inversely related to its viscosity, increased fluid temperature subsequently increases Reynold's number. As Reynold's number increases under laminar flow conditions, the resulting discharge coefficient decreases. This results in a decreased pressure drop across minor losses for a given flow rate as temperature increases. In fluid power systems, inefficiencies result in a proportion of produced power converted into thermal energy. Despite the tractor's cooling system working to reduce heat effects, hydraulic oil temperature will substantially increase during an operation until a minimum steady-state temperature can be maintained. Thus, regardless of whether valve spool position or a determined pressure drop is utilized to predict flow rate, careful consideration must be given to changes in the effective discharge coefficient due to changes in fluid temperature.

4.2. Objectives

The goal of this study was to develop an effective method to determine implement circuit flow rates during field operations without a turbine flowmeter. Specific objectives to accomplish this goal included 1) developing a compact minor loss device to predict flow rate using the standard orifice equation, 2) forming a flow rate prediction method using an input of valve spool position, and 3) assessing an effective method to compensate both flow rate prediction methods for temperature effects. The accuracy of the developed method was to be determined through comparing predicted versus measured flow rates for sample test data simulating different conditions expected for various implements.

4.3. Materials and Methods

4.3.1. Equipment / Materials Used

Two modern tractors of the same model number (6145R, Deere & Company, Moline, Ill.) were selected for use in this study. Hydraulic-related variables logged from existing machine CAN messages available on both tractors included engine speed, hydraulic fluid temperature, and estimated flow rate percentage based on valve spool position.

A testing apparatus was developed to simulate connected implement circuits and measure fluid flow rate. The apparatus (figure 4.1) featured two duplicate circuits containing a turbine flowmeter (Flo-tech Activa F6206-AVB-NN, Badger Meter, Milwaukee, Wisc.) that served as the baseline flow rate measurement and an adjustable flow control valve, or needle valve, to allow adjustment to the circuit pressure requirement. An analog pressure gauge was also incorporated into the circuit to provide the operator with an estimated circuit fluid pressure during testing.

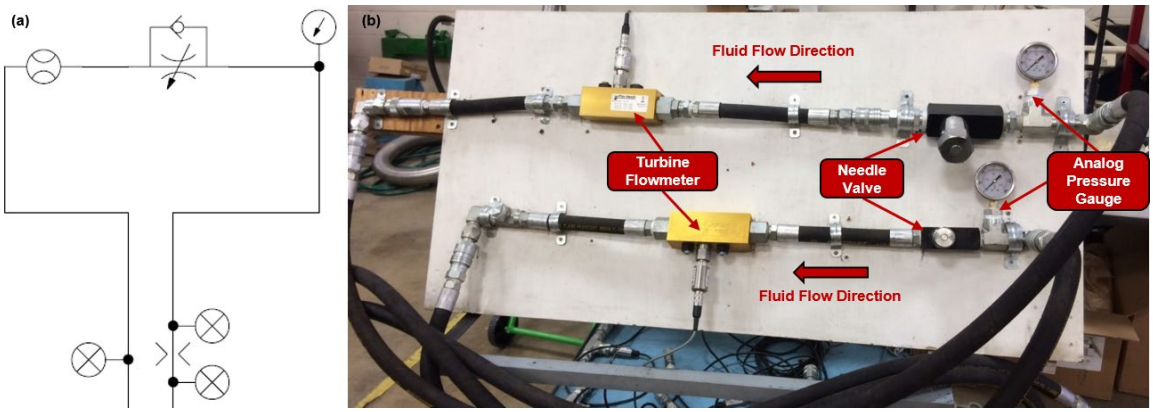

Figure 4.1: *(a) Schematic of the (b) hydraulic testing apparatus used throughout the study.*

All pressure measurements were conducted using a common electronic pressure transducer (Omega PX309, Omega Engineering Inc., Norwalk, Conn.). Pressure was measured on the extend and retract ports of each control valve and the pump and load sense diagnostic ports available on the tractor (figure 4.2). To measure control valve pressures, sensors were added to tee fittings with ISO quick couplers to allow location between the tractor control valves and implement.

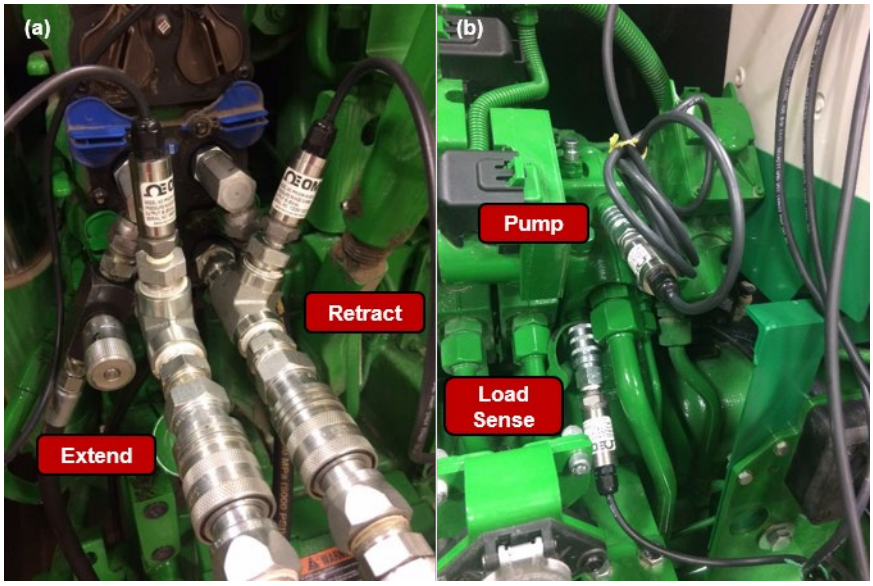

Figure 4.2: *Common pressure sensor locations include (a) on the extend and retract port immediately beyond each valve and (b) on diagnostic ports of the pump and load sense.*

4.3.2. Data Collection Method

To synchronize data collection, sensor data were published as CAN messages to the tractor's implement bus (ISOBUS). This allowed for all data to be logged with a CAN data logger. An electronic controller unit (ECU) (Danfoss MC024-110, Danfoss North America, Ames, Iowa) was programmed through a graphically programmable proprietary software (Danfoss PLUS+1 GUIDE, Danfoss North America) to convert analog sensor outputs into CAN messages. A customized electronics enclosure (figure 4.3), named the Sensor CAN Gateway (SCANGate), housed the ECU and connected it to the tractor CAN system using an implement-end ISOBUS breakaway connector (IBBC). Furthermore, the SCANGate supplied power to the sensors and connected their output readings to the ECU. For this study, three additional messages containing all added sensor data were broadcast at a frequency of 4 Hz.

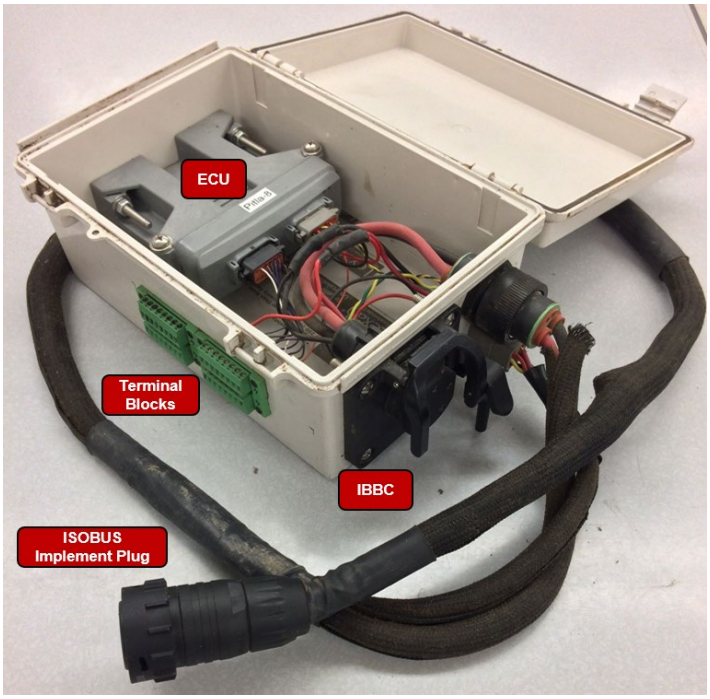

Figure 4.3: *Picture of the developed SCANGate design with hardware components labelled.*

The tractor's in-cab CAN diagnostic port was accessed to enable a standalone data-logger (Pro 2xHS v2, Kvaser AB, Mölndal, Sweden) to log CAN data to an SD card. Various filters were utilized by the data logger so that only desired messages were recorded. Given the log files were produced in a raw hexadecimal format, a MATLAB program was created to post-process test data. Steps in the data post-processing included sorting different messages by their parameter group number (PGN), converting raw data bytes into engineering units based upon the ISO 11783 standard, and resampling calculated engineering values to common time intervals.

4.3.3. Minor Pressure Drop Selection

While selecting an existing minor loss to predict flow rate in flow-limited circumstances was preferred to prevent creation of another system loss, other criteria contended with available options. No alterations to existing tractor components were preferred, limiting pressure measurement locations to diagnostic ports and between the control valve stack and implement. Thus, the only measurable existing minor losses were across the control valve's main spool using the pump and load sense diagnostic ports and the quick coupler connection in the valve stack using the load sense and control valve pressure sensors. Issues with either method exist when the system load sense would not accurately represent a flow-limited valve's load sense. As highlighted in chapter 3, this can occur in high pressure requirement scenarios or when multiple valves are flow-limited due to similar pressure requirements.

Due to potential for the system load sense to be unable to represent a flow-limited valve, only added minor losses were considered. As highlighted by Lipták and Venczel (1982), due to the anticipated quadratic relationship between flow rate and pressure drop,

the added loss needed to produce a pressure drop of sufficient magnitude to distinguish low flow rates. While a larger added loss would enable measurement of low flow rates with greater accuracy, the added loss needed to remain small enough to prevent a substantial system loss limiting implements from performing their necessary functions.

Three potential added minor losses were explored: 1) an additional ISO coupler pair using two pressure tee fittings (figure 4.4a), 2) an assembly of common fittings that reduce the passageway area from 19.05 mm (0.75”) to 9.53 mm (0.375”) (figure 4.4c), and 3) a customized orifice fitting which reduced the flow passageway to a 7.94 mm (0.313”) diameter circular opening in either flow direction (effective beta ratio of 0.417) (figure 4.4d). Each of these configurations required significantly less space than a turbine flowmeter and did not require any additional support structure to secure the sensors for harsh field conditions. A variable spool position test (discussed in greater detail in section 4.3.4.1) was used to determine which minor loss offered the best orifice flowmeter solution. The selected orifice flowmeter was to be replicated to allow indirect flow rate measurement on multiple valves simultaneously.

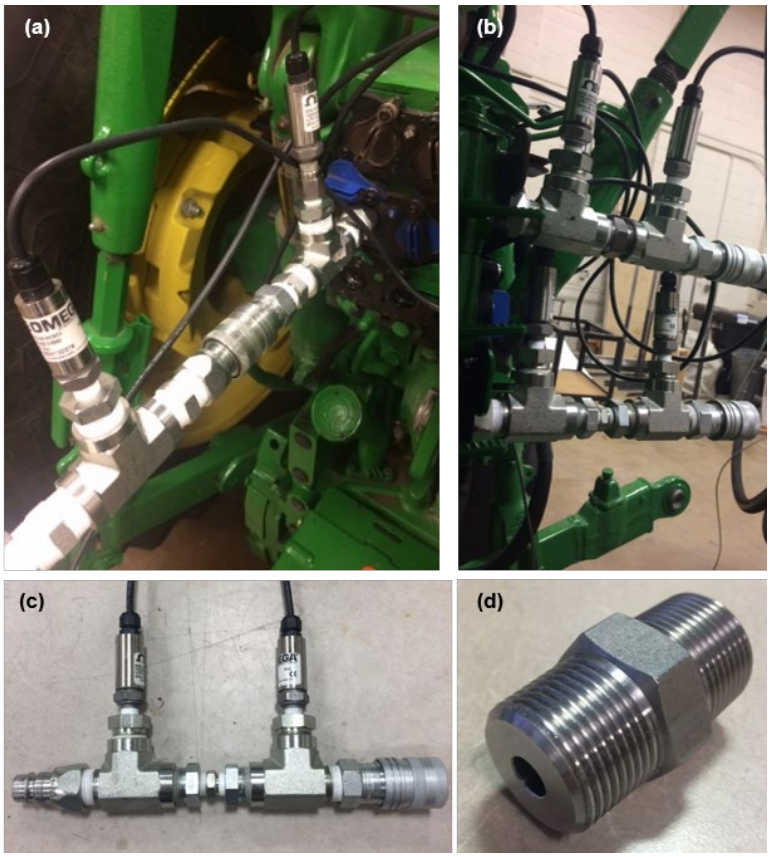

Figure 4.4: *Different proposed minor loss additions included a) an additional ISO Coupler pair using two pressure tee fittings or b) an individual assembly featuring a reduction in port size using c) standard fittings or d) a custom machined fitting.*

4.3.4. Conducted Flow Rate Relationship Tests

4.3.4.1. Variable Spool Position Test

A test was developed to simultaneously define the flow rate produced for different valve spool positions and the corresponding pressure drop experienced across an orifice flowmeter for that flow rate. Hydraulic oil was preheated to a temperature that the tractor cooling system could maintain to minimize changes in fluid viscosity throughout the test. Engine speed was kept at a non-flow-limiting magnitude and the needle valve on the tested circuit was fixed to a larger opening to prevent high-pressure conditions from occurring such that valve spool position would not accurately represent flow rate.

The control valves on both tractors featured the ability to maintain any input spool position setting over a desired time length using the valve's detent control. Both the spool position setting and detent time length were controlled from the tractor virtual terminal (figure 4.5). Two valve actuation methods were utilized. One method was to place the control valve into detent for 15 seconds for each tested spool position to obtain enough data to determine the expected flow-sufficient flow rate for that position. The other method was to place the control valve into continuous detent, and adjust the spool position every 10-20 seconds while the valve was in detent. For either method, 10-20 spool positions were tested to define trends between the magnitudes of flow rate and the CAN-reported estimated flow rate percentage.

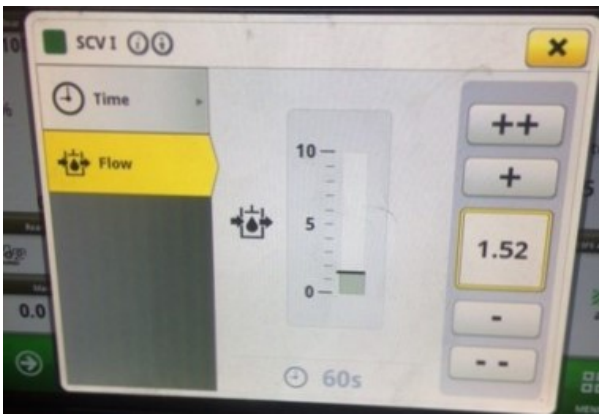

Figure 4.5: *Screen displayed by the tractor virtual terminal detailing the flow and time settings for detent control on SCV 1 of the tractor under test.*

In post-processing, the mean flow rate and pressure drop among steady-state data for each tested valve spool position were calculated. Using these mean values, the relationship between flow rate and reported valve spool position as well as flow rate and orifice flowmeter pressure drop could be assessed. If a quantifiable relationship existed between the two variables, a best-fit equation was found using MATLAB's Curve Fitting Toolbox.

To accurately predict flow rate for valves actuated in either flow direction, tests were conducted for each valve and orifice flowmeter in both flow directions. While the valve flow directions could be defined by the "extend" and "retract" nomenclature, the orifice flowmeter flow directions were defined by the nomenclature, "implement" and "tractor," which represented which direction flow was moving towards. This was due to the potential for the orifice flowmeter to be located on either valve port side. The ability to distinguish the difference between directions was feasible when post-processing test data due to the estimated flow rate message being positive when the valve was actuated in the extend direction and negative when actuated in the retract direction. Comparisons were made between different valves, replicated orifice flowmeters, and flow directions to determine whether differing relationships existed between flow rate and the associated input variable for different valves and orifice flowmeters.

4.3.4.2. Oil Temperature Analysis Tests

As the relationship between flow rate and corresponding pressure drop across a loss varies with fluid temperature, a test was conducted to analyze fluid temperature effects on the flow rate-valve spool position and flow rate-orifice flowmeter pressure drop relationships observed in the variable spool position tests. A standard CAN message for hydraulic fluid temperature broadcasted on the tractor under test was used to measure temperature. Precision in the reported message was to the nearest degree Celsius.

Each test began with the fluid temperature equivalent to the ambient laboratory temperature (23-28°C). Engine speed and circuit pressure requirements were set to levels that would not hinder the pump's ability to produce a requested flow rate. The selected valve was placed into continuous detent and a single valve spool position was maintained

throughout the test duration. Hydraulic oil temperature was monitored on the tractor's virtual terminal to determine when a stable temperature was achieved. Once this temperature was achieved, the test run for that spool position was complete.

In post-processing the test data, the mean flow rate and pressure drop across the orifice flowmeter was found for each degree Celsius observed in fluid temperature. This allowed for the evaluation of the relationship between flow rate and temperature for a given valve spool position as well as flow rate and pressure drop for varying temperatures.

To test whether flow rate-temperature relationships varied for different flow rate magnitudes and spool position settings, oil temperature analysis tests were conducted at spool positions with estimated flow rate CAN messages of 44%, 54%, 64%, 74%, and 84%. To make comparisons between the different tests, the proportion of observed flow rate to the anticipated flow rate at preheated fluid temperatures was used.

4.3.5. Flow Rate Prediction Function Methodology and Validation

Using determined flow rate prediction methods with inputs of valve spool position and pressure drop, a MATLAB function was developed to predict flow rate for given test data. Due to potential for conditions where valve spool position cannot accurately predict flow rate, the function utilized a decision matrix (figure 4.6) based upon pressure measurements at the pump and load sense diagnostic ports and between the control valve and simulated implement circuit to determine whether valve spool position or the orifice flowmeter should be used to predict flow rate for a given valve.

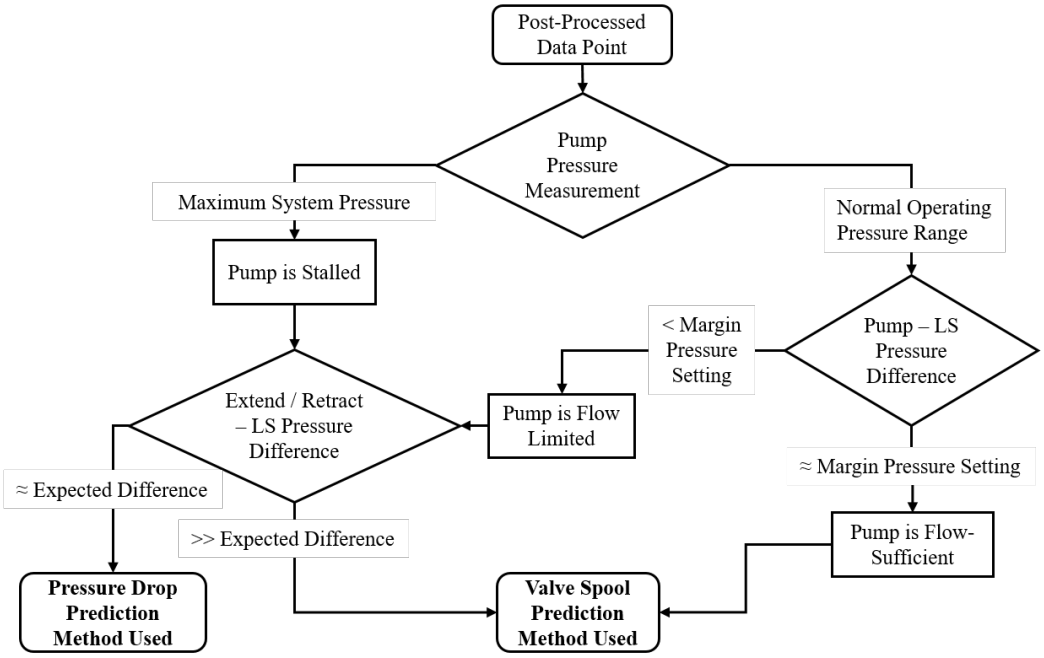

Figure 4.6: *Flowchart detailing the methods used to determine when valve spool position could be used to predict flow rate for a given data point.*

Several test datasets were processed through the developed MATLAB function to assess the accuracy of the developed methods in predicting flow rate. Several scenarios within these tests existed, including consistent steady-state flow rate at both flow-limited and flow-sufficient conditions, changes in fluid temperature, high pump pressure , actuation of multiple valves simultaneously, and transient conditions created by varying engine speed or valve spool position frequently.

After predicting flow rate for a given test dataset, another MATLAB function was developed to determine the accuracy of the flow rate prediction. By comparing the differences in predicted versus measured flow rate for each data point, a mean absolute error (MAE), mean absolute percentage error (MAPE), and root mean squared error (RMSE) were determined for a given dataset. Additionally, for tests where predominately steady-state conditions occurred, another function was used to organize the test data by

the different levels of a factor tested. This allowed for the previously mentioned statistics and mean error to be computed for each level tested.

4.4. Results and Discussion

4.4.1. Pressure Drop Prediction Method

4.4.1.1. Determination of Selected Pressure Drop

Results from a variable spool position test comparing proposed orifice flowmeters are provided graphically in figure 4.7. It was seen that the standard fittings orifice resulted in the lowest pressure drop for a given flow rate. Meanwhile, the ISO coupler pair created the largest added system loss. As anticipated, a quadratic relationship existed between flow rate and pressure drop for each added minor loss.

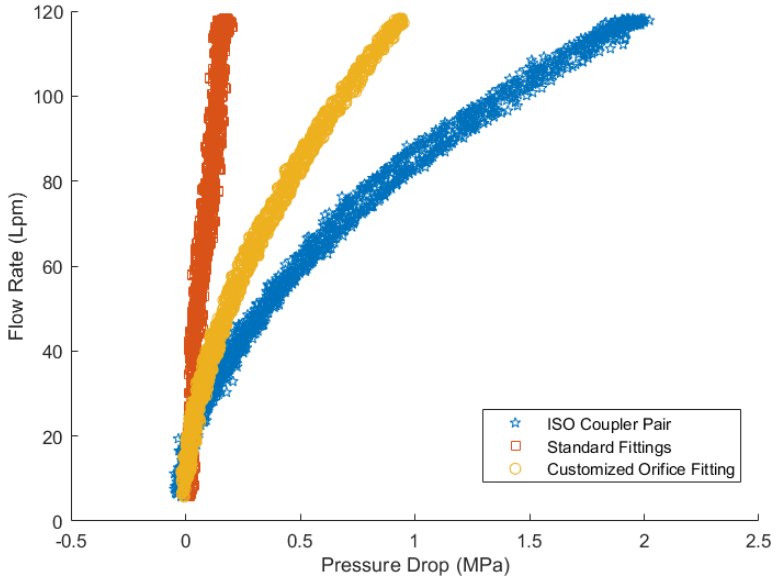

Figure 4.7: *Flow Rate – Pressure Drop Relationship for three proposed added pressure drops.*

To decipher the necessary pressure measurement precision needed to distinguish lower flower rates for each proposed orifice flowmeter, a best-fit curve was found relating flow rate and pressure drop. It was determined that a linear/cubic rational fit provided the best approximation to the observed datasets. While the structure of a power

fit more closely related to the standard orifice equation, because a negative pressure drop was observed across the ISO coupler pair and customized orifice fitting at low flow rates, the rational fit was better able to account for this phenomenon. Table 4.1 details the curve of best fit found for each proposed orifice flowmeter.

Table 4.1: Minor Loss Flow Rate Prediction Comparisons

Added Pressure Drop	Best-Fit Equation[a]	R^2 of Best-Fit Equation	Pressure Drop @ 45 Lpm – Pressure Drop @ 40 Lpm
ISO Coupler Pair	$Q = \frac{1363\Delta p + 112.6}{\Delta p^3 - 4.769\Delta p^2 + 13.89\Delta p + 7.245}$	0.9958	59.8 kPa
Standard Fittings	$Q = \frac{446.0\Delta p + 1.157}{\Delta p^3 + 3.851\Delta p^2 + 0.322\Delta p + 0.516}$	0.9135	6.5 kPa
Customized Orifice Fitting	$Q = \frac{359.5\Delta p + 12.85}{\Delta p^3 - 2.541\Delta p^2 + 3.620\Delta p + 0.986}$	0.9943	30.7 kPa

[a] Q has units of L min^{-1}; Δp has units of MPa.

Using the best-fit equations, the pressure measurement precision needed to distinguish a 40 Lpm versus 45 Lpm flow rate for each proposed orifice flowmeter was determined and provided in Table 4.1. It was determined from these values the required precision to decipher the two flow rates for the standard fittings orifice was 6.5 kPa. Because the precision of the pressure transducers used was 7 kPa, the standard fittings configuration was determined unsuitable. While the ISO coupler (59.8 kPa) provided greater precision in distinguishing the difference between 40 Lpm and 45 Lpm than the customized orifice (30.7 kPa), both methods were determined feasible. Considering lower power loss magnitude, a more condensed package, and reduced potential for fluid leakage at the quick coupler, the customized machined orifice fitting was selected for the duration of the study.

After determining the customized orifice fitting served as the best added pressure drop to use as an orifice flowmeter, further testing was conducted on two devices designed to the same dimensional specifications. These devices are distinguished by the nomenclature "Orifice 281" and "Orifice 295" below.

4.4.1.2. Flow Rate-Pressure Drop Relationship at Preheated Oil Temperature

Figure 4.8 provides a graphical representation comparing the flow rate-to-pressure drop relationship between the two replicated orifice flowmeters in both flow directions (implement and tractor). In the tractor flow direction, for both orifices tested, a negative pressure difference occurred across the device at low flow rates (<25 Lpm). To quantify the relationships between flow rate and pressure drop, a linear/cubic rational fit (eq. 7) was used. As previously mentioned, despite a power best-fit equation more closely aligning to the standard orifice equation, the rational best-fit equation provided a better correlation due to its ability to work with negative pressure drop inputs.

$$Q_{p.ss} = \frac{c_{1n,oq}\Delta p + c_{0n,oq}}{c_{3d,oq}\Delta p^3 + c_{2d,oq}\Delta p^2 + c_{1d,oq}\Delta p + c_{0d,oq}} \quad \text{(Eq. 7)}$$

Where
$Q_{p.ss}$ = predicted flow rate at steady-state temperature
Δp = measured pressure drop
$c_{n,oq}$ = nth power coefficient of orifice "o" in direction "q"

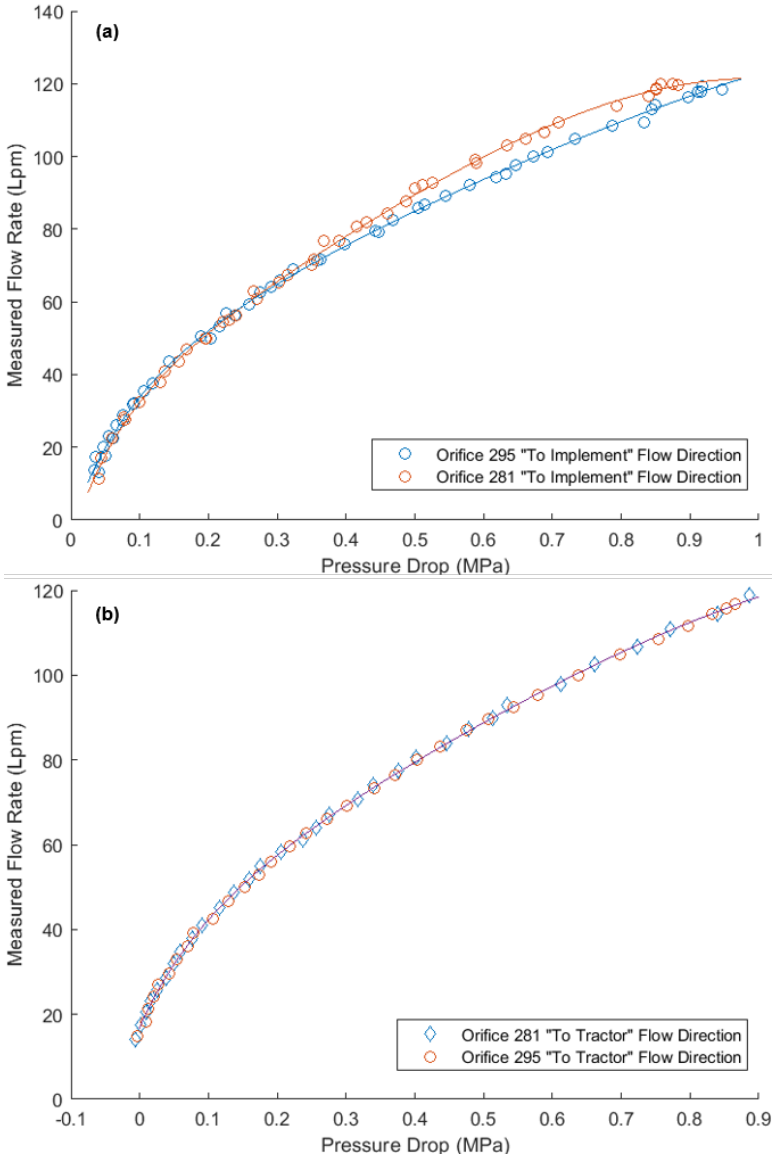

Figure 4.8: *Comparison of flow rate-to-pressure drop relationship between two customized orifice flowmeters in (a) implement flow direction and (b) tractor flow direction.*

To determine whether separate best-fit equations were needed to define the flow rate-pressure drop relationship between the two orifices and each flow direction, the 95% confidence intervals of each best-fit equation coefficient were compared. As detailed in table A.2 in appendix A, no significant differences existed between the confidence intervals of the tractor flow direction coefficients of each orifice. To validate that a

single best-fit curve was suitable for use between the two orifice flowmeters in the tractor flow direction, fit statistics defining how well each orifice dataset related to the determined best-fit curve were analyzed. As provided in Table 4.2, data correlated to the best-fit curve from both orifices had an RMSE around 0.5 L min^{-1} and MAPE less than 1%. This was an acceptable error level, allowing a single equation to be used.

Table 4.2: Orifice Statistics for Tractor Flow Direction Best-Fit Curve

	Orifice 281	Orifice 295
Root Mean Squared Error (RMSE) (Lpm)	0.5574	0.4919
Mean Absolute Error (MAE) (Lpm)	0.4446	0.3748
Mean Absolute Percentage Error (MAPE) (%)	0.9192	0.7951

While no significant differences existed between the two orifice best-fit equation coefficients in the tractor flow direction, the quadratic denominator coefficients between the two orifice equations were significantly different in the implement flow direction (table A.2). As shown in table A.3, various pressure drop magnitudes input into the two implement flow direction best-fit equations resulted in flow rate differences between 5.5% and 6.5% in magnitude. These differences further validated the need to distinguish which orifice flowmeter was used with each valve to reduce flow rate prediction error despite a single best-fit equation needed for the tractor flow direction.

When comparing the best-fit equation coefficients for the two flow directions of each orifice, both orifices had significant differences in various coefficients between the two flow directions. Both orifice 281 and 295 had significant differences in the zero-order numerator coefficient, while orifice 281 also had significant differences in the linear numerator and quadratic denominator coefficients. As detailed in table A.4, lower pressure drop magnitudes corresponding to flow rates under 70 Lpm input into the two

flow direction best-fit equations resulted in flow rate differences of 5% and greater for both orifices. These differences further validated the need to identify which flow direction was occurring when predicting flow rate using an orifice flowmeter in each valve.

From these results, identification of which orifices were used with each valve and which flow direction occurred for each data point were taken into account in the flow rate prediction algorithm to minimize flow rate prediction error when using the added pressure drop. The resulting linear/cubic rational fit equation for each orifice and flow direction is provided in table A.2 in Appendix A.

4.4.1.3. Effect of Fluid Temperature on Flow Rate-Pressure Drop Relationship

Due to the design and execution of the oil temperature tests, because temperature impacted flow rates produced for a given valve spool position on the tractor, the flow rate magnitude, in addition to the pressure drop across the orifice, varied slightly within a given test run. Rather than compare the flow rate to pressure drop ratio across different temperatures observed during the test, instead, the ratio between measured flow rate to predicted flow rate was used. The predicted flow rate was determined by inserting the orifice flowmeter pressure drop into the corresponding preheated oil flow rate-pressure drop best-fit equation found through work discussed in 4.4.1.2. This method allowed for effective comparison between different oil temperature tests conducted at different flow rate magnitudes dictated by spool position setting.

Figure 4.90 provides a graphical representation comparing the measured to predicted flow rate proportion across fluid temperatures for each oil temperature analysis test conducted. Although it was unknown what the flow rate proportion would be at cooler

temperatures, upon reaching the near steady-state preheated fluid temperature, the measured flow rate should theoretically closely match the predicted flow rate as the predicted flow rate was derived from a test conducted at a similar fluid temperature. However, in reality, subtle prediction errors based on the measured pressure drop occurred in some of the test runs, which negatively impacted the actual flow rate proportion relationship with temperature.

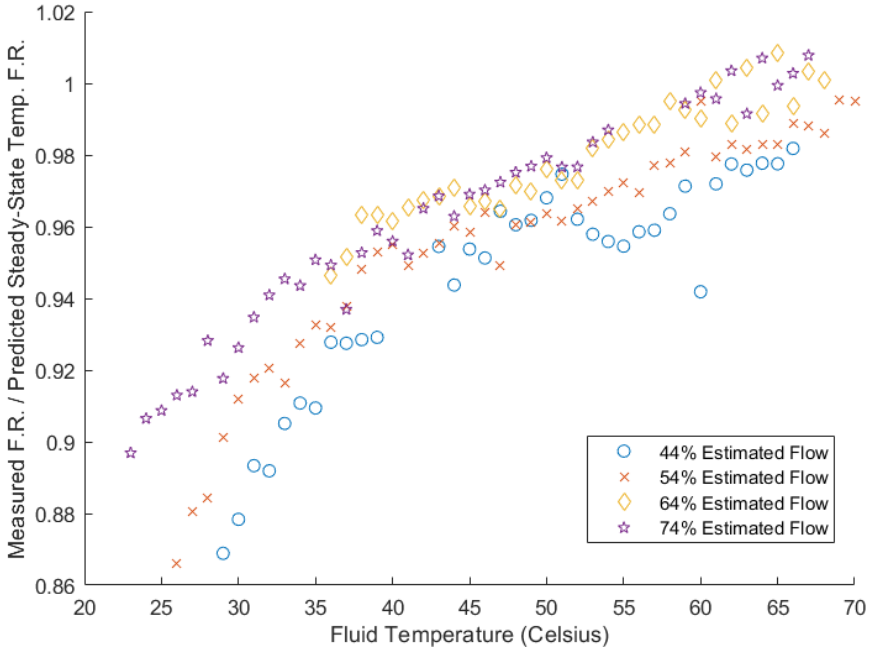

Figure 4.9: *Measured flow rate to predicted flow rate at steady-state temperature for different fluid temperatures.*

To account for errors in flow rate prediction, an adjustment was made to each observed proportion. Shown in equation 8, an offset representing the difference in predicted versus measured flow rate at 66°C was added to each predicted flow rate at different temperatures. This assisted in ensuring a temperature compensation would not adjust a steady-state temperature value that theoretically would accurately be predicted

by the steady-state best-fit equation. Using this method, a closer temperature relationship appeared to exist between the different tests (figure 4.1).

$$p_{me.T.adj} = \frac{Q_{m.T}}{Q_{ss.T} + (Q_{m.66} - Q_{ss.66})} \quad \text{(Eq. 8)}$$

where
$p_{me.T.adj}$ = adjusted measured to expected flow rate proportion
T = temperature (°C) at corresponding data point
$Q_{m.T}$ = measured flow rate (L min^{-1})
$Q_{ss.T}$ = predicted flow rate using preheated best-fit eq. (L min^{-1})
$Q_{m.66}$ = measured flow rate for data at 66°C
$Q_{ss.66}$ = predicted flow rate for data at 66°C

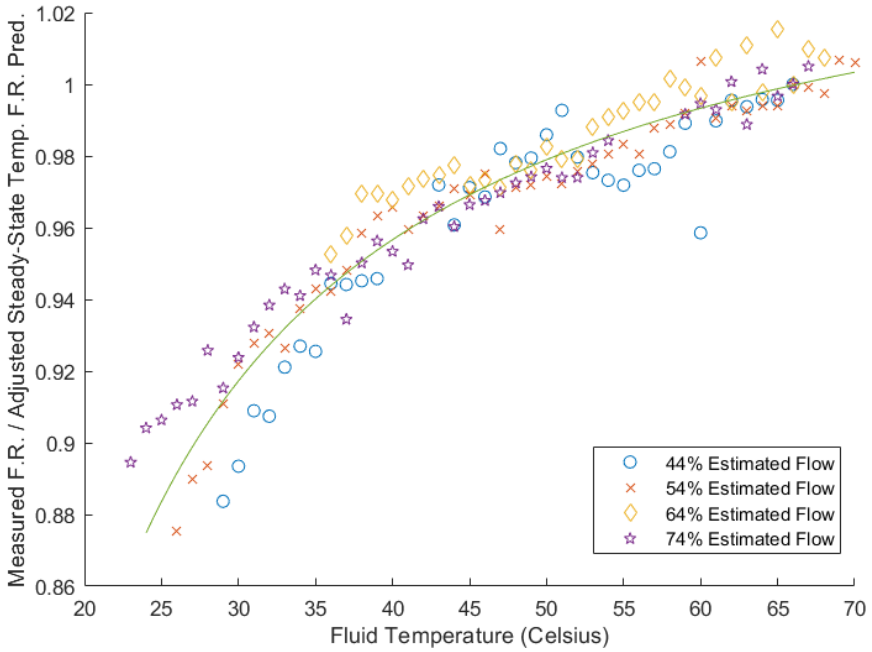

Figure 4.10: *Measured flow rate to adjusted predicted flow rate for different fluid temperatures.*

A linear/linear rational best-fit curve (eq. 9) provided the best correlation between adjusted flow rate proportions versus fluid temperature observed between four temperature test runs combined in the analysis. When comparing this best-fit curve to data from these four tests, a RMSE of 0.009 and MAPE of 0.72% existed. Given this

strong fit was associated with four varying flow rate magnitudes, it was determined that temperature effects could be compensated independently of the flow rate magnitude.

$$t_p = \left(\frac{1.060T - 7.818}{1T - 3.868}\right) \quad \text{(Eq. 9)}$$

where
t_p = temperature adjustment coefficient
T = hydraulic oil temperature (°C)

4.4.1.4. Derived Pressure Drop Prediction Method

Having determined that temperature effects on flow rate prediction can be assessed independent of flow rate magnitude, the model shown in equation 10 was determined suitable for flow rate prediction. Thus, after calculating the expected flow rate at steady state oil temperature based on a given pressure drop across an orifice flowmeter, an adjustment to the prediction can be made by multiplying a temperature compensation coefficient based on the CAN-indicated fluid temperature. Different empirical equations dependent on orifice and flow direction were to be used to determine the expected preheated oil temperature flow rate, while equation 9 from section 4.4.1.3 was used to obtain the temperature compensation coefficient.

$$Q = t_p Q_{p.ss} \quad \text{(Eq. 10)}$$

where
Q_p = predicted flow rate using orifice flowmeter (L min^{-1})
t_p = temperature compensation coefficient
$Q_{p.ss}$ = expected flow rate at steady-state temperature (L min^{-1})

4.4.2. Valve Spool Position Prediction Method

4.4.2.1. Flow Rate-Valve Spool Position Relationship at Steady-State Fluid Temperature

Figure 4.11 provides a graphical representation of the mean flow rate and pressure difference between pump and load sense for different extend direction valve spool positions conducted on valve 1 of tractor A. Despite maintaining a high engine speed and suitable pressure requirement, the pump did not satisfy the valve's flow rate request at high spool positions (86% and greater estimated flow CAN message). However, a strongly correlated best-fit curve could be used to relate flow-sufficient spool positions.

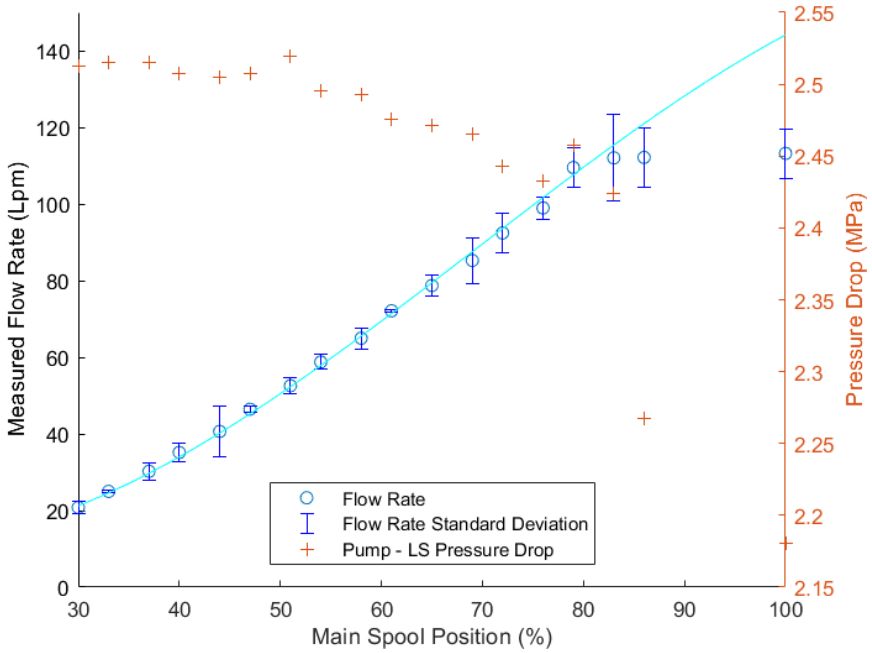

Figure 4.11: *Relationship between flow rate and pressure differential between the pump and load sense for different valve spool positions.*

Figure 4.12 compares mean flow rates measured for extend direction spool positions of a control valve on each tested tractor. From the figure, it appeared that the control valve design used on both tractors differed from one another despite both tractors being

the same make and model. Tractor B's control valve design possessed a relatively better linear relationship between flow rate and estimated flow rate percentage, while tractor A had a higher order polynomial relationship between the two quantities. Thus, different polynomial fit types were used between the two tractors.

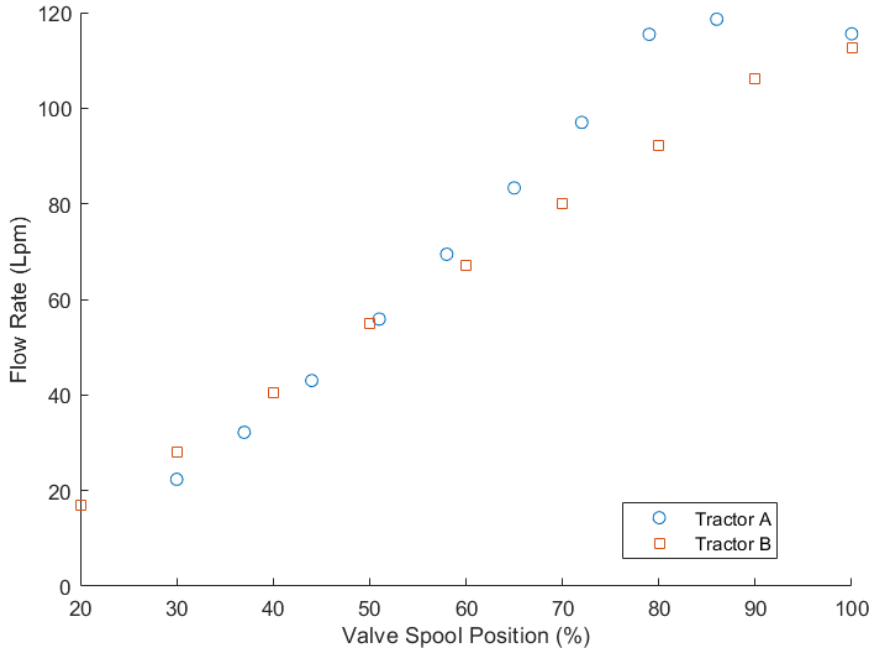

Figure 4.12: *Comparison of valve flow rates in extend direction between two tractors tested.*

Table 4.3 details the mean flow rate measured for different spool positions in the retract direction for two control valves on tractor B. Overall, valve 2 had a flow rate that was on average 3.03% higher than valve 1 for the positions tested, with higher differences occurring at low flow rates. Based on these differences, separate best-fit curves were found for each valve. When comparing the 95% confidence intervals of the coefficients for each best-fit curve (Appendix A), no two variables were determined significantly different from one another. However, to minimize prediction error, it was determined it was necessary to find different best-fit curves for each valve on each tractor.

Table 4.3: Comparison of Different Valves on Tractor B

Estimated Flow Rate (%)	Retract Direction Flow Rate (Lpm)		Difference (%)
	Valve #1	Valve #2	
20	14.17	14.90	5.18
24	20.54	21.42	4.27
30	25.81	26.93	4.33
34	32.02	32.98	2.99
40	37.80	39.10	3.43
44	45.12	46.57	3.22
50	51.75	52.96	2.34
54	58.22	59.49	2.17
60	63.99	66.05	3.22
64	70.62	73.34	3.85
70	77.36	79.96	3.36
74	83.93	86.90	3.54
80	89.97	92.57	2.89
84	97.98	100.06	2.12
90	106.56	108.44	1.76
94	114.41	114.51	0.09

Table 4.4 details the mean flow rate measured for spool positons in the extend and retract flow direction for valve 2 on tractor B. From analyzing the table, while a low difference in flow rate existed at high spool positions, high differences were seen in measured flow rate at low spool positions. Thus, separate best-fit curves were found for each control valve direction. In comparing the 95% confidence intervals for each coefficient between the two best-fit equations (Appendix A), the quadratic coefficients between the two best-fit curves were significantly different from one another. Thus, separate best-fit curves were needed between the two flow directions for each valve.

Table 4.4: Comparison of Valve Flow Directions - Tractor B

Estimated Flow Rate (%)	Extend Direction (Lpm)	Retract Direction (Lpm)	Difference (%)

20	16.95	14.17	17.89
24	22.76	20.54	10.26
30	27.99	25.81	8.11
34	34.65	32.02	7.91
40	40.59	37.80	7.12
44	48.96	45.12	8.16
50	54.96	51.75	6.02
54	61.83	58.22	6.02
60	67.20	63.99	4.89
64	74.63	70.62	5.53
70	79.97	77.36	3.32
74	87.49	83.93	4.16
80	92.25	89.97	2.51
84	99.68	97.98	1.72
90	106.19	106.56	-0.35
94	114.87	114.41	0.40
100	119.52	118.96	0.47

Based on the results, separate best-fit curves were found for each valve and valve direction for both tractors. All best-fit equations found followed a format shown in equation 11. However, the cubic term for valve equations on tractor B were determined unnecessary. The resulting equation coefficient estimates and confidence intervals are listed in Appendix A.

$$Q_{v.ss} = c_{3.vd}x^3 + c_{2.vd}x^2 + c_{1.vd}x + c_{o.vd} \quad \text{(Eq. 11)}$$

where
$Q_{v.ss}$ = predicted flow rate at steady-state temperature
x = estimated flow rate (%)
$c_{n.vd}$ = nth power coefficient of valve "v" in direction "d"

4.4.2.2. Effect of Fluid Temperature on Flow Rate-Valve Spool Position Relationship

As the valve spool position flow rate prediction method predicted a constant flow rate for a given valve spool position, a single flow-rate was predicted for a given temperature

test. Thus, rather than comparing the observed flow rate for given temperatures to the predicted flow rate at steady-state temperature, comparisons instead were made to the observed flow rate at a near-steady state temperature. A proportion was found relating the measured flow rate to the flow rate observed at 66°C for each temperature of each test.

Figure 4.13 details the relationship between measured-to-steady-state flow rate and fluid temperature for different valve spool positions for a given valve. At the lowest fluid temperatures, the resulting flow rate was as low as 95% of the measured flow rates at steady state temperature. Overall, a common relationship was maintained among different spool positions. A quadratic/linear rational empirical curve (eq. 12) provided the best fit relating the mean proportion among all tests for each temperature. When compared to the data collected from each test, the predicted proportions using the best fit curve had a .002 RMSE. Thus, a single curve could compensate flow rate prediction for fluid temperature effects independent of spool position setting under flow-sufficient conditions.

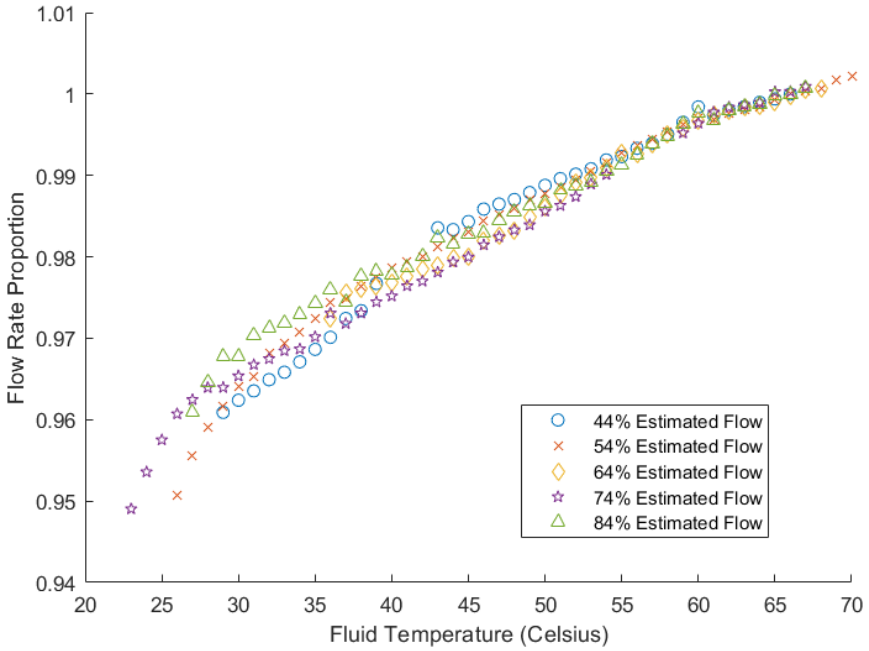

Figure 4.13: *Comparison of fluid temperature tests at different valve spool positions.*

$$t_v = \frac{.000639T^2 + 0.960T - 8.964}{T - 8.464} \qquad \text{(Eq. 12)}$$

Where:

x = fluid temperature (°C)

t_v = temperature coefficient using valve spool position

4.4.2.3. Derived Valve Spool Position Prediction Method

Because the proportion of flow rate produced at different fluid temperatures to flow rate at steady-state temperature was consistent for different flow rate magnitudes, valve spool position and fluid temperature effects could be determined independent of one another. Thus, after determining the expected flow rate at steady state temperature for a given estimated flow percentage magnitude, an adjustment to the prediction could be made by multiplying the prediction by a temperature coefficient based on the CAN-indicated fluid temperature (eq. 13). Different empirical equations dependent on valve and flow direction were to be used to determine the expected preheated oil temperature

flow rate, while equation 12 from section 4.4.2.2 was used to obtain the temperature compensation coefficient.

$$Q_v = t_v Q_{v.ss} \quad \text{(Eq. 13)}$$

where
Q_v = predicted flow rate using valve spool position method
t_v = temperature coefficient using valve spool position
$Q_{v.ss}$ = predicted flow rate at steady-state temperature

4.4.3. Flow Rate Prediction Validation Results

4.4.3.1. Steady State Test

A variable valve position test dataset which featured mostly steady-state flow conditions at varying flow rate magnitudes was used to test the prediction algorithm. Figure 4.14 provides a graphical representation of the predicted versus measured flow rates throughout the test duration.

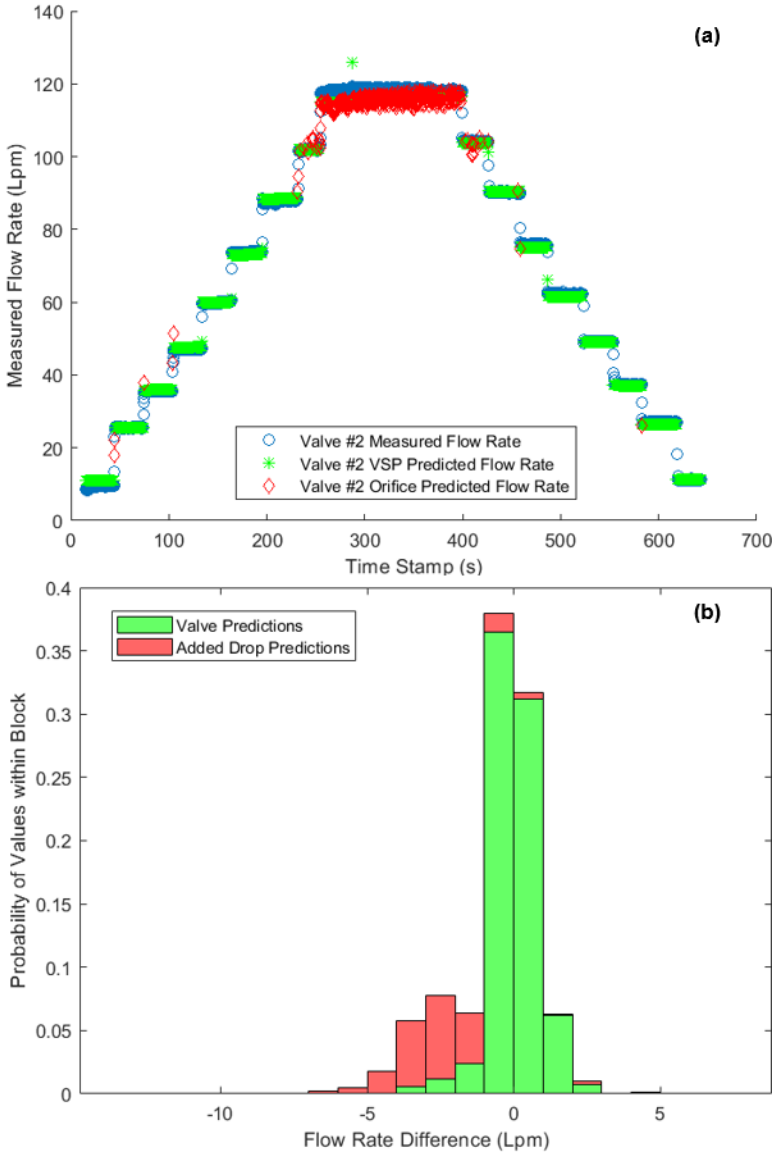

Figure 4.14: *Resulting predicted flow rate versus measured flow rate for steady-state test.*

As the orifice flowmeter was expected to predict flow rate independent of system conditions, prediction accuracy was compared between the developed flow rate prediction function using valve spool position when possible versus using only the orifice flowmeter. As shown in table 4.5, the prediction function had a lower MAE, MAPE, and RMSE than the pressure drop method. Thus, using valve spool position when possible within the prediction function resulted in a more accurate flow rate prediction.

Table 4.5: Valve Position Test Flow Rate Prediction Accuracy - Overall

Performance Statistic	Magnitude – w/ Valve Spool Position	Magnitude – Orifice Flowmeter Only
Mean Absolute Error (MAE) (Lpm)	1.032	2.294
Mean Absolute Percentage Error (MAPE) (%)	2.088	6.347
Root Mean Squared Error (RMSE) (Lpm)	1.602	2.841

To further analyze when errors occurred with both prediction methods, the associated accuracy statistics were found for each tested valve spool position. As seen in table 4.6, while using only the pressure drop method resulted in higher absolute errors and RMSE, the mean flow rate prediction for a given valve position did not greatly differ from the method using valve spool position when possible. Additionally, the overall MAPE, MAE, and RMSE values from the orifice flowmeter prediction were inflated due to higher variance in prediction at the lowest flow rates. At flow rates greater than 60 Lpm, the MAPE was no higher than 3.03%. This was likely due to the need for higher precision to detect changes in flow rate resulting from the quadratic relationship between flow rate and pressure drop.

Table 4.6: Valve Position Test Flow Rate Prediction Accuracy – Individual Levels

Measured Flow Rate (Lpm)	Prediction Function Flow Rate				Orifice Predicted Flow Rate			
	Mean Error (Lpm)	MAE (Lpm)	MAPE (%)	RMSE (Lpm)	Mean Error (Lpm)	MAE (Lpm)	MAPE (%)	RMSE (Lpm)
10.21	0.98	1.05	10.91	1.36	0.38	3.56	35.10	4.44
26.37	-0.47	0.49	1.82	0.63	0.72	2.34	8.85	2.95
36.44	0.11	0.35	0.98	0.59	-0.39	1.83	5.04	2.26
48.13	0.25	0.44	0.93	0.96	-0.26	2.47	5.13	3.03
61.19	-0.08	0.41	0.66	0.44	-0.36	1.77	2.89	2.21
74.68	-0.49	0.53	0.71	0.65	1.88	2.27	3.03	2.73
88.99	0.62	0.68	0.77	0.87	1.03	1.55	1.73	2.06
103.22	-0.07	0.50	0.47	1.37	-1.03	1.88	1.82	2.31
117.95	-2.56	2.56	2.17	2.88	2.70	2.71	2.29	3.07

4.4.3.2. Temperature Test

To validate the adjustments made based on fluid temperature, a temperature test was processed through the flow rate prediction program. Two different valve positions total were tested beginning at a fluid temperature of 22°C and ending the test at 58°C. Figure 4.15 provides a visual representation of predicted versus measured flow rates throughout the test duration.

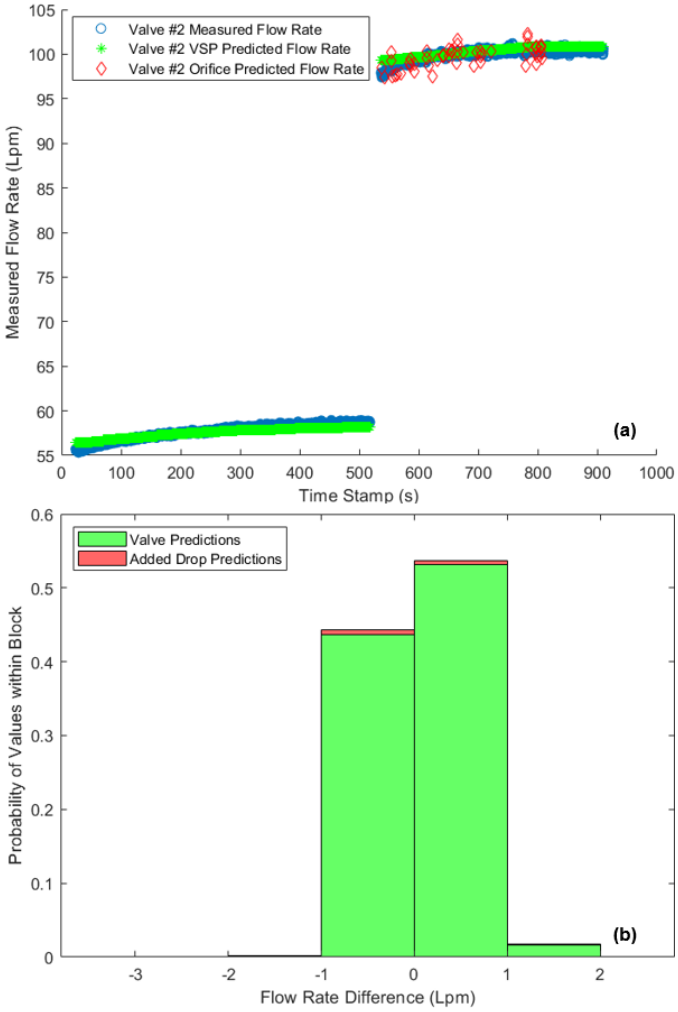

Figure 4.15: *(a) Comparison in predicted versus measured flow rate and (b) error distribution for a steady state test with high variance in fluid temperature.*

Table 4.7 presents the improvement level in accuracy the program achieved when utilizing the temperature compensation adjustment for both the prediction using only the pressure drop and for the method incorporating valve spool position when possible. Similar to the steady state test results, incorporating valve position when possible provided a more accurate flow rate prediction. While temperature compensation improved both predictions, the level of improvement was greater in the added pressure drop method. This aligns to the larger compensation factor seen at low temperatures for the added drop versus valve spool position prediction method from the temperature compensation development results.

Table 4.7: Temperature Test Flow Rate Prediction Accuracy

Performance Statistic	No Temperature Compensation		Temperature Compensation	
	Prediction Program	Only Added Drop	Prediction Program	Only Added Drop
MAE (Lpm)	1.256	3.983	0.347	0.898
MAPE (%)	1.892	6.084	0.491	1.261
RMSE (Lpm)	1.535	4.569	0.435	1.140

4.4.3.3. Maximum System Pump Pressure Test

Another variable valve spool position test, but with an additional valve not connected to any circuit also continuously actuated, was processed through the prediction program. This served as a valid test to determine the accuracy in valve prediction with the valve's pre-spool compensator engagement required to maintain flow rate. Additionally, it tested the ability for the orifice flwometer to predict flow rate at high pump pressures. The vast majority of flow rate data were in steady-state conditions. Figure 4.16 provides a visual representation of the predicted and measured flow rates throughout the test duration.

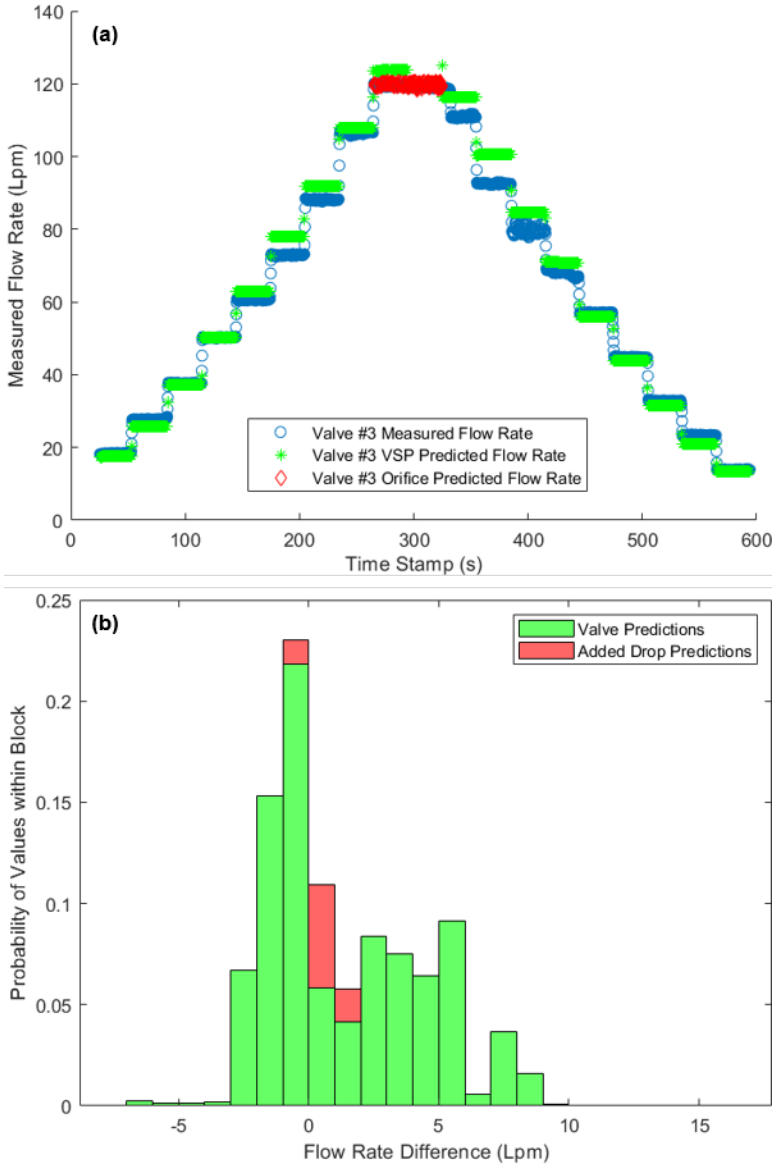

Figure 4.16: *(a) Comparison in predicted versus measured flow rate and (b) error distribution for a variable valve position test with a stalled pump.*

As provided in table 4.8, the prediction program error was higher for this test in comparison to the steady-state test. It was inferred this increased error stemmed from differences in flow rate produced for a given spool position between being the highest load sense and using the pre-spool compensator to maintain flow rate when other circuits had a higher load sense. However, with a mean absolute error below 5%, it was deemed a

separate prediction algorithm for instances with the pre-spool compensator engaged to maintain desired flow rate was not necessary. While utilizing valve spool position when possible in the prediction program still resulted in a reduced error versus solely using the orifice flowmeter, the difference in error decreased from the steady-state test.

Table 4.8: Maximum System Pressure Pump Test Flow Rate Prediction Accuracy

Performance Statistic	Prediction Program	Orifice Flowmeter Only
Mean Absolute Error (Lpm)	2.424	2.888
Mean Absolute Percentage Error (%)	4.076	6.887
Root Mean Squared Error (Lpm)	3.247	3.782

4.4.3.4. Multiple Valve Test – Steady State Conditions

A multiple valve test with one valve (valve 1) maintained at a constant spool position while making adjustments to the other (valve 2) in increments similar to the variable valve position test was processed through the flow rate prediction program. Two repetitions of this actuation method were performed during the test; however, the second repetition, which began at a time stamp of 375 seconds, had a third valve attached to no circuit actuated to generate the maximum system pressure. Comparisons in the measured versus predicted flow rate are provided in figure 4.17. As seen in the figure, while the prediction error magnitude did not greatly change between the two repetitions in valve 2, the error magnitude increased in valve 1 when the third valve was actuated. Similar to comparisons between the maximum system pressure versus steady-state test data, prediction accuracy decreased when a flow-sufficient valve went from being the highest load sense valve to a lower load sense valve.

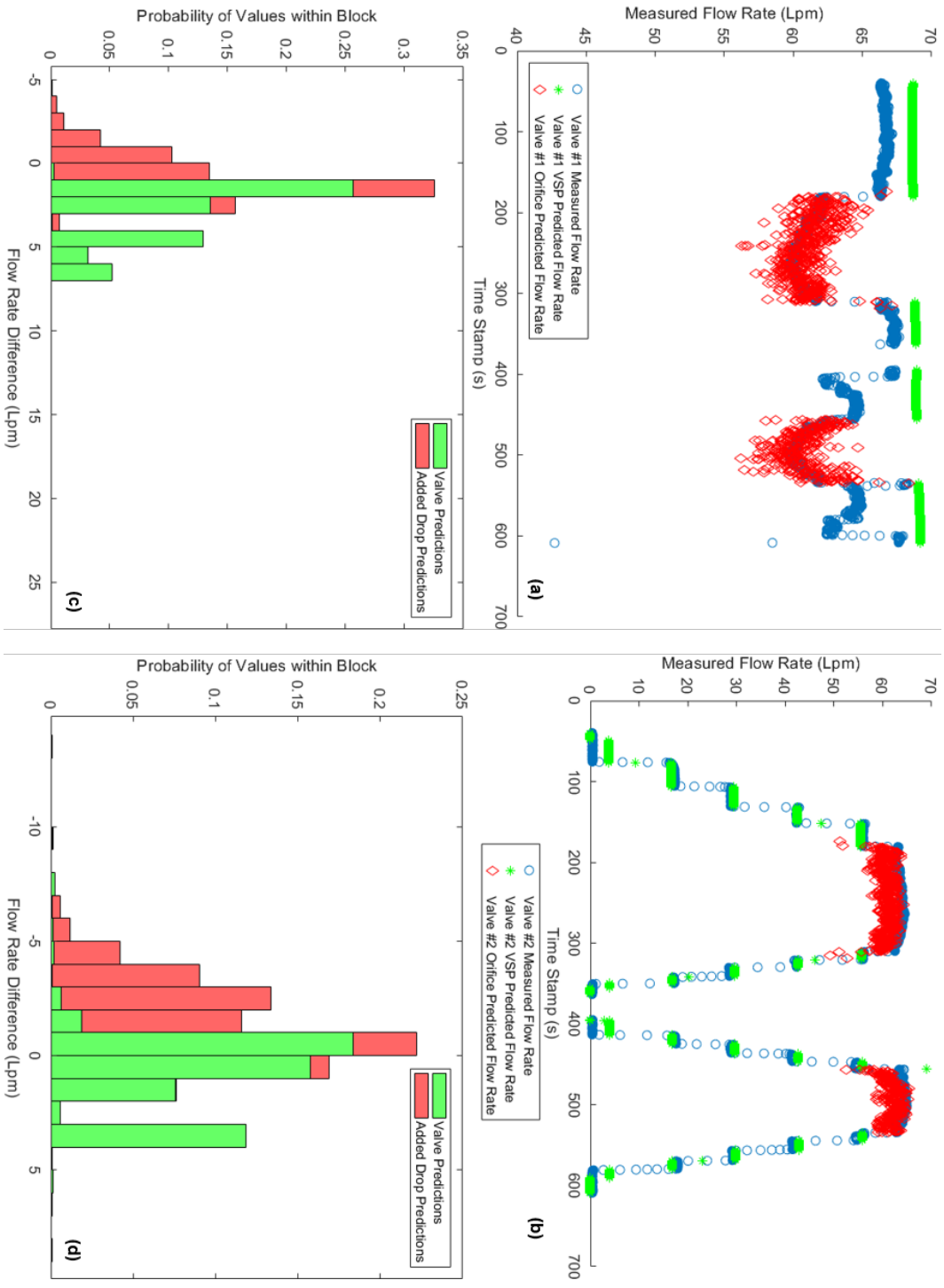

Figure 4.17: *Comparison in predicted versus measured flow rate for (a) valve 1 and (b) valve 2 and error distribution for both (c) valve 1 and (d) valve 2 for steady state multiple valve test.*

When analyzing the resulting prediction accuracy statistics, it is notable that while valve 2 had a lower MAE and RMSE than valve 1, the MAPE of valve 2 was 89.9%.

Due to the program predicting a positive flow rate at a low valve spool position where minimal flow rate was occurring, the percentage error was inflated by these data points. When excluding these low flow rate conditions, which was not expected during actual field operations, the MAE for valve 2 dropped to 3.66%.

Table 4.9: Steady-State Multiple Valve Test Flow Rate Prediction Accuracy

Performance Statistic	Valve #1	Valve #2
Mean Absolute Error (Lpm)	2.240	1.758
Mean Absolute Percentage Error (%)	3.50	89.9
Root Mean Squared Error (Lpm)	2.859	2.354

4.4.3.5. Multiple Valve Test – Transient Conditions

In addition to the steady-state multiple valve test, a multiple valve test with a high proportion of transient flow rate data was processed through the flow rate program. Changes in flow rate frequently occurred due to changes in engine speed or valve position in either valve. This resulted in both valves featuring both flow-sufficient and flow-limited conditions. Figure 4.18 shows the changes in flow rate and the associated prediction at given times throughout the test. As seen in table 4.10, while the error was slightly higher in valve 2, both valves had MAPEs below 6%.

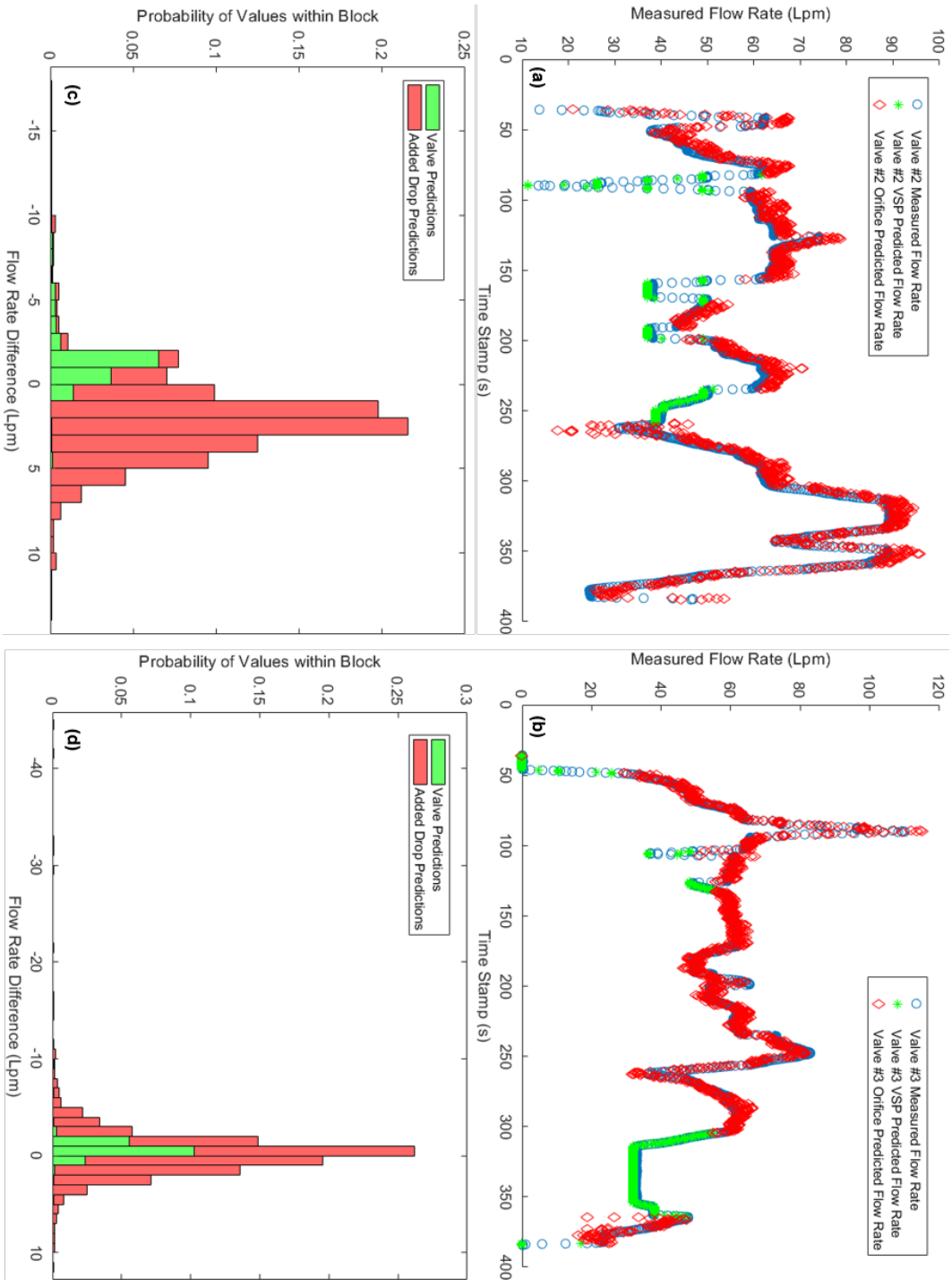

Figure 4.18: *Comparison in predicted versus measured flow rate for (a) valve 2 and (b) valve 3 and error distribution for both (c) valve 2 and (d) valve 3 for transient multiple valve test.*

Table 4.10: Transient Multiple Valve Test Flow Rate Prediction Accuracy

Performance Statistic	Valve #2	Valve #3
Mean Absolute Error (Lpm)	2.633	1.653
Mean Absolute Percentage Error (%)	5.334	3.573
Root Mean Squared Error (Lpm)	3.319	3.175

4.5. Conclusions

From variable valve spool position tests conducted at flow-sufficient conditions, strongly correlated best-fit curves were found relating flow rate to both valve spool position and the pressure drop across the customized orifice flowmeter developed for this study. However, tests conducted across varying hydraulic oil temperatures determined that the flow rate relationship to either valve spool position or pressure drop changed at different fluid temperatures due to changes in fluid properties. Analysis between different temperature tests determined that the change in flow rate at different temperatures was a proportion of the expected flow rate magnitude at the determined preheated temperature of 66℃. Thus, the finalized flow rate prediction equation used for both valve spool position and pressure drop featured a temperature compensation coefficient that adjusted the steady state flow rate prediction by a proportion determined by the measured fluid temperature.

The developed flow rate prediction program that incorporated the flow rate prediction equations met prediction accuracy goals across a variety of tests processed through the program. While predicting flow rate using the orifice flowmeter method alone resulted in a similar mean error for different positions held over several seconds, the prediction program incorporating valve spool position when possible consistently produced a lower mean absolute and root mean squared error. The error magnitude varied for different

tests. Higher errors were seen for instances when the orifice flowmeter predicted lower flow rate magnitudes, a valve's spool position predicted flow rate but the valve did not have the highest pressure requirement in the system, and the proportion of transient data was higher. However, even at these conditions, the mean absolute error was maintained below 3 Lpm, and the mean absolute percentage error was held below 5.5 percent. Based on the prediction accuracy results from this test, it was determined that the combination of instrumentation and flow rate prediction program could be used in place of turbine flowmeters to predict hydraulic flow rate for implement hydraulic circuits. This work validated the ability to use these methods for agricultural machinery performance studies in field conditions.

Chapter 5: Analysis of Hydraulic Power Requirements and Machinery Performance Characteristics for Small Grain Planting Operations

5.1. Introduction

For agricultural row crop producers, a critical component to enable success for their operation is the selection of properly-sized implements and tractors that power them to accomplish required tasks throughout the year. For a given implement, the size selected may be determined from a wide variety of factors, including but not limited to the expected usage per year, amount of time available to accomplish the work within the growing season, ownership costs, capital labor costs, and power requirements the tractor must provide for the given field terrain and operator preferences (Edwards, 2017).

While the producer must pair a tractor that is capable of providing sufficient power to an implement, selecting a tractor with a far greater power capability in comparison to the requirement has drawbacks, including reduced efficiency and increased costs (White, 1977). Thus, there is an incentive for pairing a tractor to an implement that provides sufficient power, but minimize drawbacks with increased power capabilities.

While some producers may select a tractor for their operation based on the implements to be used with it, others may select their implement based on their tractors in their fleet. While a tractor may possess the overall power capability to work with a particular implement, it may not have the ability to provide the power take off (PTO) or hydraulic power components the implement demand. Examples include modern large tractors that do not feature an optional PTO or older tractors fitted with hydraulic pumps that produce insufficient flow rate requirements. There are potential alternatives to

account for the lack of these power components, including the addition of a PTO-powered hydraulic pump to the implement to provide additional hydraulic power or conversion kits for implement functions normally powered by the PTO to instead be hydraulically powered. Nonetheless, the ability for the producer to know the overall implement power requirements, as well as of each power form, would be beneficial in selecting implements for operations based on the tractor's capabilities.

The American Society of Agricultural and Biological Engineers (ASABE) developed Standard D497.7, entitled "Agricultural Machinery Management Data," to assist in predicting implement power requirements. The standard provides empirical equations that can be used to estimate either draft force or rotational power requirements for a given implement. However, the standard lists several equations with an allowable error of 50%. Additionally, the studies conducted to determine the empirical coefficients provided in the standard were developed in the 1990's (Harrigan and Rotz, 1995; Rotz and Muhtar, 1992). Due to the high allowable error range of the empirical equations and the date of the current standard's origin, the usefulness of the predicted power requirements using the standard is limited.

5.2. Objectives

The goal of this study was to assess the performance of similar tractor designs paired with two different no-till air drills for small grain planting operations. Specific objectives included 1) assessing tractor power usage across different terrain, 2) determining time and fuel requirements per area for different fields planted with the given machinery, and 3) analyzing hydraulic power requirements for both implements.

5.3. Materials and Methods

5.3.1. Machinery Background

Two different small grain planting operations were analyzed in this study. A wheat crop was planted with a row crop tractor (8320R, Deere & Company, Moline, Ill.) and no-till air drill (NTA2007, Great Plains Manufacturing, Salina, Kan.) with a 6.1 m (20 ft.) working width. A rye cover-crop was planted with a similar row crop tractor model (8320RT, Deere & Company, Moline, Ill.), but with tracks rather than tires, and a no-till air drill (JD 1990, Deere & Company, Moline, Ill.) with a 12.2 m (40 ft.) working width. Both crops were planted in rows spaced 19.05 cm (7.5 in.) apart. Both tractor and planter combinations are shown in figure 5.1. In total, roughly 647.5 hectares (1600 acres) of rye cover crop and 55.5 hectares (137 acres) of wheat crop planting operations were analyzed.

Figure 5.1: *(a) JD 8320R with Great Plains NTA2007 no-till air drill used throughout wheat planting operation and (b) JD 8320RT and (c) JD 1990 no-till air drill used throughout rye planting operation.*

The planter used for the wheat crop featured a hydraulically-powered fan for the material delivery system. In addition to planting seed, dry fertilizer was also applied on each row with the operation. Other implement functions that used tractor hydraulic power included weight transfer and wing folding, opener lifting, and visual field markers. In comparison, the planter used for the rye cover crop also used tractor hydraulic power for a fan to move seed to each opener, opener lifts, and wing folding. However, unlike the planter used for wheat planting, downforce to keep the openers engaged was done using the opener lift circuit as opposed to using weight transfer using the wing folding circuit for rye planter. Pressure control valves were used to control the fluid pressure magnitude supplied to both the downforce function on the rye planter and the weight transfer function on the wheat planter. Additionally, the wheat planter featured a bypass valve within the weight transfer circuit to reduce wasted power when used with load-sensing, closed center hydraulic systems. However, the operator for the wheat planting opted to leave this bypass valve closed due to past issues during operation. Neither implement possessed functions that required the tractor power take off (PTO).

5.3.2. Data Collection Method

Numerous desired machine operating parameters were available in a standard controller area network (CAN) message format on each tractor's ISOBUS. Table 5.1 details the list of messages that were available for logging. However, hydraulic pressure and flow rate measurements needed to assess hydraulic power were not available through standard CAN messages. Thus, the addition of sensors to the tractor were needed to measure these quantities.

Table 5.1: Standard CAN Messages Available for Interpretation on Tested Tractors

Parameter Group Number (PGN) (Hexadecimal)	Reported Variables of Interest
F004	Engine Speed, Engine Torque
FE11 FE12 FE13 FE14	Estimated Hydraulic Valve Flow Rate Percentage (from Valve Spool Position)
FE43	PTO Speed
FE45	3 Point Hitch Position, Draft Sense
FE48	Wheel-Indicated Vehicle Speed, Total Distance
FE68	Hydraulic Fluid Temperature
FEE3*	Reference Engine Torque, Engine Lug Curve Data Points
FEE8	GPS Bearing, Vehicle Speed, Pitch, and Altitude
FEF2	Fuel Rate
FEF3	GPS Latitude, Longitude Coordinates

*Message typically published following SAE J1939 Transport Protocol (PGN: EB00)

Efforts were made to convert all sensor signals into CAN messages published on the ISOBUS. Thus, all data could be recorded with a standalone CAN data logger (Pro 2xHS v2, Kvaser AB, Mölndal, Sweden) plugged into the tractor's CAN diagnostic port. A customized electronics enclosure, named the Sensor CAN Gateway (SCANGate), was developed to power the added sensors and convert sensor signals into CAN messages that were published on the ISOBUS using an electronic controller unit (ECU) (Danfoss MC024-110, Danfoss North America, Ames, Iowa). In total, 3 additional CAN messages were published to the ISOBUS at 4 Hz. To connect the ECU into the tractor's ISOBUS, an implement-end ISOBUS breakaway connector (IBBC) plug on the SCANGate connected into the tractor's IBBC. While the planter used for wheat planting did not

feature any ISOBUS components, the planter used for the rye planting had ISOBUS components that also required connection to the tractor IBBC. To allow the implement to also connect into the ISOBUS, the planter's IBBC was plugged into a second breakaway connector on the SCANGate.

Due to the preference of not placing sensor cables in the cab, and in being closer to the sensor locations, the SCANGate was mounted behind the tractor cab. Specific locations varied between the two tractors due to available room with each tractor design (figure 5.2). Thus, customized mounting brackets were used with each tractor to properly secure the SCANGate.

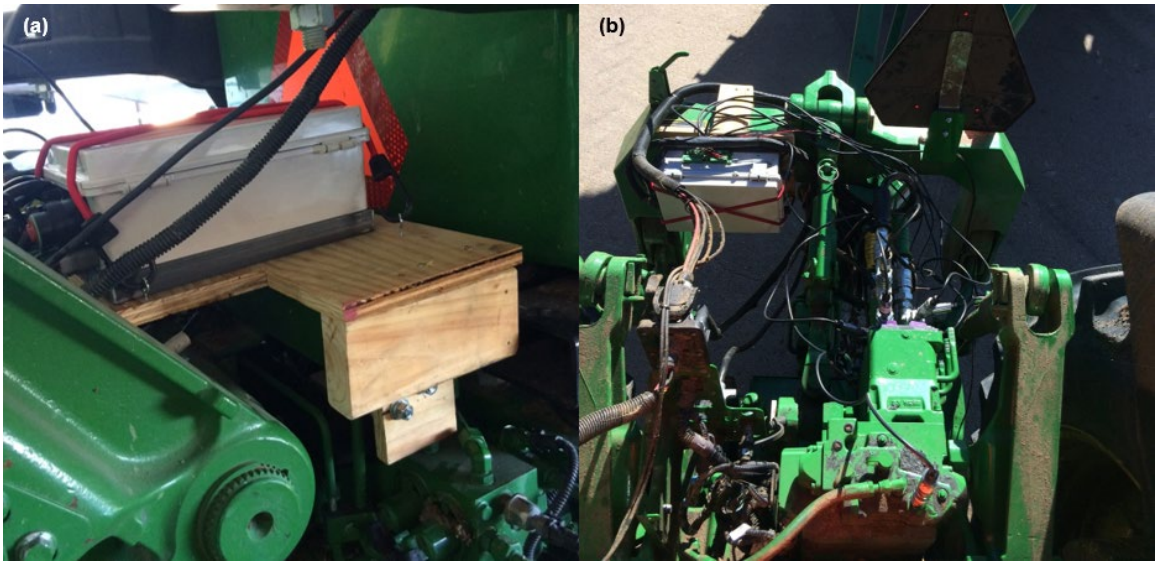

Figure 5.2: *Location of the SCANGate varied between the two tractors. The device was mounted (a) directly behind the tractor cab for the rye cover crop tests and (b) on the quick hitch for the wheat tests.*

5.3.3. Hydraulic Power Sensor Instrumentation and Calibration Testing

All hydraulic pressure measurements were conducted using a common electronic pressure transducer model (Omega PX309, Omega Engineering Inc., Norwalk, Conn.). Because flowmeters required significant upstream and downstream uninterrupted flow

lengths (Badger Meter, 2018), a flow rate prediction method was used for field data collection.

Due to the load sensing hydraulic system design on both tractors, flow rate could be estimated using valve spool position when the pump produced sufficient flow to satisfy each valve position's requested flow rate. However, at least one valve's spool position would not accurately predict flow rate if the total requested flow rate could not be provided by the pump. Thus, a customized orifice flowmeter (figure 5.3) was added to each implement hydraulic circuit of interest to predict flow rate in these circumstances. The selected added pressure drop featured a customized orifice fitting which reduced the flow passageway to a 7.94 mm diameter circular opening in either flow direction (effective beta ratio of 0.417).

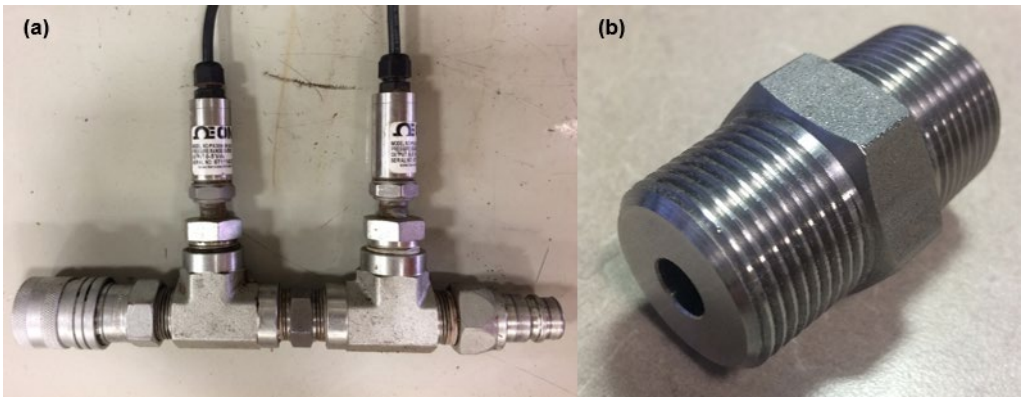

Figure 5.3: *(a) Added system loss used to predict flow rate in flow-limited circumstance. System loss featured a (b) customized orifice fitting with a 7.94 mm diameter opening.*

Pressure was measured on both the extend and retract ports of each control valve in order to determine each circuit's pressure requirements. With pressure sensors already utilized on one port side with the orifice flowmeter, a single pressure sensor in a separate fitting assembly was added to the other port side when possible. However, for the fan circuits on both planters, a return line was connected to the tractor's sump port to

eliminate back pressure instances from occurring that could damage the fan. Thus, it was always assumed the return supply had no backpressure for fan circuits. Therefore, power could be determined solely from the pressure measurement at the flow outlet with the orifice flowmeter sensors.

In addition to pressure measurements utilized for flow rate prediction and implement pressure demands, as detailed in chapter 3, pump and load sense pressures needed measured to determine whether valve spool position accurately predicted flow rate on all valves at a given time. At high pump pressures and instances where the difference between pump and load sense pressures was less than the nominal margin pressure value, at least one valve would be flow-limited. Therefore, pressure sensors were added to the pump and load sense test diagnostic ports on each tractor. Although both tractors had pump pressure diagnostic ports available behind the tractor cab, neither tractor had load sense diagnostic ports in the same location. Instead, load sense diagnostic ports were available at the hydraulic pump located underneath the chassis.

Calibration tests were conducted on each tractor to determine the relationship between valve spool position and flow rate. Prior testing discussed in chapter 4 found that the actual-to-estimated flow rate relationship varied for different valves and valve actuation directions. Thus, tests were conducted on each valve of interest in both actuation directions. A simulated implement circuit containing a turbine flowmeter (Flo-tech Activa F6206-AVB-NN, Badger Meter, Milwaukee, Wisc.) to serve as the baseline flow rate measurement and a needle valve to allow adjustment to the circuit pressure requirement was connected to the tractor. The calibration test was conducted at an engine speed and implement load setting that would not hinder the valve's requested flow

rate from being attained. Upon actuating the valve into continuous detent for a given direction at a low spool position, the spool position was gradually increased in the smallest possible increments (0.04 on a dimensionless scale of 0 to 10) until the valve spool was fully open. From there, valve spool position was gradually decreased until fully closed. While there was concern that the reported estimated flow rate message would not account for valve hysteresis effects, results from testing showed no difference in flow rate magnitude for given estimated flow rate messages values regardless of the valve spool direction. Calibration testing revealed a linear relationship observed between flow rate and reported estimated flow rate percentage correlating to lower flow rates, but a nonlinear relationship seen between the two variables at spool positions correlating to higher flow rates. Thus, piece-wise empirical calibration equations were utilized to predict flow rate using valve spool position. Equations found from the tests are listed in appendix A.

5.3.4. Post-Data Processing Program

All data were analyzed post-operation using a customized Matlab program developed for this study. Various methods in the post-processing analysis are discussed below.

As the CAN data logger produced all log files in a raw format, the first step in the program was to convert the raw messages into engineering measurements. This involved sorting different messages by their parameter group number (PGN), converting raw data bytes into engineering units based upon the ISO 11783 standard, and resampling calculated engineering values to common time intervals. While standard functions within Matlab's Vehicle Network Toolbox application would also convert the raw log files, it

was determined a customized function that only accounted for data bytes of interest resulted in a faster processing time.

While the post-processed dataset contained all of the necessary pressure readings to determine implement hydraulic power requirements, further work was needed to determine the predicted flow rate. A Matlab function was developed to determine flow rate through each hydraulic control valve of interest. The function predicted flow rate using both the valve spool position method and the orifice flowmeter for all data points. Flow rate prediction using these methods required utilization of the estimated flow rate, pressure drop across the orifice flowmeter, and fluid temperature at each data point. From work conducted in chapter 4, it was preferred to use the valve spool position method over the orifice flowmeter to predict flow rate when valve spool position accurately represented flow rate. Thus, following a process shown in figure 5.4 using different pressure measurements, it was determined when the valve spool position method was accurate. Thus, the predicted flow rate was derived from the valve spool position prediction when valid and the orifice flowmeter method when the valve spool position prediction was invalid.

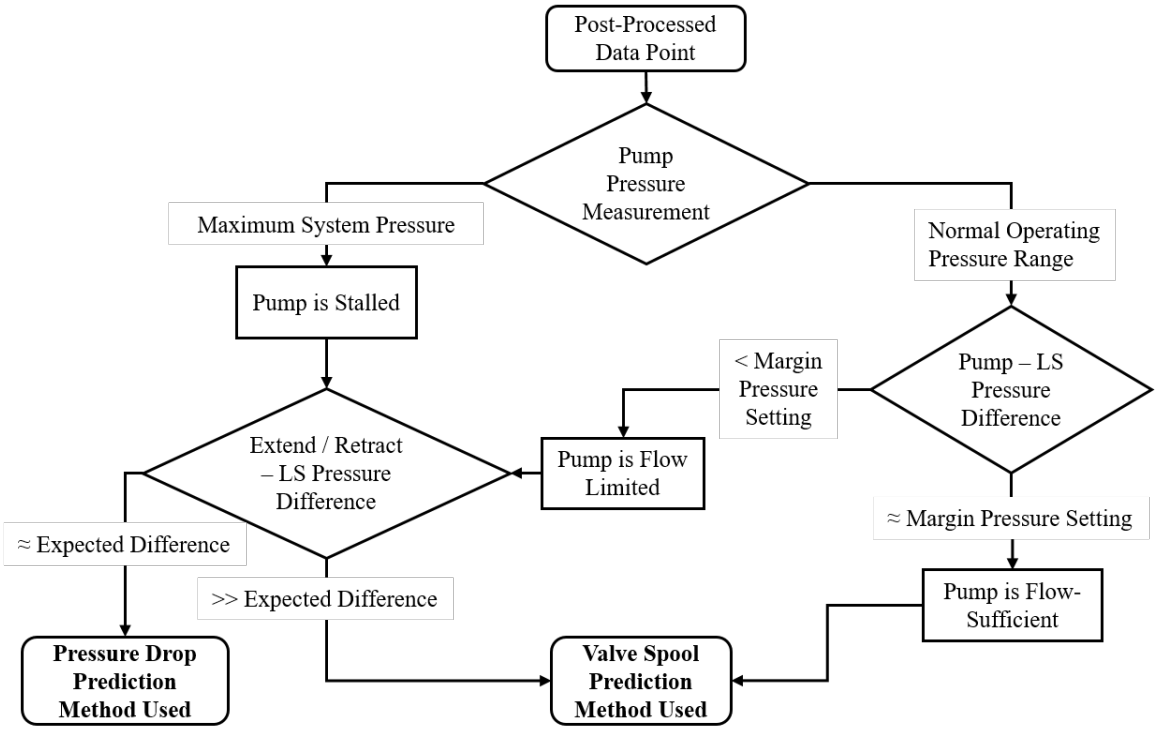

Figure 5.4: *Flow chart defining the determination of whether a given post-processed data point could be predicted using valve spool position.*

Upon determining all predicted flow rates, the next step in the program was to analyze the field data. In general, there were four different vehicle states that occurred throughout the field operation. These states were when the planter was actually planting seed (working), the tractor was being repositioned so it could begin planting again within a field (turning), the tractor was stopped for any potential reason (stoppage), and the tractor was being moved from one field to the next (traveling). It was critical to decipher these different states to be able to determine field efficiency and make comparisons in performance characteristics both within and amongst each vehicle state.

To understand when each vehicle state occurred within a data file, the standard CAN messages for vehicle wheel speed and hydraulic control valve estimated flow rate associated with the planter's folding and opener circuits were used. To effectively

determine all notable characteristics of each vehicle state occurrence, data were processed chronologically. A function was utilized to determine whether the first valve actuation for the folding circuit was to fold or unfold the implement. If the first actuation was unfolding, the implement began in a traveling mode; otherwise, it was either working, turning, or stopped initially. After determining the status of the first point, a decision matrix utilizing the CAN messages of interest was used to determine each data point's vehicle status (figure 5.5).

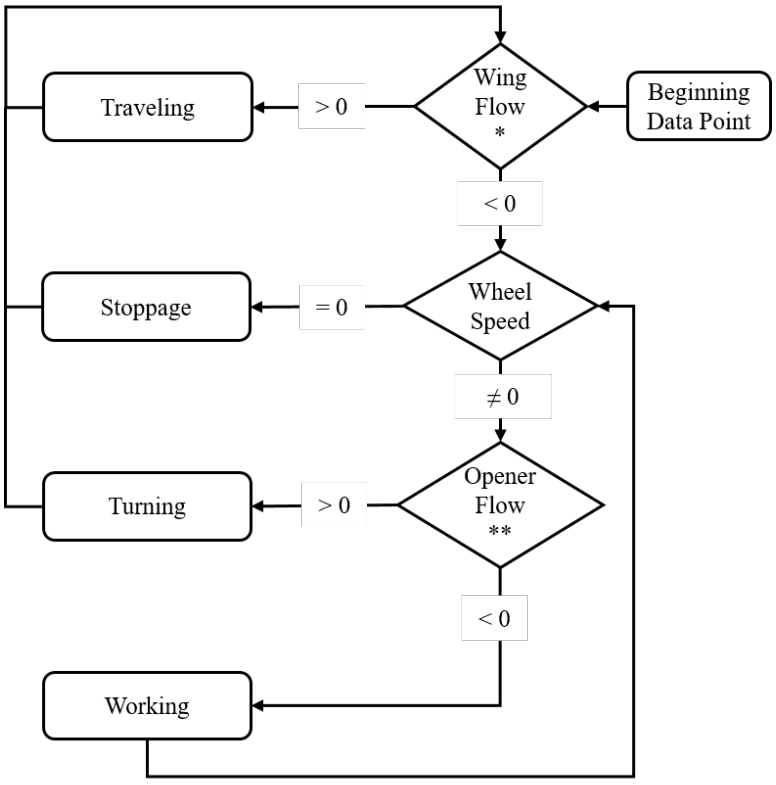

Figure 5.5: *Flow chart defining decision matrix used to distinguish different work states.*

With distinction between different vehicle states, numerous performance characteristics were determined. These included field efficiency both including and

excluding stoppage occurrences and the total time and fuel usage of the field operation excluding traveling states and stoppages if desired. Additionally, upon estimating the effective field size using the implement width and sum of all work pass lengths, the time and fuel requirements per acre were determined. Finally, comparisons were made in fuel and power values between each of the states.

In addition to comparisons within a given field, comparisons were made between different fields. The standard CAN message for elevation reported from the GPS was used to determine topographic traits of each field. Two statistics from the work pass elevation data were determined. The mean standard deviation in reported elevation within each row quantified how much change in elevation existed within each row. An increasing amount of elevation change within a row resulted in varying pitches both potentially within the row and from one row to the next. The standard deviation of the mean reported elevations of each work pass quantified the change in elevation from one row to the next. An increasing standard deviation in mean elevation amongst the work passes indicated an increasing tractor roll angle throughout the operation.

For field comparisons, characteristics of the working vehicle state were analyzed. The effects of field terrain on fuel rate, ground speed, engine torque, and engine speed were explored. To better understand each field, work passes were sorted by uphill versus downhill passes. While it was expected that the pitch CAN message would aid in distinguishing the difference between rows, it was determined that a positive pitch was reported for terrain where no change in elevation existed between points. Additionally, when comparing fields, the mean positive pitch magnitude between points with no

elevation change slightly varied between fields. Thus, a function was used to adjust all pitch data to correct for the error in measurement.

5.4. Results and Discussion

5.4.1. Comparison of Implement Hydraulic Power Requirements

Due to being the state that required a substantially higher overall power requirement, hydraulic power requirements were analyzed across working states only. During a work pass, the fan and downforce circuits were actuated continuously for both planters. As the opener circuit was only actuated at the beginning and end of turning states and the wing circuit was only actuated at the beginning and end of travel states, they were excluded from implement hydraulic power requirement analysis.

A statistical analysis was conducted to determine whether differences existed in flow rate and pressure requirements for both circuits among uphill versus downhill passes, vehicle speeds, and fluid temperatures. Due to the wheat being planted on ground with minimal elevation change, only the rye fields were considered for the analysis. Results provided in greater detail in appendix B concluded that slope and vehicle speed did not affect the resulting flow rate and pressure requirements for either circuit. Fluid temperature, however, resulted in a higher pressure but lower flow rate for both circuits. However, these differences would only exist at the beginning of a field operation. Differences in fan flow rate and pressure requirements existed among the tested fields. This was presumed to be due to differences in operator setting between fields. Given these results, implement hydraulic power requirements were able to be determined independent of different field and operating conditions.

Mean estimates and confidence intervals were found for the mean work pass flow rate and pressure requirements for each circuit for both planters (table 5.2). In comparing planters, the wheat planter had a significantly higher fan flow rate but lower fan pressure requirement than the rye planter. While the downforce and weight transfer circuit flow rates were not significantly different from one another, the rye planter had a significantly higher pressure requirement.

Table 5.2: Mean Work Pass Hydraulic Flow Rate and Pressure Requirements

	Flow Rate (Lpm)		Pressure (MPa)	
Circuit	Mean Value	95% C.I.	Mean Value	95% C.I.
Rye Fan	38.27	(38.14,38.41)	15.80	(15.78,15.82)
Rye Downforce (D.F.)	14.77	(14.08,15.46)	19.47	(19.44,19.50)
Wheat Fan	47.83	(47.44,48.21)	13.24	(13.19,13.29)
Wheat Weight Transfer (W.T.)	15.28	(14.92,15.63)	18.95	(18.94,18.96)

Taking the product of the flow rate and pressure measured in each circuit, an estimated implement hydraulic power requirement was determined. Table 5.3 details the inferred implement hydraulic power requirement at the mean estimate and confidence interval bounds (from table 5.2) for each circuit for both planters. In comparing planters, the wheat fan circuit had a slightly higher power requirement than the rye fan circuit, but the downforce and weight transfer circuit power requirements did not greatly differ. The slightly higher fan power requirement in the wheat planter could potentially be due to the incorporation of fertilizer with the planter. Given the wheat planter contained half the number of row units (32) versus the rye planter (64), the corresponding power requirement per row unit was over double the magnitude for the wheat planter versus the rye planter.

Table 5.3: Mean Work Pass Hydraulic Power Requirements and Tractor Delivery

	Implement Requirements (kW)		Tractor Power (kW)	
Planter	Mean Estimate	Corresponding Power at C.I. Bounds	Mean Estimate	Corresponding Power at C.I. Bounds
Rye Fan	10.08	(10.04,10.12)	17.21	(16.92,17.51)
Rye D.F.	4.789	(4.567,5.011)		
Wheat Fan	10.55	(10.46,10.64)	19.93	(19.68,20.17)
Wheat W.T.	4.829	(4.715,4.942)		

Due to both tractors having a hydraulic system featuring a single pump, the magnitude in hydraulic power produced by the tractor was a function of the sum of implement circuit and primary tractor function flow rates and the highest pressure requirement among all the implement circuits. Primary tractor hydraulic function flow rates were excluded from measurement in this study. However, the estimated power required from the pump for the implement alone using individual circuit estimates (from table 5.2) was determined (table 5.3). From this table, it was seen that the rye planter required less tractor hydraulic power than the wheat planter. In addition, the pump power efficiency was better for the rye planter (86.4%) versus the wheat planter (77.2%) due to the wheat planter fan's lower pressure and higher flow rate requirement. A fan motor with a smaller displacement would assist in improving the efficiency of the wheat planter. With similar pump pressure magnitudes, the addition of primary tractor functions into the hydraulic power calculations would not greatly affect the performance relationship between the two planters.

Due to the weight transfer and downforce circuit design using pressure control valves, fluid pressure produced by the pump was at its maximum magnitude when the circuit was actuated despite the actual pressure requirement of the circuit being less than the stalled

pump pressure. While the implement's downforce or weight transfer circuit power requirements were determined as a function of the measured flow rate and pressure measurement on the delivered flow side only, in reality, the pressure magnitude was determined by the tractor's stalled pump pressure setting. If the bypass valve in the weight transfer circuit on the wheat planter had been properly used, the pressure requirement would have instead been determined by the bypass valve setting. While the bypass valve would have increased the circuit's flow rate, the tractor's pump would have more efficiently provided power. If the implement circuit could be paired with the tractor's hydraulic system to provide only the necessary pressure requirement, a notable pressure reduction could occur without the increase in flow rate.

5.4.2. Effect of Different Field Terrain on Vehicle Performance

Figure 5.6 illustrates the within-row and among-row elevation variance observed for each tested field between both crops. As seen in the figure, a far greater terrain variety existed for the rye cover crop planting applications versus the wheat planting. Thus, analysis of differing terrain on effective fuel rates and produced engine power was done only for selected rye fields.

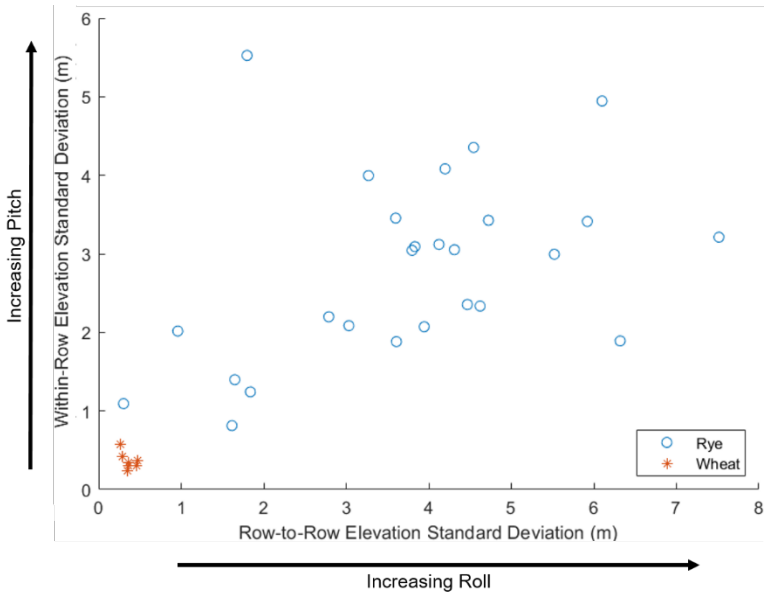

Figure 5.6: *Breakdown of estimated pitch and roll for different conducted fields using elevation work pass data.*

In total, four fields were selected for analysis of differing field terrains. These fields were selected on the premise of analyzing a field with low pitch and roll, high pitch but low roll, high roll but low pitch, and a high pitch and roll. Table 5.4 breaks down each selected field's standard deviation both within each row and among rows. Higher standard deviations in elevation within each row indicated a field with higher pitch characteristics. Higher standard deviations in mean elevation among different rows indicated a field with higher roll characteristics. Figure 5.7 details the geographical vehicle state breakdown for each field.

Table 5.4: Selected Field Pitch and Roll Characteristics

Field Type	Within-Row Elevation Standard Deviation (m)	Among-Row Elevation Standard Deviation (m)
Flat Field	1.24	1.84
Pitch Field	5.53	1.80
Roll Field	1.89	6.32
Pitch and Roll Field	4.95	6.10

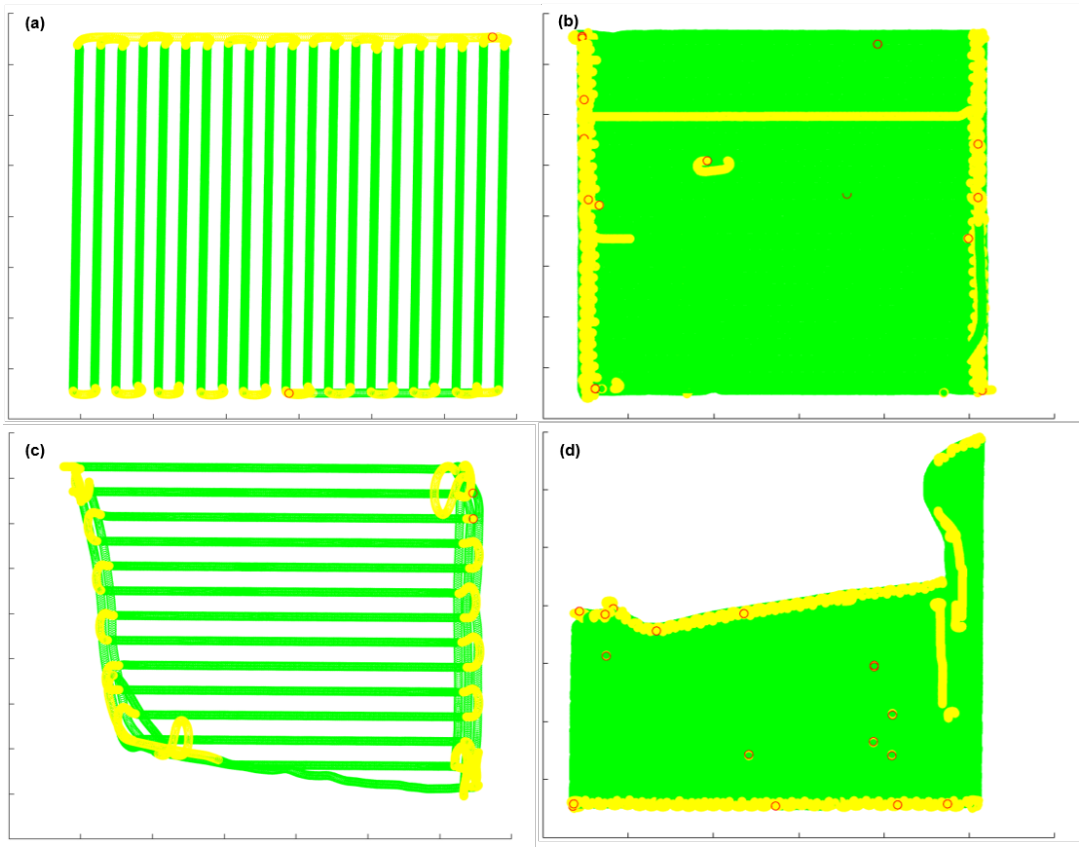

Figure 5.7: *Field shape and vehicle state differentiation for the selected (a) high pitch, low roll field, (b) high pitch, low roll field, (c) low pitch, low roll field, and (d) low pitch, high roll field. Different marker colors distinguish working (green), turning (yellow), and stopped (red) vehicle states.*

Figure 5.8 provides the engine speed and torque measurements, along with the corresponding fuel rate, over working data seen for the pitch and roll field. From this figure, it can be seen that the engine attempted to maintain a given engine speed throughout the field work, but instances occurred where the engine speed became governed by the respected engine torque due to limitation in engine power. Additionally, the figure illustrates that fuel rates greater than 60 L/h indicated instances where the engine was on the lug curve.

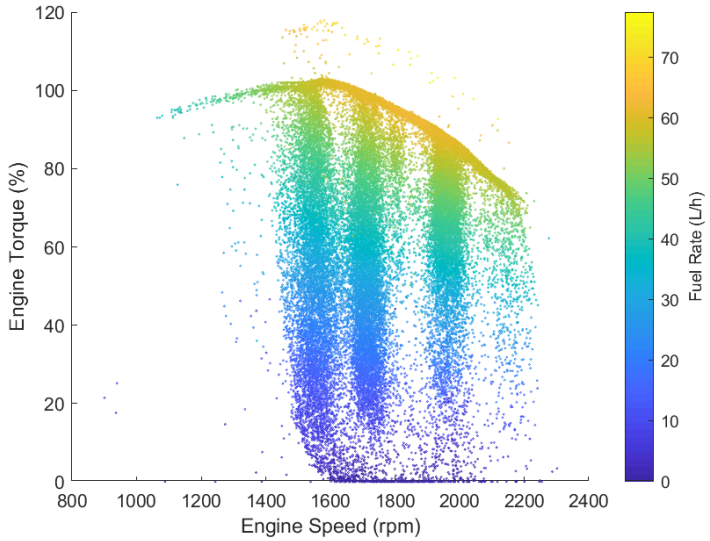

Figure 5.8: *Torque vs engine speed for work passes on the pitch and roll field.*

Figure 5.9 provides a graphical representation of the relationship seen between engine power and fuel rate for the pitch and roll field. As shown in the figure, based on the collected data, a linear relationship existed between engine power and fuel rate. Thus, analysis of fuel rate could be used to also characterize power requirements.

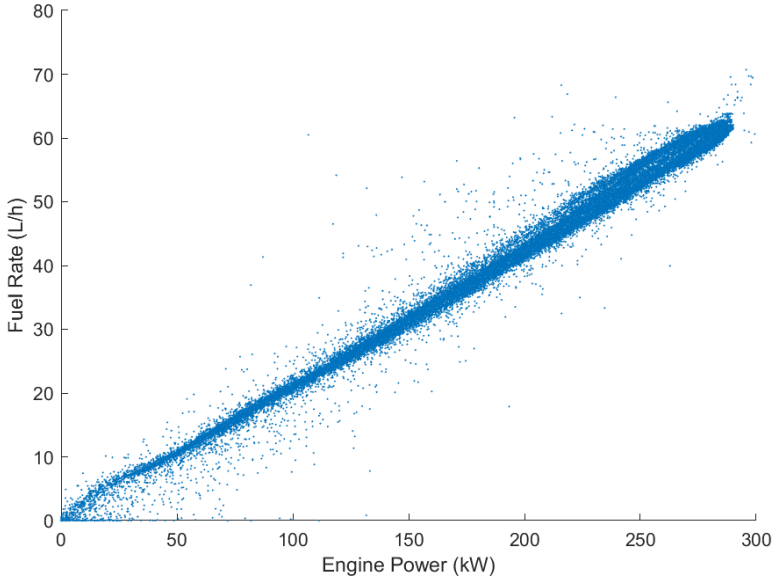

Figure 5.9: *Relationship between fuel rate and engine power seen in the pitch and roll field.*

To understand the effects of power-limited circumstances on vehicle ground speed, the relationship between engine torque and ground speed was analyzed. According to the operator, while a constant ground speed was attempted to be maintained during working vehicle states, a reduction in ground speed was required to cross ditches within a given work pass. Figure 5.10 illustrates the engine torque versus ground speed relationship for the selected pitch and roll field. Two vehicle ground speeds (9.5 km/h and 16 km/h) appeared to contain all power-sufficient data. While the tractor was able to maintain the 9.5 km/h set point, it appeared there were several instances within the field where the 16 km/h ground speed set point could not be maintained due to the tractor's engine becoming power-limited, indicated by fuel rates approaching and exceeding 60 L/h. Thus, vehicle speeds between 10 and 15 km/h predominately represented instances where the engine was power limited, resulting in speeds below the desired 16 km/h setting.

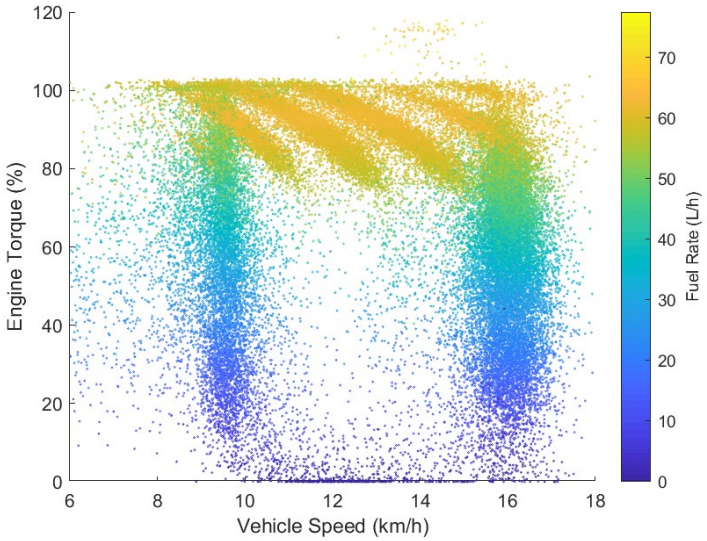

Figure 5.10: *Torque versus GPS-indicated ground speed for roll and pitch field.*

Figure 5.11 illustrates the proportion of vehicle speed observed for each of the four field types. While all four fields had a proportion of field data in the 9-11 km/h range,

the pitch and roll field had a far higher percentage in the range (26.3%) versus the next closest field (15.8% for the roll field). When comparing the low pitch, low roll field versus the pitch field, both of which had a similar percentage of working vehicle state data in the 8-11 km/h range, the flat field had a higher percentage of data in the desired 15-17 km/h range (64.6%) versus the high pitch, low roll field (54.7%). When observing when power-limited instances occurred between uphill and downhill passes for the high pitch, low roll field, as illustrated in figure 5.12, nearly twice the proportion of uphill pass data (42.3%) fell in the 11-15 km/h region versus the downhill pass data (21.7%). A similar observation was seen in the high pitch, high roll field (38.8% for uphill passes versus 19.8% for downhill passes). Thus, an increasing pitch resulted in a higher percentage of data points in a presumed-power limited condition for this operation.

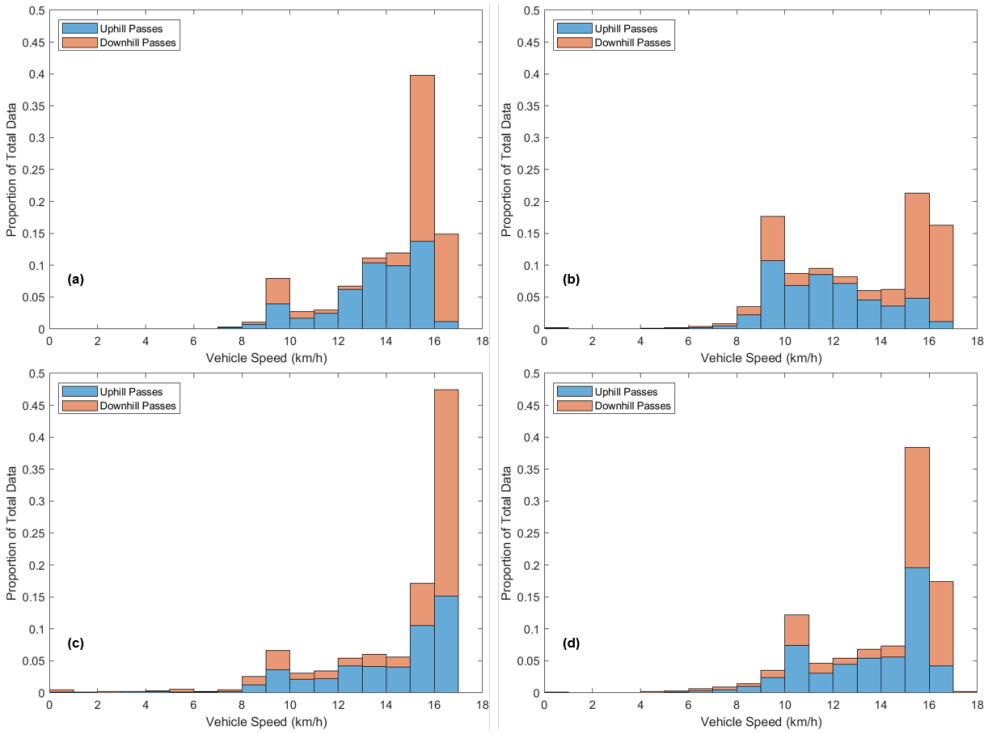

Figure 5.11*: Vehicle speed distribution over working vehicle state data for the selected (a) high pitch, low roll field, (b) high pitch, high roll field, (c) low pitch, low roll field, and (d) low pitch, high roll field.*

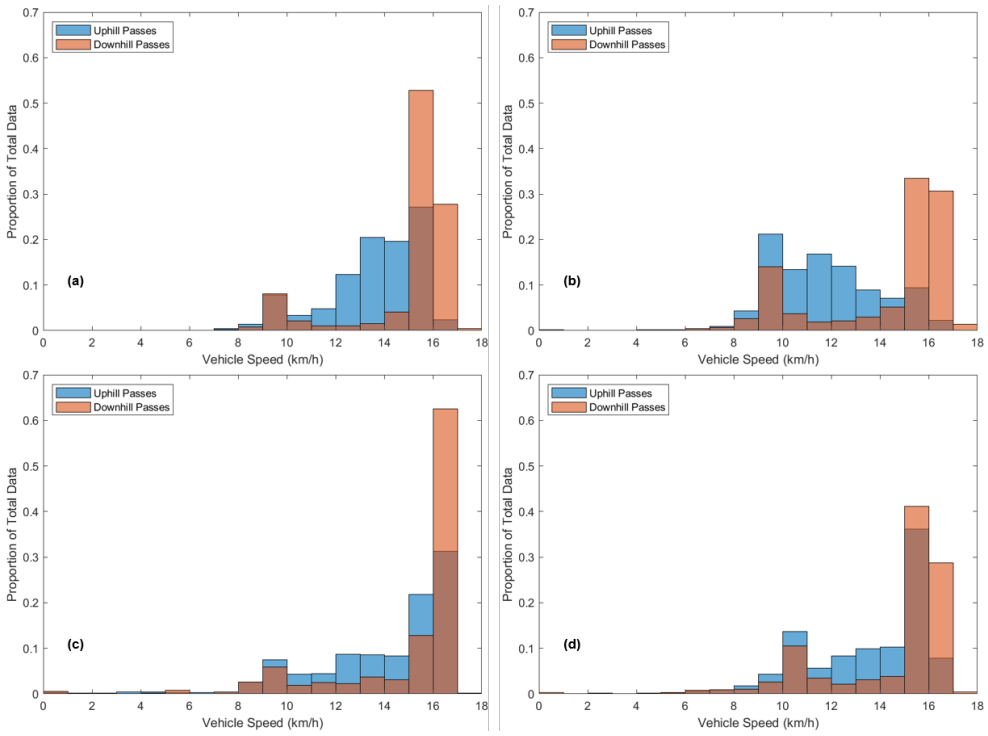

Figure 5.12: *Proportion of uphill and downhill data at given vehicle speeds for the selected (a) high pitch, low roll field, (b) high pitch, high roll field, (c) low pitch, low roll field, and (d) low pitch, high roll field.*

Figure 5.13 illustrates the variation in fuel rate for working vehicle state conditions for each field. As anticipated from the results of the ground speed analysis, a higher proportion of working vehicle state data had a fuel rate magnitude of 60 L/h or greater for the high pitch, low roll field (33.2%) versus the low pitch low roll field (23.1%). When comparing uphill versus downhill passes for the high pitch, high roll field (figure 5.14), 45.8% of uphill pass data had a fuel rate above 60 L/h, while downhill passes only had 18.5% of its data above 60 L/h. However, while the pitch field's uphill passes possessed a greater proportion of data with fuel rates 60 L/h or greater than the low pitch, low roll field, downhill passes had a lower mean fuel rate (46.47 L/h) versus the low pitch, low roll field downhill passes (49.41 L/h).

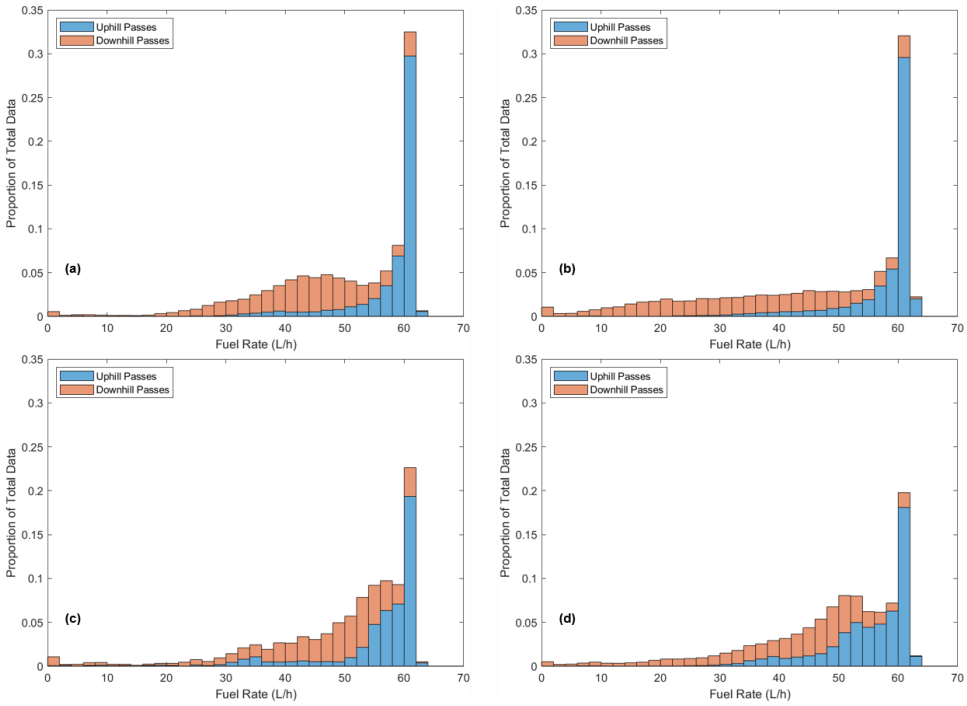

Figure 5.13: *Proportion of working vehicle state data at given fuel rates for the selected (a) pitch field, (b) pitch and roll field, (c) flat field, and (d) roll field.*

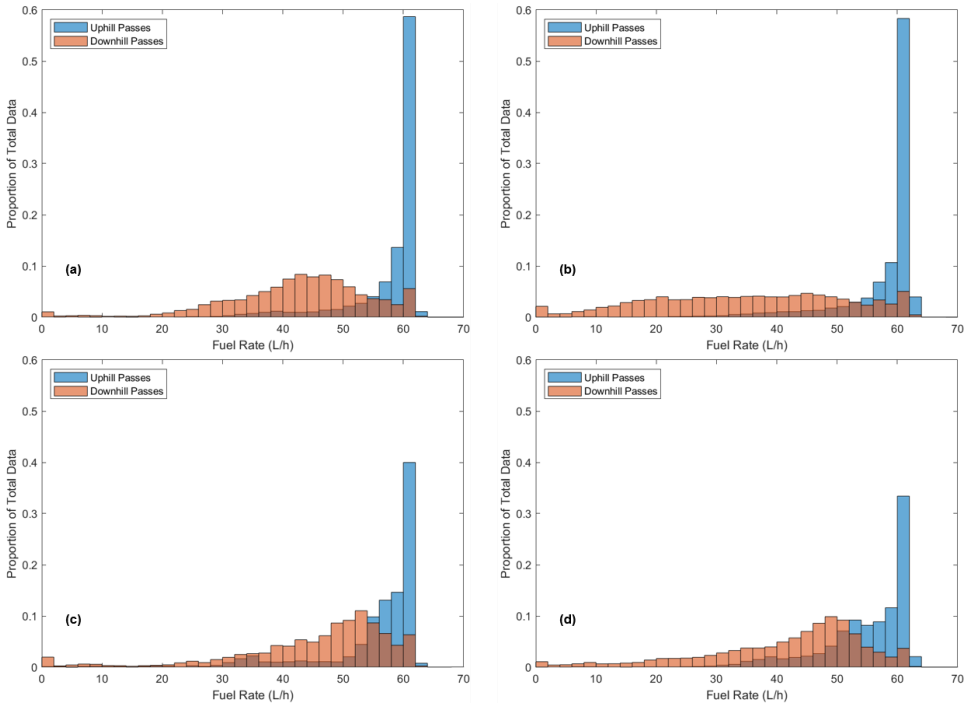

Figure 5.14: *Proportion of uphill and downhill work passes at given fuel rates for the selected (a) pitch field, (b) pitch and roll field, (c) flat field, and (d) roll field.*

Table 5.5 shows the mean vehicle speed and fuel rate seen for each of the four fields examined. Despite the high pitch, high roll field having a greater spread in distribution of fuel rate and vehicle speeds than the low pitch, low roll field, both fields had nearly identical mean ground speeds and fuel rates. From this result, it appeared the resulting mean fuel rate was determined by the vehicle's mean ground speed instead of the amount of elevation change within the field.

Table 5.5: Mean Vehicle Speed and Fuel Rate for Selected Fields

	Mean Vehicle Speed (km/h)	Mean Fuel Rate (L/h)
Flat Field	14.38	50.34
Pitch Field	14.30	50.30
Roll Field	13.87	48.81
Pitch and Roll Field	12.94	46.63

While the tractor used for the rye cover crop planting became power-limited at various instances throughout the field operation, the tractor used with the wheat planting operation was power-sufficient throughout the operation. Shown in figure 5.15, the engine's lug curve could not be defined based on the measured engine speed and torque across the field operation, indicating a lack of power-limited occurrences.

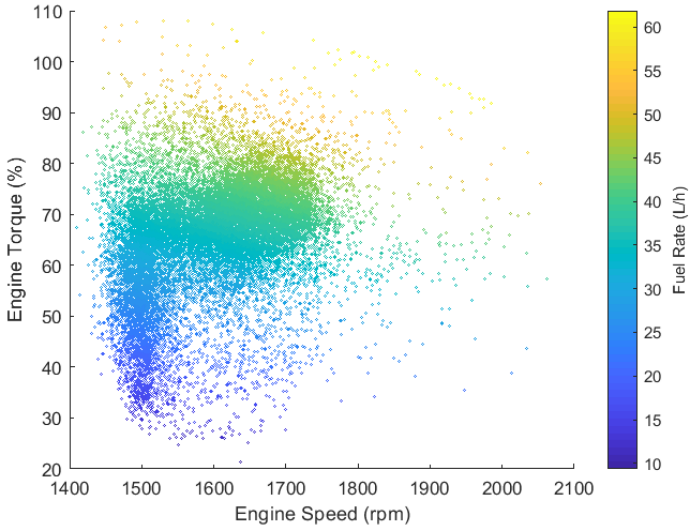

Figure 5.15: *Engine speed and torque and respective fuel rate map for selected wheat field planting operation.*

Figure 5.16 shows the distribution in vehicle speeds and fuel rates for the wheat planting working state data. With 76.5% of vehicle speeds between 8 and 10 kilometers per hour, it is apparent the desired ground speed for the operation was around 9 km/h. Additionally, with similar distributions in fuel rates between uphill and downhill work passes, it appears the field terrain had minimal effect on changes in field power requirements as anticipated by the low variation in elevation.

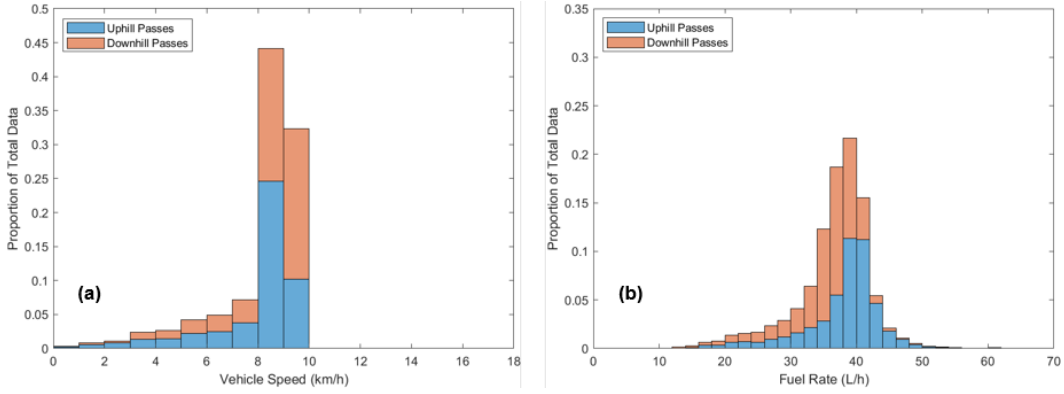

Figure 5.16: *Distribution of (a) vehicle speed and (b) fuel rate over working states for selected wheat planting field.*

From these results, while the rye tractor was appropriately sized for the rye planter, a reduction in tractor size would be possible to accomplish the same field work with wheat planter. Several factors contribute to lower power requirements for the wheat planter versus the rye planter, including a lower operating ground speed, half the working width, and less field elevation variability in the wheat fields versus the rye fields.

5.4.3. Comparison of Field Performance Characteristics

Based on the apparent relationship seen between mean fuel rate and mean vehicle speed, the relationship between the two quantities was compared among each field logged. As mean vehicle speed increased, so also increased the corresponding fuel rate (figure 5.17). Also seen within the figure, the mean vehicle ground speed was generally independent of the field's pitch, with several examples of high pitch fields with a high vehicle speed and low pitch fields with a low vehicle speed. It is presumed that vehicle speed was determined based on whether the previous crop was corn or soybeans and how many ditches were located within the field.

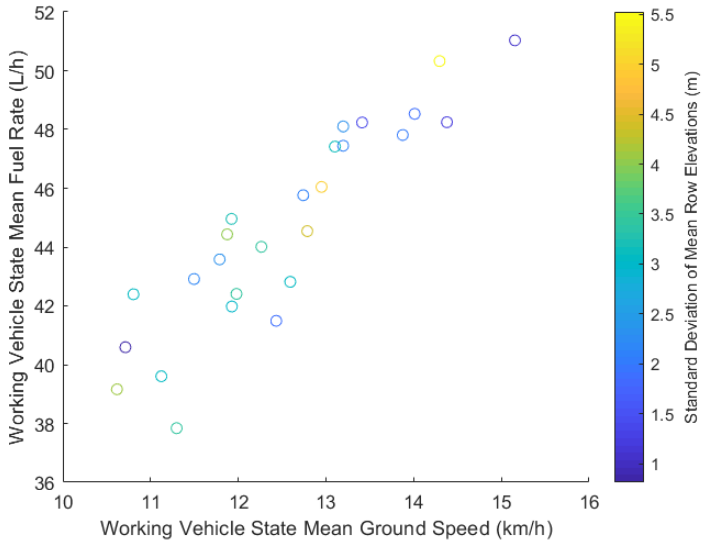

Figure 5.17: *Mean working state fuel rate versus ground speed for all rye fields*

While increasing vehicle speed resulted in higher mean fuel rates, the effects of vehicle speed on time and fuel requirements per area were also analyzed. The fuel requirement for working and turning vehicle states generally decreased per area as vehicle speed increased (figure 5.18). Additionally, considering only time needed for working and turning, the area planted per time consistently increased as mean working state vehicle speed increased (figure 5.19). With a goal of minimizing fuel and time requirements, the operator is at an advantage to plant at higher ground speeds. However, the planter's seed placement ability at higher speeds for given terrain conditions may hinder the operator from being able to go faster. While a far lower number of wheat fields were logged, the same trend was seen in the reduction of fuel and time requirements per area by maintaining a higher mean vehicle speed.

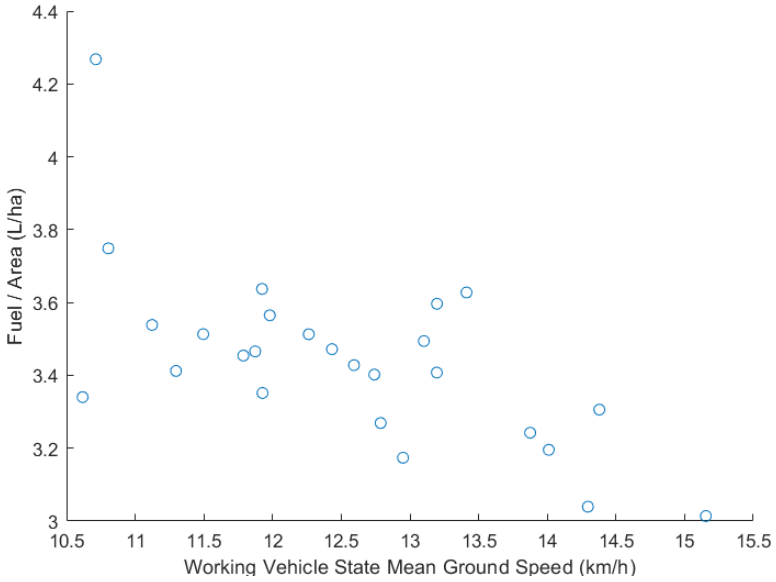

Figure 5.18: *Comparison in fuel requirements per area for rye fields of varying mean vehicle speeds*

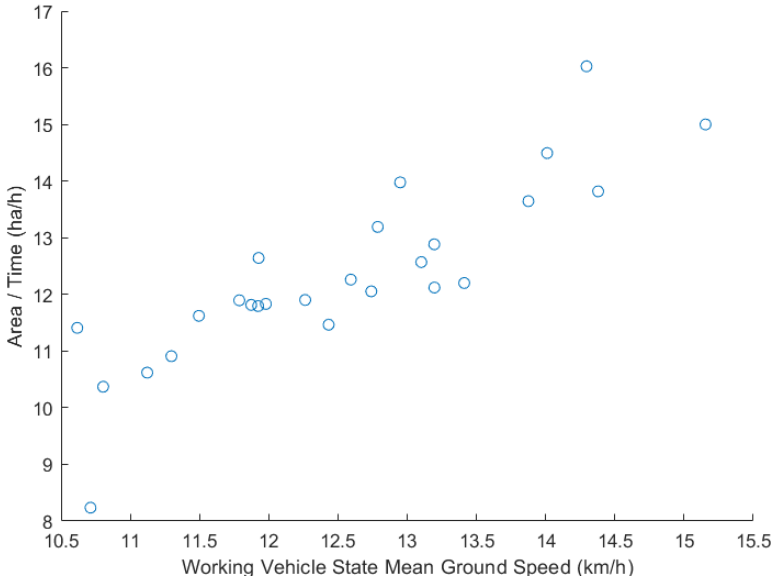

Figure 5.19: *Comparison in effective area covered per time for rye fields of varying mean vehicle speeds.*

A comparison in various performance characteristics between the wheat and rye planting operations is provided in table 5.6. As seen from the table, the tractor and planter combination used for the rye planting far outperformed the tractor and planter combination used with the wheat planting. Benefits of a lower field cost and increased

planting rate stemmed from the increased planter width, faster maintained ground speed, and a higher mean field efficiency, which were dependent on turning time for each field.

Table 5.6: Comparison of Machinery Performance Characteristics between Crops

	Overall Means	
Measurement	Wheat Fields	Rye Fields
Working Width (m)	6.1	12.2
*Efficiency (%)	73.4	84.7
**Ground Speed (km/h)	8.486	12.46
*Area / Time (ha/h)	3.311	12.56
*Fuel / Area (L/ha)	9.309	3.400

* Only considers working and turning states, ** Only considers working states

5.5. Conclusions

Using standard hydraulic control valves and wheel-indicated ground speed CAN messages published on the selected tractors, different vehicle states were able to be classified for planter field operations. This allowed for power and fuel analysis to be conducted for working states among different fields.

In analyzing hydraulic power demand for the rye planter, a statistical analysis determined that factors such as field terrain and vehicle speed had no significant interaction effect on hydraulic power requirements of the fan and downforce circuits actuated during the working state. Comparisons between the rye and wheat planters found that while the overall implement hydraulic power demand was similar between the two implements, the rye planter required less tractor hydraulic power due to a more efficient design with more similar pressure requirements between the fan and downforce circuit. Analyzing from a per-row unit basis, the wheat planter required over twice the amount of power per row unit compared to the wheat planter. Testing of more implements of differing sizes and manufacturers is needed to determine the relationship

between row unit and overall hydraulic power demand, but results from this study found could not determine a relationship existed.

As for overall time, fuel, and power requirements, in comparing the two tractor-implement pairings, the rye planting far outperformed the wheat planting operation. The wheat planting required 274% more fuel and 377% more time to cover the same area the rye planter required. Several factors likely contributed to the stark difference between the operations. These included the rye planter having a larger working width, a higher vehicle speed, and a tractor that was less oversized to handle the implement power requirements. Comparisons within fields of the rye planting operation found that time and fuel requirements per area decreased as vehicle speed increased, validating improved efficiency when a higher percentage of the tractor's power capability was used.

Based on the results from this study, it was determined that the tractor-implement pairing used for the rye planting operation offered both a lower hydraulic power requirement and reduced time and fuel costs to the operator in comparison to the tractor-implement pairing used with the wheat planting operation. From the data analyzed, it appeared a lower power tractor was feasible for usage with the wheat planter than what was used. If the ownership costs associated with a lower power tractor are substantially lower than the increased operating costs and the producer can afford the increased time requirement, the producer may still be financially ahead to use the wheat planter versus the rye planter. However, this study concluded when considering the operating costs alone, the rye planting operation was the better option of the two.

Chapter 6: Overall Conclusions and Future Work

From the studies discussed in detail throughout this thesis, multiple accomplishments were made in improving the ability to conduct field performance studies investigating implement power requirements.

The development of the Sensor CAN Gateway (SCANGate) allowed for a CAN data logger to serve as the sole data acquisition system for field machinery performance studies where added sensors were needed in addition to logging existing CAN messages on the machine to measure all necessary variables. The box converted sensor readings into CAN messages that were published on the ISOBUS. The SCANGate was used across all studies in this thesis.

For field studies involving the measurement of implement hydraulic power requirements, an effective method predicting flow rate utilizing valve spool position and an added minor loss to the system was developed. Usage of this method provided a more compact solution versus using a turbine flowmeter to measure flow rate.

Finally, for machinery performance field operation studies, differentiation between vehicle states was established using standard hydraulic valve and wheel-indicated ground speed CAN messages. This allowed for numerous performance analyses to be conducted among common vehicle states between differing field shapes, implement sizes, vehicle speeds, and topography characteristics.

Going forward, the inclusion of variables needed to determine drawbar and power take off (PTO) power requirements should be added to field analysis studies to truly determine the requirements for different implements. This would provide the ability for

numerous analyses to be conducted comparing similar implements but with differing sizes or designs.

Additionally, further work discussing fuel and time requirements per area for different tractor and implement combinations could be explored. For example, while for this study, it was determined the larger implement used less fuel per area than the smaller implement, perhaps when downsizing the tractor on the smaller implement, this relationship may change. Another factor to further assist producers would be incorporating machinery ownership costs. This, combined with fuel and time costs, would help a producer to determine the most economical machinery cost solution for their operation.

As agricultural machinery technology continues to advance, value exists in determining expected power requirements associated with implements and the performance and associated costs with different combinations of tractor and implement pairings. In an industry striving to meet the global food demands in the coming years, work devoted in this field will assist in equipping producers with the proper machinery needed utilized in the most cost effective and sustainable method.

References

Al-Aani, F. S., Darr, M. J., Covington, B. R., Powell, L. J. (2016). The Performance of Farm Tractors as Reported by CAN-BUS Messages. Presented at the 2016 ASABE Annual International Meeting, American Society of Agricultural and Biological Engineers. https://doi.org/10.13031/aim.20162461746

Badger Meter. (2018). Turbine Flow Sensors, Activa, Ultima, Classic, and Quad: User Manual.

Breidi, F., Garrity, J., Lumkes, J. (2017). Design and Testing of Novel Hydraulic Pump/Motors to Improve the Efficiency of Agricultural Equipment. *Transactions of the ASABE*, *60*(6), 1809–1817. https://doi.org/10.13031/trans.11557

Build and Price. (2019). Retrieved from https://www.caseih.com/northamerica/en-us/Pages/Build-and-Price-Iframe.aspx?series=STEIGER%20TRACTORS

Burgun, C., Lacour, S., Delacroix, A., Descombes, G., Doyen, V. (2013). Computing time and fuel requirements to assess efficiency of a field work from conventional laboratory tests : application to a plowing operation. *AGRICULTURAL AND FOOD SCIENCE*, 15.

Cundiff, J. S. (2001). *Fluid Power Circuits and Controls: Fundamentals and Applications*. CRC Press.

Darr, M. (2012). CAN Bus Technology Enables Advanced Machinery Management. *Resource Magazine*, *19*(5), 10–11. https://doi.org/10.13031/2013.42312

Deere & Company. (2018). *MY18 Tractors 6145R, 6155R, 6155RH, 6175R, 6195R, and 6215R*. Mannheim, DE: John Deere GmbH & Co.

Dell, T. W. (2017). *Hydraulic Systems for Mobile Equipment*. United States: The Goodheart-Willcox Company, Inc.

DEMCO Harvest Equipment. (2018). Retrieved from https://www.demco-products.com/assets/users/documents/AG11008_Rev24_Harvest_Brochure_LR.pdf

Edwards, W. (2017). Farm Machinery Selection. *Ag Decision Maker*, *File A3-28*.

Hanigan, M. (2018). *Volumetric yield sensing in a combine harvester*. Iowa State University. Retrieved from https://lib.dr.iastate.edu/cgi/viewcontent.cgi?article=7376&context=etd

Harrigan, T. M., Rotz, C. A. (1995). Draft relationships for tillage and seeding equipment. *Applied Engineering in Agriculture*, *11*(6), 773–783.

Hollingshead, C. L. (2011). *Discharge Coefficient Performance of Venturi, Standard Concentric Orifice Plate, V-Cone, and Wedge Flow Meters at Small Reynolds Numbers*. Utah State University.

Kortenbruck, D., Griepentrog, H. W., Paraforos, D. S. (2017). Machine operation profiles generated from ISO 11783 communication data. *Computers and Electronics in Agriculture*, *140*, 227–236. https://doi.org/10.1016/j.compag.2017.05.039

Kvaser. (2019). J1939 Introduction. Retrieved May 11, 2019, from https://www.kvaser.com/about-can/higher-layer-protocols/j1939-introduction/

Lacour, S., Burgun, C., Perilhon, C., Descombes, G., Doyen, V. (2014). A model to assess tractor operational efficiency from bench test data. *Journal of Terramechanics*, *54*, 1–18. https://doi.org/10.1016/j.jterra.2014.04.001

Lipták, B. G., Venczel, K. (1982). *Instrument Engineers' Handbook: Process Measurement*. Radnor, Pennsylvania: Chilton Book Co.

Love, L. J. (2012). *Estimating the Impact (Energy, Emissions and Economics) of the US Fluid Power Industry* (No. ORNL/TM-2011/14, 1061537). https://doi.org/10.2172/1061537

Manring, N. (2005). *Hydraulic Control Systems*. Hoboken, NJ: John Wiley & Sons, Inc.

Marx, S. E., Luck, J. D., Hoy, R. M., Pitla, S. K., Blankenship, E. E., Darr, M. J. (2015). Validation of machine CAN bus J1939 fuel rate accuracy using Nebraska Tractor Test Laboratory fuel rate data. *Computers and Electronics in Agriculture*, *118*, 179–185. https://doi.org/10.1016/j.compag.2015.08.032

McLaughlin, N. B., Heslop, L. C., Buckley, D. J., Amour, G. S., Compton, B. A., Jones, A. M., Van Bodegom, P. (1993). A general purpose tractor instrumentation and data logging system. *Transactions of the ASAE*, *36*(2), 265–273.

Molari, G., Mattetti, M., Perozzi, D., Sereni, E. (2013). Monitoring of the tractor working parameters from the CAN-Bus. *Journal of Agricultural Engineering*, *44*(2s). https://doi.org/10.4081/jae.2013.s2.e77

Nebraska Tractor Test Laboratory. (2016a). *Nebraska OECD Tractor Test 2146 - Summary 1009 John Deere 6145R Autoquad-Plus Diesel 20 Speed*. University of Nebraska-Lincoln. Retrieved from https://tractortestlab.unl.edu/John%20Deere%206145R.pdf

Nebraska Tractor Test Laboratory. (2016b). *Nebraska OECD Tractor Test 2165 - Summary 1046 Case IH Steiger 620 Quadtrac Diesel 16 Speed*. University of

Nebraska-Lincoln. Retrieved from https://tractortestlab.unl.edu/Case%20IH%20Steiger%20620.pdf

Options for 9370R Cab Tractor. (2019). Retrieved April 22, 2019, from https://configure.deere.com/cbyo/#/en_us/configure/67221761

Pitla, Santosh K., Luck, J. D., Werner, J., Lin, N., Shearer, S. A. (2016). In-field fuel use and load states of agricultural field machinery. *Computers and Electronics in Agriculture*, *121*, 290–300. https://doi.org/10.1016/j.compag.2015.12.023

Pitla, S.K., Lin, N., Shearer, S. A., Luck, J. D. (2014). Use of Controller Area Network (CAN) Data To Determine Field Efficiencies of Agricultural Machinery. *Applied Engineering in Agriculture*, 829–838. https://doi.org/10.13031/aea.30.10618

Roeber, J. B. W., Pitla, S. K., Kocher, M. F., Luck, J. D., Hoy, R. M. (2016). Tractor hydraulic power data acquisition system. *Computers and Electronics in Agriculture*, *127*, 1–14. https://doi.org/10.1016/j.compag.2016.05.012

Rohrer, R. (2017). Investigation of Petroleum Use in Off-road Agricultural Machinery and Analysis of J1939 Controller Area Network (CAN) Data for Advanced Machinery Testing.

Rotz, C. A., Muhtar, H. A. (1992). Rotary power requirements for harvesting and handling equipment. *Applied Engineering in Agriculture*, *8*(6), 751–757.

Srivastava, A. K., Goering, C. E., Rohrbach, R. P., Buckmaster, D. R. (2012). *Engineering principles of agricultural machines*. St. Joseph, MI: ASABE.

Stone, M. L., Benneweis, R. K., Van Bergeijk, J. (2008). Evolution of electronics for mobile agricultural equipment. *Transactions of the ASABE*, *51*(2), 385–390.

Stone, M. L., McKee, K. D., Formwalt, C. W., Benneweis, R. K. (1999). ISO 11783: An Electronic Communications Protocol for Agricultural Equipment. Presented at the Agricultural Equipment Technology Conference, Louisville, KY: ASAE. Retrieved from https://elibrary.asabe.org/data/pdf/6/ddp2002/lecture23.pdf

Stoss, K. J., Sobotzik, J., Shi, B., Kreis, E. (2013). Tractor Power for Implement Operation: Mechanical, Hydraulic, and Electrical: an Overview. Presented at the Agricultural Equipment Technology Conference, Kansas City, MO: ASABE. Retrieved from https://elibrary.asabe.org/azdez.asp?AID=42518&T=2

Voss, W. (2018). SAE J1939 Programming with Arduino - SAE J1939/21 - Transport Protocol (TP). Retrieved May 11, 2019, from https://copperhilltech.com/blog/sae-j1939-programming-with-arduino-sae-j193921-transport-protocol-tp/

White, R. G. (1977). Matching Tractor Horsepower and Farm Implement Size. *Extension Bulletin*, *E-1152 SF 11*(SF 1). Retrieved from https://archive.lib.msu.edu/DMC/Ag.%20Ext.%202007-Chelsie/PDF/e1152.pdf

Appendix A– Flow Rate Prediction Equations

A.1. Orifice Best-Fit Determination Tables

$$y_{ss} = \frac{Ax + B}{1x^3 + Cx^2 + Dx + E} \quad \text{(Eq. 14)}$$

where
y_{ss} = flow rate at steady-state fluid temperature (L min^{-1})
x = pressure difference across added loss (MPa)
A,B,C,D,E determined by orifice and flow direction.

Table A.1: Orifice Flowmeter Flow Rate Prediction Coefficients

Orifice Number / Direction	*A*	*B*	*C*	*D*	*E*
281 / I	120.9	-1.287	-1.791	1.583	0.1926
281 / T	232.4	8.688	-2.189	2.635	0.5119
295 / I	314.8	-1.102	-2.632	3.625	0.5612
295 / T	232.4	8.688	-2.189	2.635	0.5119

*I = Implement Flow Direction, T = Tractor Flow Direction

Table A.2: Orifice Flowmeter Flow Rate Prediction Coefficient 95% Confidence Intervals

	A	*B*	*C*	*D*	*E*
281 / I	(77.53, 164.3)	(-2.071, -0.5030)	(-1.893, -1.690)	(1.285, 1.882)	(0.06809, 0.3171)
281 / T	(171.5, 293.3)	(5.794, 11.58)	(-2.386, -1.992)	(2.110, 3.160)	(0.3478, 0.6760)
295 / I	(88.63, 541.0)	(-2.873, 0.6689)	(-3.356, -1.908)	(1.605, 5.644)	(0.0449, 1.078)
295 / T	(171.5, 293.3)	(5.794, 11.58)	(-2.386, -1.992)	(2.110, 3.160)	(0.3478, 0.6760)

*I = Towards Implement Flow Direction, T = Towards Tractor Flow Direction

Table A.3: Comparison of Implement Flow Direction Flow Rates between Orifices

Pressure Drop (MPa)	Orifice 281 Flow Rate (Lpm)	Orifice 295 Flow Rate (Lpm)	Difference (%)
0.025	7.51	10.41	38.55
0.075	25.80	27.49	6.58
0.125	37.94	39.22	3.38
0.175	47.30	48.19	1.88
0.225	55.20	55.56	0.65
0.275	62.27	61.94	0.53
0.325	68.82	67.67	1.68
0.375	75.03	72.95	2.77
0.425	80.98	77.91	3.79
0.475	86.69	82.63	4.68
0.525	92.16	87.16	5.42
0.575	97.36	91.54	5.98
0.625	102.24	95.78	6.31
0.675	106.72	99.89	6.40
0.725	110.73	103.87	6.20
0.775	114.20	107.70	5.69
0.825	117.06	111.39	4.84
0.875	119.24	114.91	3.63
0.925	120.70	118.24	2.04
0.975	121.41	121.36	0.05

Table A.4: Comparisons of Expected Flow Rate for Different Flow Directions

Pressure Drop (MPa)	Tractor Flow Direction (Lpm)	Implement Flow Direction (Lpm)		Difference in Directions (%)	
	Both Orifices	281	295	281	295
-0.01	13.11	X	X	X	X
0.04	29.30	14.02	16.37	-52.13	-44.14
0.09	40.44	29.87	31.41	-26.15	-22.32
0.14	49.04	40.96	42.13	-16.48	-14.08
0.19	56.19	49.79	50.53	-11.40	-10.07
0.24	62.46	57.39	57.56	-8.12	-7.85
0.29	68.16	64.28	63.72	-5.68	-6.51
0.34	73.45	70.72	69.30	-3.72	-5.66
0.39	78.46	76.84	74.47	-2.06	-5.09
0.44	83.25	82.72	79.35	-0.64	-4.69
0.49	87.85	88.36	84.01	0.58	-4.38
0.54	92.29	93.75	88.49	1.59	-4.12
0.59	96.56	98.86	92.83	2.38	-3.87
0.64	100.67	103.62	97.03	2.94	-3.62
0.69	104.58	107.97	101.10	3.24	-3.33
0.74	108.29	111.83	105.03	3.27	-3.01
0.79	111.77	115.13	108.83	3.01	-2.63
0.84	114.98	117.78	112.46	2.44	-2.19
0.89	117.89	119.75	115.93	1.58	-1.67
0.94	120.49	120.99	119.19	0.42	-1.07

A.2. Lab Study Tractor Valve Position Flow Rate Predictive Equations

$$y_{ss} = Ax^3 + Bx^2 + Cx + D \quad \text{(Eq. 15)}$$

where
y_{ss} = flow rate (L min^{-1})
x = valve spool position (%)
A,B,C,D determined by tractor, valve number, and actuation direction

Table A.5 Tractor A (JD 6145R) Valve Position Flow Rate Coefficients

Valve / Direction	A	B	C	D
1E	-1.77E-4	0.0352	-0.4609	6.925
1R	-1.51E-4	0.0314	-0.3714	3.924
2E	-1.22E-4	0.0265	0.0897	-0.9486
2R	-2.74E-4	0.0496	-1.123	16.49
3E	-4.11E-5	0.0159	0.5139	-7.014
3R	-2.63E-4	0.0504	-1.320	19.75

*E = Extend Direction, R = Retract Direction

Table A.6: Tractor A (JD 6145R) Coefficient 95% Confidence Intervals

	A	B	C	D
1E	(-2.261E-4, -1.275E-4)	(0.0271, 0.0432)	(-0.8833, -0.0386)	(-0.1765, 14.03)
1R	(-1.65E-4, -1.37E-4)	(0.0290, 0.0339)	(-0.5026, -0.2402)	(1.743, 6.104)
2E	(-2.55E-4, 1.15E-5)	(5.52E-3, 0.0475)	(-0.9472, 1.127)	(-16.90, 15.00)
2R	(-3.48E-4, -2.01E-4)	(0.0369, 0.0624)	(-1.816, -0.4308)	(4.836, 28.14)
3E	(-6.49E-5, -1.73E-5)	(0.0122, 0.0196)	(0.3333, 0.6946)	(-9.755, -4.273)
3R	(-3.61E-4, -1.65E-4)	(0.0335, 0.0674)	(-2.244, -0.3962)	(4.190, 35.30)

*E = Extend Direction, R = Retract Direction

Table A.7: Tractor B (JD 6145R) Valve Position Flow Rate Coefficients

Valve / Direction*	A	B	C	D
1E	0	3.38E-4	1.269	-7.704
1R	0	2.59E-3	1.023	-6.507
2E	0	4.32E-3	1.277	-8.934
2R	0	1.74E-3	1.136	-8.145

*E = Extend Direction, R = Retract Direction

Table A.8: Tractor B (JD 6145R) Coefficient 95% Confidence Intervals

	A	B	C	D
1E	X	(-6.22E-4, 1.298E-3)	(1.163, 1.375)	(-10.23, -5.183)
1R	X	(1.77E-3, 3.41E-3)	(0.9256, 1.121)	(-9.106, -3.908)
2E	X	(-3.45E-4, 1.21E-4)	(1.189, 1.365)	(-11.17, -6.694)
2R	X	(9.87E-4, 2.49E-3)	(1.049, 1.223)	(-10.42, -5.866)

*E = Extend Direction, R = Retract Direction

A.3. Field Study Tractor Valve Position Flow Rate Predictive Equations

$$y_{ss} = \begin{cases} C_L x + D_L \; for \; x \leq 55 \\ Ax^3 + Bx^2 + Cx + D \; for \; x > 55 \end{cases} \quad \text{(Eq. 16)}$$

where
y_{ss} = flow rate (L min^{-1})
x = valve spool position (%)
A,B,C,D,C_L,D_L determined by tractor, valve number, and actuation direction

Table A.9: Wheat Tractor (JD 8320R) Valve Position Flow Rate Coefficients

Valve / Direction*	C_L	D_L	*A*	*B*	*C*	*D*
1E	0.8737	-18.68	-9.19E-5	0.0359	-1.734	32.6
1R	0.8596	-10.41	6.54E-4	-0.1608	14.95	-407.6
2E	0.8966	-17.69	-1.67E-4	0.0476	-2.231	38.74
2R	0.8448	-10.05	2.80E-4	-0.0834	9.807	-297.1
3E	0.9204	-19.37	-3.69E-4	0.0925	-5.440	113.1
3R	0.8879	-11.00	-6.18E-5	-7.13E-3	4.094	-153.1
4E	0.905	-20.39	-2.19E-4	0.0649	-3.906	85.74
4R	0.9597	-10.79	2.84E-4	-0.0911	10.50	-301.1

*E = Extend Direction, R = Retract Direction

Table A.10: Wheat Tractor (JD 8320R) Coefficient 95% Confidence Intervals

	C_L	D_L	A	B	C	D
1E	(0.8477, 0.8997)	(-19.78, -17.58)	(-4.02E-4, 2.19E-4)	(-0.0364, 0.1081)	(-7.252, 3.784)	(-105.5, 170.7)
1R	(0.8116, 0.9077)	(-12.27, -8.547)	(-3.18E-4, 9.90E-4)	(-0.2380, -0.8363)	(9.128, 20.76)	(-551.5, -263.7)
2E	(0.8732, 0.9200)	(-18.68, -16.69)	(-3.56E-4, 2.145E-5)	(3.75E-3, 0.0915)	(-5.580, 1.117)	(-44.96, 122.4)
2R	(0.7950, 0.8946)	(-12.03, -8.067)	(-3.59E-5, 5.97E-4)	(-0.1570, -9.84E-3)	(4.189, 15.43)	(-437.7, -156.6)
3E	(0.9037, 0.9372)	(-20.08, -18.66)	(-6.37E-4, -1.01E-4)	(0.0301, 0.1549)	(-10.20, -0.6769)	(-5.977, 232.1)
3R	(0.8367, 0.9391)	(-12.99, -9.02)	(-4.46E-4, 3.22E-4)	(-0.965, 0.0821)	(-2.723, 10.91)	(-323.5, 17.36)
4E	(0.8784, 0.9316)	(-21.55, -19.23)	(-5.56E-4, 1.18E-4)	(-0.0136, 0.1434)	(-9.898, 2.086)	(-64.19, 235.7)
4R	(0.8963, 1.023)	(-13.18, -8.396)	(-1.71E-5, 7.389E-4)	(-0.197, 0.0149)	(2.415, 18.58)	(-503.2, -99.03)

*E = Extend Direction, R = Retract Direction

Table A.11: Rye Tractor (JD 8320RT) Valve Position Flow Rate Coefficients

Valve / Direction	C_L	D_L	A	B	C	D
2E	0.9118	-17.30	4.55E-4	-0.1015	9.510	-257.6
2R	0.8664	-10.67	4.56E-4	-.1186	11.86	-332.8
4E	0.8825	-16.36	2.34E-4	-0.0503	5.588	-160.8
4R	0.9053	-11.00	8.59E-4	-0.2075	18.35	-483.1

*E = Extend Direction, R = Retract Direction

Table A.12: Rye Tractor (JD 8320RT) Coefficient 95% Confidence Intervals

	C_L	D_L	A	B	C	D
2E	(0.8894, 0.9341)	(-18.22, -16.37)	(6.023E-5, 8.499E-4)	(-0.1935, -.00964)	(2.495, 16.52)	(-433.0, -82.29)
2R	(0.8262, 0.9066)	(-12.22, -9.11)	(7.58E-5, 8.38E-4)	(-0.2065, -0.0291)	(5.093, 18.64)	(-502.3, -163.4)
4E	(0.8567, 0.9082)	(-17.45, -15.27)	(-5.49E-5, 5.22E-4)	(-0.1175, 0.01684)	(0.4617, 10.71)	(-288.9, -32.61)
4R	(0.8485, 0.9621)	(-13.14, -8.857)	(6.29E-4, 1.09E-3)	(-0.2604, -0.1546)	(14.36, 22.33)	(-581.8, -384)

*E = Extend Direction, R = Retract Direction

Appendix B – Field Hydraulic Power Variable Statistical Analyses

A statistical analysis was conducted to determine whether geographical topography, vehicle speed, or fluid temperature impacted the resulting flow rate and pressure requirements for the fan and downforce circuits on the rye planter. The mean flow rate and pressure seen within each work pass for both circuits for different fields served as the data sets used in the analysis. Each variable was blocked by field to exclude effects that may vary within each field. Table B.1 details the associated levels with each factor tested. In addition to main effects, interaction effects were tested between field and slope, and slope and vehicle speed. The SAS outputs below detail results from the analysis.

Table B.1: Factors and Levels Tested for Implement Hydraulic Variable Field Statistical Analysis

Factors (SAS variable)	Levels shown in SAS Program	Description of Level
Field Number (field_num)	1-23	Given field where data was collected
Field Topography (slope)	1	Work pass defined as uphill for a given field
	2	Work pass defined as downhill for a given field
Vehicle Ground Speed (spd)	0	Mean work pass ground speed less than 10.5 km/h
	1	Mean work pass ground speed between 10.5 km/h and 14 km/h
	2	Mean work pass ground speed greater than 14 km/h
Hydraulic Oil Temperature (temp)	0	Mean work pass oil temperature below 50°C
	1	Mean work pass oil temperature between 50°C and 65°C
	2	Mean work pass oil temperature greater than 65°C

The SAS System

The GLIMMIX Procedure

Model Information	
Data Set	WORK.HYD_DATA
Response Variable	fr
Response Distribution	Gaussian
Link Function	Identity
Variance Function	Default
Variance Matrix	Diagonal
Estimation Technique	Restricted Maximum Likelihood
Degrees of Freedom Method	Residual

Class Level Information		
Class	Levels	Values
field_num	24	11-15.2_field1 11-15.2_field2 11-15.3_field1 11-15.3_field2 11-15.5_field1 11-15.6_field1 11-15.7_field1 11-15.9_field3 11-15.9_field4 11-20.3_field1 11-20.3_field2 11-20.3_field3 11-20.3_field4 11-20.4_field2 11-21.1_field2 11-27.2_field1 11-27.2_field2 11-27.2_field4 11-27.2_field5 11-27.2_field6 11-27.4_field1 11-27.4_field2 11-27.4_field3 11-27.4_field4
slope	2	1 2
spd	3	0 1 2
temp	3	0 1 2

Number of Observations Read	1131
Number of Observations Used	1131

Type III Tests of Fixed Effects				
Effect	Num DF	Den DF	F Value	Pr > F
field_num	23	1077	22.20	<.0001
slope	1	1077	0.18	0.6735
spd	2	1077	1.62	0.1989
slope*spd	2	1077	0.70	0.4987
temp	2	1077	38.22	<.0001
field_num*slope	23	1077	0.87	0.6460

temp Least Squares Means								
temp	Estimate	Standard Error	DF	t Value	Pr > |t|	Alpha	Lower	Upper
0	36.7812	0.3743	1077	98.26	<.0001	0.05	36.0467	37.5157
1	36.6686	0.2456	1077	149.32	<.0001	0.05	36.1868	37.1505
2	38.5825	0.08416	1077	458.47	<.0001	0.05	38.4174	38.7477

Differences of temp Least Squares Means									
temp	_temp	Estimate	Standard Error	DF	t Value	Pr > |t|	Alpha	Lower	Upper
0	1	0.1126	0.4298	1077	0.26	0.7934	0.05	-0.7308	0.9560
0	2	-1.8013	0.3754	1077	-4.80	<.0001	0.05	-2.5379	-1.0647
1	2	-1.9139	0.2477	1077	-7.73	<.0001	0.05	-2.3999	-1.4279

Figure B.1: *SAS output detailing results for the fan flow rate. From the results, significant differences only existed between fields and fluid temperatures.*

The SAS System

The GLIMMIX Procedure

Model Information	
Data Set	WORK.HYD_DATA
Response Variable	hi_press
Response Distribution	Gaussian
Link Function	Identity
Variance Function	Default
Variance Matrix	Diagonal
Estimation Technique	Restricted Maximum Likelihood
Degrees of Freedom Method	Residual

Class Level Information		
Class	Levels	Values
field_num	24	11-15.2_field1 11-15.2_field2 11-15.3_field1 11-15.3_field2 11-15.5_field1 11-15.6_field1 11-15.7_field1 11-15.9_field3 11-15.9_field4 11-20.3_field1 11-20.3_field2 11-20.3_field3 11-20.3_field4 11-20.4_field2 11-21.1_field2 11-27.2_field1 11-27.2_field2 11-27.2_field4 11-27.2_field5 11-27.2_field6 11-27.4_field1 11-27.4_field2 11-27.4_field3 11-27.4_field4
slope	2	1 2
spd	3	0 1 2
temp	3	0 1 2

Number of Observations Read	1131
Number of Observations Used	1131

Type III Tests of Fixed Effects				
Effect	Num DF	Den DF	F Value	Pr > F
field_num	23	1077	88.72	<.0001
slope	1	1077	0.39	0.5317
spd	2	1077	0.37	0.6918
slope*spd	2	1077	1.27	0.2806
temp	2	1077	79.92	<.0001
field_num*slope	23	1077	1.52	0.0559

temp Least Squares Means								
temp	Estimate	Standard Error	DF	t Value	Pr > |t|	Alpha	Lower	Upper
0	16.3709	0.04674	1077	350.23	<.0001	0.05	16.2792	16.4627
1	15.7587	0.03067	1077	513.88	<.0001	0.05	15.6985	15.8188
2	15.7863	0.01051	1077	1502.14	<.0001	0.05	15.7657	15.8069

Differences of temp Least Squares Means									
temp	_temp	Estimate	Standard Error	DF	t Value	Pr > |t|	Alpha	Lower	Upper
0	1	0.6123	0.05368	1077	11.41	<.0001	0.05	0.5069	0.7176
0	2	0.5847	0.04688	1077	12.47	<.0001	0.05	0.4927	0.6766
1	2	-0.02761	0.03093	1077	-0.89	0.3723	0.05	-0.08829	0.03308

Figure B.2: *SAS output detailing results for the fan pressure requirements. From the results, significant differences only existed between fields and fluid temperatures.*

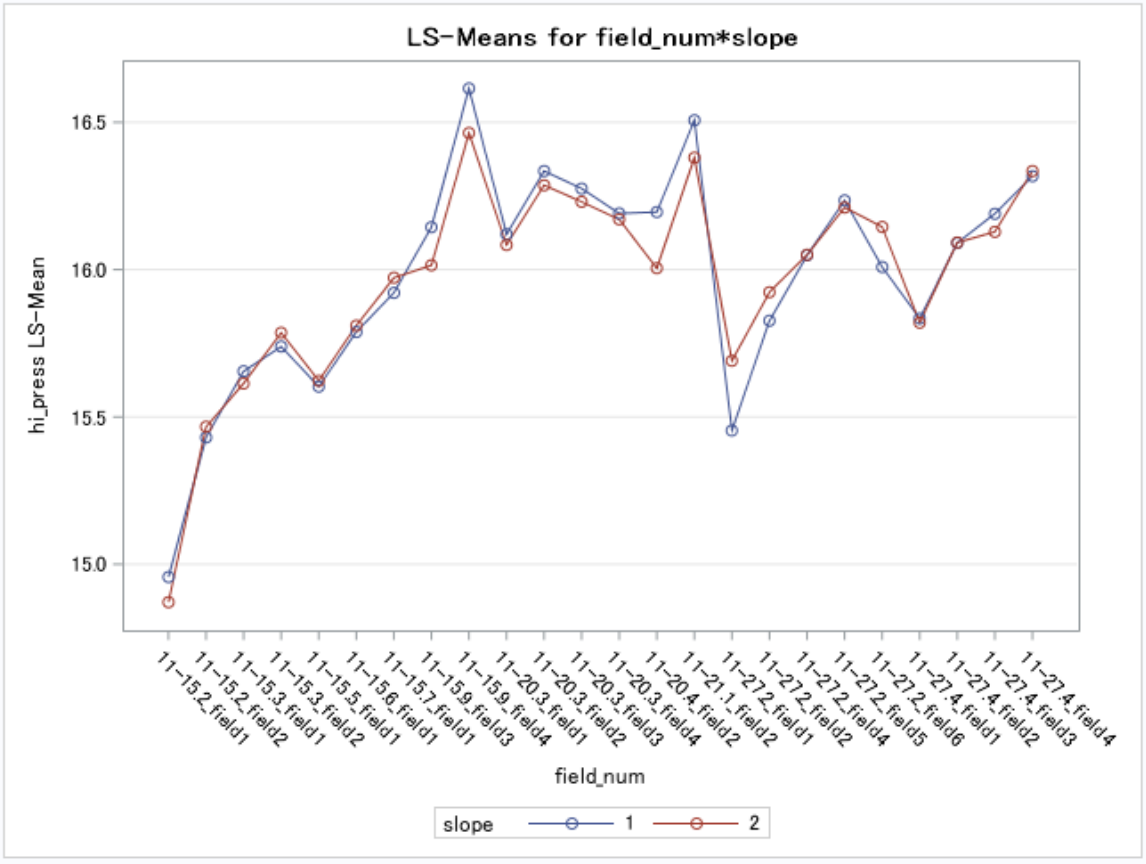

Figure B.3: *Plot illustrating differences in pressure between uphill versus downhill passes across different fields. From this figure, it is seen that overall, despite a lower p-value, great deviation does not exist.*

The SAS System

The GLIMMIX Procedure

Model Information	
Data Set	WORK.HYD_DATA
Response Variable	fr
Response Distribution	Gaussian
Link Function	Identity
Variance Function	Default
Variance Matrix	Diagonal
Estimation Technique	Restricted Maximum Likelihood
Degrees of Freedom Method	Residual

Class Level Information		
Class	Levels	Values
field_num	2	10-21.1_field1 10-21.2_field1
slope	2	1 2
spd	2	0 1
temp	3	0 1 2

Number of Observations Read	66
Number of Observations Used	66

Type III Tests of Fixed Effects				
Effect	Num DF	Den DF	F Value	Pr > F
field_num	1	58	3.53	0.0652
slope	1	58	0.05	0.8199
spd	1	58	0.76	0.3878
slope*spd	1	58	0.69	0.4110
temp	2	58	5.00	0.0100
field_num*slope	1	58	2.42	0.1254

temp Least Squares Means								
temp	Estimate	Standard Error	DF	t Value	Pr > |t|	Alpha	Lower	Upper
0	11.2944	1.1013	58	10.26	<.0001	0.05	9.0899	13.4989
1	14.7929	0.7909	58	18.70	<.0001	0.05	13.2098	16.3760
2	15.0294	0.4713	58	31.89	<.0001	0.05	14.0859	15.9728

Differences of temp Least Squares Means									
temp	_temp	Estimate	Standard Error	DF	t Value	Pr > |t|	Alpha	Lower	Upper
0	1	-3.4985	1.1981	58	-2.92	0.0050	0.05	-5.8968	-1.1003
0	2	-3.7350	1.2733	58	-2.93	0.0048	0.05	-6.2838	-1.1862
1	2	-0.2365	0.9365	58	-0.25	0.8016	0.05	-2.1111	1.6382

Figure B.4: *SAS output detailing results for the downforce flow rate analysis. From the results, significant differences only existed between fluid temperatures.*

The SAS System

The GLIMMIX Procedure

Model Information	
Data Set	WORK.HYD_DATA
Response Variable	hi_press
Response Distribution	Gaussian
Link Function	Identity
Variance Function	Default
Variance Matrix	Diagonal
Estimation Technique	Restricted Maximum Likelihood
Degrees of Freedom Method	Residual

Class Level Information		
Class	Levels	Values
field_num	2	10-21.1_field1 10-21.2_field1
slope	2	1 2
spd	2	0 1
temp	3	0 1 2

Number of Observations Read	66
Number of Observations Used	66

Type III Tests of Fixed Effects				
Effect	Num DF	Den DF	F Value	Pr > F
field_num	1	58	1.14	0.2908
slope	1	58	0.10	0.7476
spd	1	58	1.11	0.2959
slope*spd	1	58	2.92	0.0930
temp	2	58	13.26	<.0001
field_num*slope	1	58	2.30	0.1348

temp Least Squares Means								
temp	Estimate	Standard Error	DF	t Value	Pr > |t|	Alpha	Lower	Upper
0	19.6444	0.03799	58	517.05	<.0001	0.05	19.5683	19.7204
1	19.4638	0.02728	58	713.38	<.0001	0.05	19.4091	19.5184
2	19.4235	0.01626	58	1194.59	<.0001	0.05	19.3910	19.4561

Differences of temp Least Squares Means									
temp	_temp	Estimate	Standard Error	DF	t Value	Pr > |t|	Alpha	Lower	Upper
0	1	0.1806	0.04133	58	4.37	<.0001	0.05	0.09790	0.2634
0	2	0.2208	0.04393	58	5.03	<.0001	0.05	0.1329	0.3088
1	2	0.04022	0.03231	58	1.24	0.2182	0.05	-0.02446	0.1049

Figure B.5: *SAS output detailing results for the downforce pressure requirements. From the results, significant differences only existed between fluid temperatures.*